CANCER NANOTECHNOLOGY: ENGINEERING MULTIFUNCTIONAL NANOSTRUCTURES FOR TARGETING TUMOR CELLS AND VASCULATURES

A Dissertation
Presented to
The Academic Faculty

by

Gloria J. Kim

In Partial Fulfillment
of the Requirements for the Degree
Doctor of Philosophy in the
School of Biomedical Engineering

Georgia Institute of Technology
May 2007

CANCER NANOTECHNOLOGY: ENGINEERING MULTIFUNCTIONAL NANOSTRUCTURES FOR TARGETING TUMOR CELLS AND VASCULATURES

Approved by:

Dr. Shuming Nie, Advisor
School of Biomedical Engineering
Georgia Institute of Technology

Dr. Larry V. McIntire
School of Biomedical Engineering
Georgia Institute of Technology

Dr. L. Andrew Lyon
School of Chemistry and Biochemistry
Georgia Institute of Technology

Dr. Niren Murthy
School of Biomedical Engineering
Georgia Institute of Technology

Dr. Mark R. Prausnitz
School of Chemical and Biomolecular Engineering
Georgia Institute of Technology

Date Approved: April 6, 2007

To: Mom, Dad, Steven, and Onkel

ACKNOWLEDGEMENTS

First of all, I would like to thank my advisor Dr. Shuming Nie for providing academic freedom, continuous guidance and unwavering support. I still remember his response when I said I would join his lab: "Welcome – and just call me Shuming." Little did I know then that this was an invitation to a relationship that may last a lifetime. Shuming's door, and more importantly, his mind, has always been open to me. I can without reservation discuss research or general issues in life with him. He is passionate about his work and readily admits to what he knows or does not know. Once I had suggested a word for a title of the manuscript and he wanted to know what it *exactly* meant. He immediately pulled out an old dictionary and looked it up. This is one image of Shuming that is indelibly seared on my mind. Along with everything I learned from him, I know the image will inspire me to remain humble and inquisitive as a scientist and as a human being.

Next I convey my appreciation to past and present Nie Research Group members. We literally built the lab together when Shuming moved to Atlanta. They are my friends and colleagues who offered their insights on research, gave constructive criticism, and had great fun together in culinary adventures and at various events. Especially, I want to mention Amit, Dominic, Gang, Tushar, Michelle Bluman and Dr. Yong Kyu Lee by name.

Research is never a one-person endeavor. I would like to acknowledge my collaborators from the labs of Drs. Shin (Drs. Kwang Jae Cho and Xu Wang – multidrug resistance studies), Yang, and Chung (Dr. Chunmeng Shi – prostate cancer studies) for

their help. I also acknowledge Dr. Giannakakou's lab at Cornell University for the tubulin staining protocols and Dr. Nicolaou's lab (Ben Pratt) at UCSD for input on the site-specific synthesis.

Additionally, I want to thank Dr. Prausnitz, who almost became my advisor and has been a constant presence in every step in the Ph.D. program. Also, my sincere appreciation to committee members Drs. McIntire, Murthy and Lyon for taking their time and providing comments that helped shape the dissertation in its final form.

When I came to Atlanta, I learned my undeniably Korean last name Kim has great power. Many of the new Korean friends I made here actually came to me first, offering their friendship and assistance. Drs. Yong-Kyu Yoon, Jung-Hwan Park, and Hak Joon Sung – now all freshly minted professors – have been of invaluable help and influence in my professional and personal life.

With the friends I made in Baltimore as a student at Johns Hopkins I still share a special bond. I am very grateful for their support.

Finally, I want to express my thanks and love to my family: My parents for giving me my magnificent brother Steven, an amazing childhood that spanned four continents, supporting me throughout this journey, and keeping me well rooted despite being thousands of miles apart; my brother Steven for just being him, and; Onkel, aunt Chae Young, and aunt Chae Yol for their love and encouragement. I am very fortunate to have a professor as Dad, a teacher as Mom, and a dentist as my younger brother. I will constantly aspire to be as accomplished in my field as they are in their respective fields.

TABLE OF CONTENTS

LIST OF TABLES

LIST OF FIGURES

LIST OF SYMBOLS AND ABBREVIATIONS

A549 cells	Human lung carcinoma cells
bFGF	Basic fibroblast growth factors
CPG	Carboxypeptidase G
Da	Dalton (molecular weight)
DCC	Dicyclo-hexylcarbodiimide
DLS	Dynamic light scattering
DMSO	Dimethyl sulfoxide
DOX	Doxorubicin
EDA	Ethylene diamine
EDTA	Ethylenedinitrilotetraacetic acid
EPR	Enhanced permeation and retention
EtOAc	Ethyl acetate
FA	Folic acid
FDA	Food and Drug Administration
FITC	Fluorescein isothiocyanate
FR	Folate Receptor
GPC	Gel permeation chromatography
HPLC	High-performance liquid chromatography
HPMA	N-(2-hydroxypropyl)methylacrylamide
i.v.	Intravenous
IU	International units
KB cells	Human nasopharyngeal epidermoid carcinoma cells

mAb	Monoclonal antibody
MDR	Multidrug resistance
MMP	Matrix metalloproteinase
MTT	3-(4,5-Dimethylthiazol-2-yl)-2,5-diphenyltetrazolium bromide
MW	Molecular weight
NHS	N-hydroxysuccinimide
NMR	Nuclear magnetic resonance
PBS	Phosphate-buffered saline
PEG	Polyethylene glycol
PG	Poly-l-glutamic acid
Pgp	Glycoprotein P
RES	Reticuloendothelial system
SAR	Structure activity relationship
TEM	Transmission electron microscopy
TLC	Thin layer chromatography
VEGF	Vascular endothelial growth factor

SUMMARY

Significant progress has been made in the development of new agents against cancer and new ways of delivering existing and new agents. Yet, the major challenge to target and selectively kill cancer cells while affecting as few healthy cells as possible remains. Nanometer-sized particles have novel optical, electronic, and structural properties that are not available from either individual molecules or bulk solids. When linked with tumor targeting moieties such as tumor-specific ligands or monoclonal antibodies, these nanoparticles can be used to target cancer-specific receptors, tumor biomarkers as well as tumor vasculatures with high affinity and precision. Recently, the use of nanoparticles for drug delivery and targeting has emerged as one of the most exciting and clinically important areas in cancer nanotechnology.

In this work, we tested the hypothesis that our novel ternary biomolecular nanostructures of folic acid, biodegradable polymer (polysaccharide heparin and poly-l-glutamic acid) and paclitaxel will improve the delivery and tumor-specific distribution of the anticancer drug. The design included three principles: 1) Passive targeting via EPR effect; 2) active targeting via a tumor-specific ligand; and 3) prodrug that would unleash the anti-cancer agent at the tumor site once specific delivery had been accomplished.

First, self-assembled heparin-paclitaxel-FA and PG-paclitaxel-FA nanostructures were synthesized. Their physicochemical properties were examined and biological efficacy was tested. The conjugates had significantly improved solubility in water, paving the way for cremophor-free formulation. Second, *in vitro* cellular toxicity and targeting ability of the nanostructures were investigated. In KB cancer cell lines with high FR

expression, the ternary conjugates were efficiently taken up. In normal cell lines with minimal FR expression level or A549 cancer cells that are FR-negative, no detectable association was found. Competitive assay with FA provided proof that the uptake was indeed via the folate receptor. Third, *in vivo* investigation in human xenograft mice models was carried out. Since the conjugates were highly water soluble, they were suspended in saline for i.v. administration. In the highly FR-positive KB tumor model, ternary nanostructures proficiently inhibited tumor growth without inducing systemic toxicity or side effects. The dramatic tumor shrinkage observed in groups treated with heparin-paclitaxel-FA was on par with the best results reported in the literature found on polymer-drug conjugate investigation. The ternary nanostructures displayed remarkable anti-angiogenic effect on tumor vasculature. Heparin-paclitaxel-FA was also very effective in drug resistant KB tumors, potentially overcoming multidrug resistance through FR targeting and tumor vasculature inhibition. Studies using other cancer models are in progress to determine the spectrum of applicability of these ternary nanostructures.

The design principles applied in these nanoparticles can be extended to delivery and targeting of diagnostic and imaging agents. The ability to engineer multifunctional nanostructures will have a significant impact on cancer diagnostics, molecular profiling, and the integration of cancer therapy and imaging.

CHAPTER 1

INTRODUCTION

1.1 Motivation

The primary objective of this dissertation is to develop novel self-assembled therapeutic nanostructures to improve drug delivery and targeting in tumor and its vasculature. About 1.4 million new cases of cancer will be diagnosed in the United States in 2006, and more than 550,000 people will die of the disease [1]. Cancer is the second leading cause of death in this country. Conventional cancer therapy and diagnostics involve application of catheters, surgery, biopsy, chemotherapy and radiation. Most current anticancer agents do not greatly differentiate between cancerous and normal cells, leading to systemic toxicity and adverse effects. Consequently, systemic application of these drugs often causes severe side effects in other tissues (e.g. bone marrow suppression, cardiomyopathy, neurotoxicity), which greatly limits the maximal allowable dose of the drug. In addition, rapid elimination and widespread distribution into non-targeted organs and tissues requires the administration of a drug in large quantities, which is not economical and often complicated due to non-specific toxicity.

Nanotechnology could offer a less invasive alternative, thus enhancing the life expectancy and quality of life of the patient. The diameter of human cells spans from 10,000 to 20,000 nanometers. The size of cell organelles ranges from a few to a few hundred nanometers. Nanoscale devices can readily interact with biomolecules on the

cell surface and within the cells in a noninvasive manner and leaving the behavior and biochemical properties of those molecules intact. In their "mesoscopic" size range of 10-100 nm in diameter, nanoparticles have more surface areas and functional groups that can be linked to multiple optical, radioisotopic, or magnetic diagnostic and therapeutic agents. When linked with tumor targeting ligands such as monoclonal antibodies, these nanoparticles can be used to target tumor antigens (biomarkers) as well as tumor vasculatures with high affinity and specificity.

1.2 Pharmacokinetics and Drug Targeting

Drug targeting is achieved when the biodistribution of drug is altered to favor its accumulation in the target tissue. This subject can be understood from the perspective of pharmacokinetics. Pharmacokinetics is the study of drug and drug carrier dynamics inside the body and includes the quantitative assessment of absorption, uptake, metabolism and elimination processes. Most relevant to our discussion is the concept of clearance, which is fundamental to pharmacokinetics.

Clearance by a specific organ, CLi , is defined as

$$CL_i = \frac{Q_i (C_{i,a} - C_{i,v})}{C_{i,v}}$$

where Q_i is the plasma flow rate perfusing the organ. $C_{i,a}$ and $C_{i,v}$ respectively represent the drug carrier concentrations in the influent and effluent blood plasma. Let α be the amount of drug molecules loaded per drug carrier, the rate of drug accumulation in a specific organ can be written as

$$\frac{dX_i}{dt} = CL_i \cdot \alpha \cdot C_p$$

which, after integration yields X_i, the total amount of drugs in a specific organ.

$$X_i = CL_i \cdot \alpha \int_{t=0}^{\infty} C_p dt = CL_i \cdot \alpha \cdot AUC_p$$

AUC_p represents the "area under the concentration-time curve" for plasma. A useful parameter is the drug targeting ratio $F_{target.}$ It equals the fraction of the total dose delivered to the target site and can be calculated as:

$$F_{target} = \frac{CL_{target}}{CL_{total}}$$

It is clear that a successful strategy of increased F_{target} involves maximizing CL_{target} while minimizing CL_{total}. Physically, this means that the drug needs to be retained in the body for a long enough time to allow the drug to reach the target. Once at the target site, drugs must be taken up effectively by the target tissue.

1.3 Targeting Strategies

Passive Targeting

The principle of passive targeting is to decrease total body clearance of the drug carrier (CL_{total}). As seen from the equation that defines drug targeting ratio in the preceding section, a prolonged circulation in the plasma results in a higher fraction of drug carriers distributed to the tumor tissues.

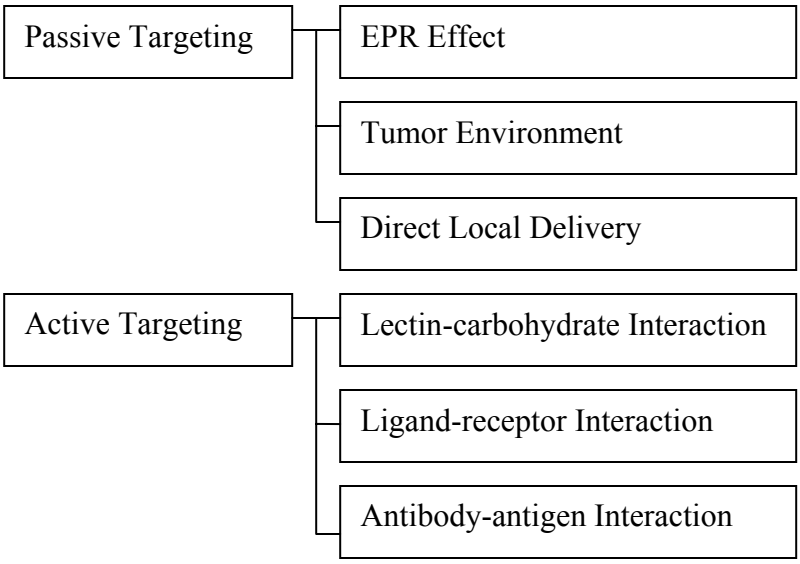

Figure 1.1: Targeting Schemes in Nanoscale Drug Delivery.

The strategies to minimize body clearance have been considered for two organs, the liver and the kidney, because they are known to be the major elimination sites in the body. Hashida and Takakura reviewed the current status of the macromolecular drug delivery systems [2], relating the physiological features of these two organs to the clearance of macromolecules. The glomerular capillaries in the kidney are fenestrated, with the pores of radii estimated to be 20-30 nm. The basement membrane acts as a size and charge barrier, which appears to hinder the transport of molecules greater than 6 nm. In the liver, the basement membrane is absent and the capillaries are characterized by having fenestrate of about 100 nm and endothelial gaps from 100 nm to 1000 nm. The passage of macromolecules is not restricted.

However, cellular uptake of the drug carriers can be lowered by decreasing the interaction between the cells and the carriers. In general, cationic molecules tend to bind to the cell surface and strongly anionic species facilitate receptor-mediated endocytosis.

Consistent with these features, macromolecules with a size greater than approximately 6 nm (MW ~50,000) have exhibited a marked inhibition on renal clearance. A slightly anionic carrier, for example, carboxymethyl dextran, appears to elicit the least uptake by liver cells and its hepatic clearance is similar to that of the fluid phase endocytosis (~10 μL/hr in mice).

EPR Effect

Most capillaries in normal tissues are continuous, with small pore radii of 6.7-8.0 nm and large pore radii of 20-28 nm. By observing the transvascular transport of liposomes in an implanted dorsal skin chamber of a tumor-bearing mouse, Jain's laboratory[3] has determined the cutoff pore size of the tumor vessel to be 400-600 nm. This feature is attributed to the expression of angiogenic factors and various collagen degrading enzymes [4].

Solid tumors have a diffusion-limited maximal size of about $2mm^3$ and will remain at this size until angiogenesis occurs[5, 6], thus granting them access to the circulation.[7, 8] Rapid vascularization to serve fast-growing cancerous tissues leads to leaky, defective architecture devoid of basement membrane and impaired lymphatic drainage. This provides a structural window of opportunity for large drug carriers to selectively reach malignant tissues while sparing most of the normal tissues. (Liver, bone marrow, spleen and kidney are the key exceptions.) This enhanced permeation and retention (EPR) effect[9-11] was first described by Matsumura et al[12]. While the macromolecules could readily extravasate into the tumor tissue, their paths to return to the circulation were blocked.

For such passive targeting mechanism to work, the size and surface properties of drug delivery nanoparticles must be controlled to avoid uptake by the reticuloendothelial system (RES)[13]. To maximize circulation times and targeting ability, the optimal size should be less than 100 nm in diameter and the surface should be hydrophilic to circumvent clearance by macrophages. A hydrophilic surface of the nanoparticles safeguards against plasma protein adsorption, and can be achieved through hydrophilic polymer coating (polyethylene glycol (PEG), poloxamines, poloxamers, polysaccharides) or the use of branched or block copolymers[14, 15]. The covalent linkage of amphiphilic copolymers (polylactic acid, polycaprolactone, polycyanonacrylate) chemically coupled to PEG) [15-17]is generally preferred, as it avoids aggregation and ligand desorption when in contact with blood components[13].

Prodrug Activation by Tumor Environment

An alternative passive targeting strategy is to utilize the unique tumor environment in a scheme called tumor-activated prodrug therapy. The drug is conjugated via a tumor-specific linkage which renders the drug inactive until it reaches the target where cleavage occurs by an intrinsic enzyme and the drug is unleashed [18].

Overexpression of the matrix metalloproteinase (MMP) MMP-2 in melanoma has been shown in a number of preclinical as well as clinical investigations. Mansour et al.[19] reported a water-soluble maleimide derivative of doxorubicin (DOX) incorporating an MMP-2 specific peptide sequence (Gly-Pro-Leu-Gly-Ile-Ala-Gly-Gln) that rapidly and selectively binds to the cysteine-34 position of circulating albumin. The albumin-doxorubicin conjugate is efficiently and specifically cleaved by MMP-2, releasing a doxorubicin tetrapeptide (Ile-Ala-Gly-Gln-DOX) and subsequently doxorubicin. pH and

redox potential have been also explored as drug release triggers at the tumor site[20]. However, their specificity and *in vivo* efficacy has met with limitations as the linkages per se do not differentiate the cancerous tissues from the normal tissues.

Direct Local Delivery

Yet another passive targeting method is the direct local delivery of anticancer agents to tumors. This approach has the obvious advantage of excluding the drug from the systemic circulation. However, administration can be highly invasive, as it involves injections or surgical procedures. For some tumors such as lung cancers that are difficult to access, the technique is nearly impossible to use.

Active Targeting

Active targeting is achieved by increasing the uptake clearance at the target site (CL_{target}). The common approach is conjugating to the nanoparticle a targeting component that provides preferential accumulation of nanoparticles in the tumor bearing organ, in the tumor itself, individual cancer cells, intracellular organelles or specific molecules in cancer cells. Without specific ligands, drug delivery systems are presumably internalized by tumor cells via fluid-phase endocytosis, a slow and non-specific cellular process. The targeting ligands enable the conjugate to be taken up via the route of receptor-mediated endocytosis. Since glycoproteins cannot remove polymer-drug conjugates that have entered the cells via endocytosis [21, 22], this active targeting mechanism provides an

alternative route for overcoming multi-drug resistance (MDR).

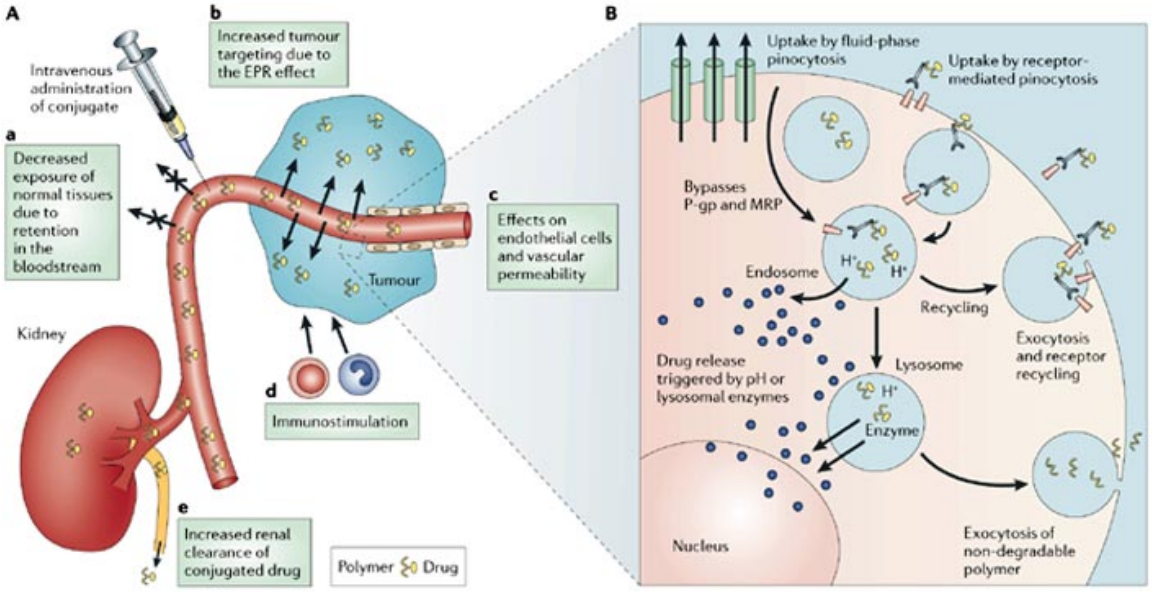

Figure 1.2: Mechanism of Action of Polymer–drug Conjugates. A. Hydrophilic polymer-drug conjugates administered intravenously can be designed to remain in the circulation — their clearance rate depends on conjugate molecular weight, which governs the rate of renal elimination. a. Drug covalently bound by a linker that is stable in the circulation is largely prevented from accessing normal tissues and biodistribution is initially limited to the blood pool. b. The blood concentration of drug conjugate drives tumor targeting due to the increased permeability of angiogenic tumor vasculature providing the opportunity for passive targeting due to the EPR effect. c. Conjugation of ligands enables specific receptor-mediated targeting of tumor cells. d. Circulating low levels of conjugate (slow drug release) might additionally lead to immunostimulation. e. If the polymer–drug linker is stable in the circulation, relatively high level of renal elimination can increase the elimination rate. B. At the tumor interstitium, polymer-conjugated drug is internalized by tumor cells through either fluid-phase pinocytosis, receptor-mediated pinocytosis following non-specific membrane binding (due to hydrophobic or charge interactions) or ligand–receptor interaction. Depending on the linkers used, the drug will usually be released intracellularly. Intracellular delivery can bypass mechanisms of resistance associated with membrane efflux pumps such as p-glycoprotein or multidrug resistance protein (MRP). If >10-fold, EPR-mediated targeting will also enable the circumvention of other mechanisms of drug resistance. Non-biodegradable polymeric platforms must eventually be eliminated from the cell by exocytosis. (Reprinted by permission from Macmillan Publishers Ltd: Nature Reviews Cancer, copyright 2006) [23]

When employing this strategy, several factors need to be taken into account. First, since tumor cells are derived from host cells, the surface antigens of tumor cells are never unique. The difference between the host and the tumor cells is the level of expression. Thus the antigen chosen should give enough selectivity between the tumor and the host tissues. Second, although a tight binding between the ligand and the antigen is essential, a high binding affinity may hinder even distribution [24]. This problem is more severe with a large polymer-drug conjugate. Jain has found that the pathophysiology of the solid tumor causes the build-up of a positive osmotic pressure [25]. The barrier to the movement deep into the tumor core increases with the size of the molecules [3]. Third, the antigen must be internalized by the tumor cells in order to facilitate receptor-mediated endocytosis. Antigen shedding has a negative impact on the effectiveness of this tumor-targeting approach.

Lectin-carbohydrate is one of the classic examples for targeted drug delivery[26]. Lectins are proteins of nonimmunological origin, capable of recognizing and binding to glycoproteins expressed on cell surfaces. Lectin interactions with certain carbohydrates are very specific. Carbohydrate moieties can be used to target drug delivery systems to lectins (direct lectin targeting), and lectins can be used as targeting moieties to target cell surface carbohydrates (reverse lectin targeting). However, drug delivery systems based on lectin-carbohydrate have mainly been developed to target whole organs[27], which can pose harm to normal cells. Therefore, in most cases the targeting moiety is directed towards specific receptors or antigens expressed on the plasma membrane or elsewhere at the tumor site.

The cell surface receptor for folate is inaccessible from the circulation to healthy cells due to its location on the apical membrane of polarized epithelia but is overexpressed on the surface of various cancers ovary, brain, kidney, breast and lung malignancies. Surface plasmon resonance studies revealed that folate-conjugated PEGylated cyanoacrylate nanoparticles had a 10-fold higher affinity for the folate receptor than free folate did [17]. Folate receptors are often organized in clusters and bind preferably to the multivalent forms of the ligand. Furthermore, confocal microscopy demonstrated selective uptake and endocytosis of folate-conjugated nanoparticles by tumor cells bearing folate receptors. Interest in exploiting folate receptor targeting in cancer therapy and diagnosis has rapidly increased, as attested by many conjugated systems including as proteins, liposomes, imaging agents, and neutron activation compounds[15, 17, 28-34].

Tumor targeting by antibodies with engineered properties is in its infancy, but holds much promise. The monoclonal antibody (mAb) BR96 (anti-sialyl Lewis Y antigen) conjugated with doxorubicin has proved highly efficacious in tumour xenograft studies, [35] but, unfortunately, has shown little or no efficacy in Phase II trials for metastatic breast cancer[36] and advanced gastric adenocarcinoma[37], respectively. Moreover, dose-limiting gastrointestinal toxicities were observed in the breast cancer trial because the immunoconjugate bound to antigen-positive normal cells in gastric mucosa, small intestine and pancreas[36]. Calicheamicins[38-40] and maytansinoids[41] are the most extensively evaluated of numerous small-molecule toxins used for direct antibody arming, but indirect arming has met with better success. For example, anti-ERBB2 immunoliposomes loaded with doxorubicin show greater antitumor activity than free

drug or drug loaded in non-targeted liposomes in several tumor xenograft models[42, 43]. Moreover, the systemic toxicity of the immunoliposome-targeted doxorubicin was much less than that of free doxorubicin. Bispecific antibodies, which are non-natural antibodies with two different epitopes, have been used most widely for delivering immune effector cells and, to a lesser extent, for delivery of radionuclides, drugs and toxins to tumors[44, 45]. Still, concern about immunogenicity remains.

Alternatively, tumor vasculatures can be targeted to allow targeted delivery to a wide range of tumor types. A number of angiogenesis inhibitors are undergoing clinical trials. Antiangiogenic therapy prevents neovascularization by inhibiting proliferation, migration and differentiation of endothelial cells[46, 47]. Vascular endothelial growth factor (VEGF) is expressed in many solid tumors[48]. A potent angiogenesis stimulating protein, it also increases the permeability of tumor blood vessels, leading to swelling of the tumor and ultimately hindering the ability of cancer cells to recruit blood supply through angiogenesis. VEGF has been utilized in liposomes and polymeric nanospheres to deliver angiostantin and endostatin[49, 50]. The $\alpha_v\beta_3$ integrin is one of the most specific biomarkers that can differentiate newly formed capillaries from their mature counterparts[51]. Although all endothelial cells use integrin receptors to attach to the extraluminal submatrix, one unique receptor ($\alpha_v\beta_3$ integrin) is found on the luminal surface of the endothelial cell only during angiogenesis[52]. High affinity $\alpha_v\beta_3$ selective ligands, Arg-Gly-Asp (RGD) have been identified by phage display studies. The cyclic form containing a conformationally constrained RGD has a higher binding affinity than the linear form[53]. Doxorubicin-loaded PEG nanoparticles conjugated to cyclic RGD[54] and paclitaxel-cyclic RGD nanoparticles[55] have been reported.

1.4 Polymer-drug Linkages

Since the inception of polymer-drug conjugate first proposed by Ringsdorf in the 1970s [56], the development of polymer-drug conjugates, especially for anti-cancer targeting, has moved forward with promising results (Table 1.1). With proper physiochemical characteristics, the polymer backbone can improve drug properties, for example, by enhancing drug solubility, preventing drug degradation and lowering excretory clearance. Drug molecules are attached to a polymer backbone via biodegradable linkers. Homing signals are covalently joined to the polymer to help localize the polymer-drug conjugates to the target site.

Table 1.1: Polymer-drug Conjugates in Clinical Trials as Anticancer Agents. (Adapted by permission from Macmillan Publishers Ltd: Nature Reviews Drug Discovery, copyright 2003)[11]

Conjugate	Company	Linkage
HPMA* copolymer-doxorubicin	Pharmacia	Amide
HPMA copolymer-galactosamine	Pharmacia	Amide
HPMA copolymer-paclitaxel	Pharmacia	Ester
HPMA copolymer-camptothecin	Pharmacia	Ester
HPMA copolymer-platinate	Access Pharmaceuticals	Malonate
Polyglutamate-paclitaxel	Cell Therapeutics	Ester
Polyglutamate-camptothecin	Cell Therapeutics	Ester
PEG-camptothecin	Enzon	Ester

*N-(2-hydroxypropyl)methylacrylamide

After the polymer-drug conjugates reach the target tissues, a mechanism is needed to release covalently attached drugs such that the active components can exert their pharmacological properties. As reviewed by Veronese et al. [57], a variety of chemical linkages can used to form drug-polymer conjugates. The hydrolysis rate

constants of these linkages depend on the chemical nature of the linkage, the structure of the polymer, and surrounding conditions [58].

The pH of the tumor interstitium rarely declines below pH 6.5 and the sites of the greatest acidity in the tumors are often far from the tumor microvasculature [59-61]. However, the pH within endosomes is markedly lower than in the surrounding milieu, reaching pH 5.5 [62-64]. Because actively targeted polymer-drug conjugates are internalized by the endocytic pathway, the concept of pH-responsive linkage remains attractive. Theoretically, this strategy is applicable to any target that features a pH decrease. The ideal linkage should be stable in the physiological pH, but undergo destabilization under acidic condition, thus resulting in the release of their contents into the cytoplasm before degradation by the lysosomal enzymes.

The frameworks of the pH-responsive amphiphiles feature the pH-sensitive functionality in the desired location of the molecule. In general, these pH-sensitive functionalities include acetals, ketals, vinyl ethers, hydrazones, and ortho esters. The mechanism and catalysis for hydrolysis of acetals, ketals, and ortho esters have been discussed in detail by Cordes et al [65].

For anti-cancer applications, hydrazone and cis-aconityl linkers have been investigated, as they are both relatively stable in physiological pH and are capable of liberating the bound drugs at low pH. The hydrazone linkage has a half-life of about 1-2 days at pH 5-6 whereas less than 20% of the linkage was broken over 30 days at pH 7.5 [66, 67]. Examples of polymer-drug conjugates containing the hydrazone linkage are HPMA-doxorubicin [68], PEG-doxorubicin [69] and PEG-paclitaxel [66]. The cis-aconityl

linkage has a half-life of 3 hours at pH 4.0 and 96 hours at pH 7.5 [70]. HPMA-doxorubicin [68] is one of the examples employing this linkage.

As mentioned in the discussion about passive targeting, with the exception of via the mediation of an intrinsic enzyme such as MMP, the linkages by themselves are not tumor-specific and rely on EPR to reach the tumor site. Therefore, a mechanism to direct the conjugates to their destination, that is, active targeting is essential to be able to take advantage of the versatility of drug-polymer linkages available.

1.5 Scope and Organization of this Work

In this work, we conceptualized novel ternary biomolecular nanostructures of folic acid (FA), biodegradable polymer and paclitaxel that will improve the delivery and tumor-specific distribution of the anticancer drug. The design incorporates both passive targeting and active targeting with an efficient drug release mechanism. This goal has been accomplished through 1) synthesis and characterization of the self-assembled nanoparticles; 2) *in vitro* cellular toxicity and targeting studies in cancer cell lines overexpressing the folate receptor; and 3) *in vivo* investigation in the nude mouse xenograft model and subsequent analysis of the effects on the tumor and its vasculature. The application of these nanoparticles can be extended to delivery and targeting of diagnostic and imaging agents. The ability to design multifunctional nanostructures will have a significant impact on cancer diagnostics, molecular profiling, and the integration of cancer therapy and imaging.

This dissertation is organized in six chapters and one appendix. Chapter 2 describes the design concept and criteria of the ternary nanostructures for enhanced cancer therapy. Chapter 3 describes the synthesis and *in vitro* characterization of two ternary nanostructures, heparin-paclitaxel-FA and poly-l-glutamic acid-paclitaxel-FA. Chapter 4 addresses the *in vivo* efficacy of the novel nanostructures in targeting tumor and its vasculature. Comparison studies with existing paclitaxel regimen including Abraxane™ as are covered as well. In chapter 5, the potential of overcoming drug resistance is explored. Chapter 6 summarizes of the work presented and identifies issues to be addressed in the future. It closes by offering a perspective on cancer nanotechnology. Appendix A briefly describes an ongoing study utilizing the ternary nanoparticles in a highly metastatic prostate cancer model.

CHAPTER 2

DESIGN CONCEPT AND CRITERIA

2.1 Concept

We have conceptualized a ternary nanostructure that potentially provides a broadly applicable platform technology for not only improving tumor-specific targeting, but also a superior way of administering hydrophobic anticancer drugs that often have formulations ridden with systemic side-effects. The nanostructure consists of three elements that are covalently linked: a hydrophobic anticancer drug, a hydrophilic polymeric carrier, and a tumor-specific ligand (Figure 2.1).

By linking a hydrophilic polymer to a hydrophobic drug, we are essentially creating an amphiphilic copolymer with random grafted side chains. In aqueous solution, this amphiphilic structure spontaneously assembles into nanoparticles of diameters about 100 nm. This self-assembled nanostructure has three built-in mechanisms for improving a cancer drug's efficacy and simultaneously reducing its toxicity, leading to dramatically improved therapeutic indices.

The first mechanism is the passive targeting via enhanced permeability and retention (EPR) effect [9, 11-13]. Extensive research in liposome drug delivery systems has shown that this is an effective mechanism for cancer drug delivery [71]. The second mechanism is the use of a tumor-specific ligand to target high-affinity receptors that are known to be overexpressed in many human tumor cells. This active tumor targeting

leads to efficient drug uptake by receptor-mediated endocytosis. In contrast to free drug diffusion across the cell membrane, multi-drug resistance proteins such as glycoproteins [72-75] cannot pump out the polymer-drug conjugates that have entered the cells by endocytosis, leading to the possibility of overcoming drug resistance. The third mechanism involves covalent conjugation of drug to the polymer via a labile bond. This covalent bond transforms the drug to a prodrug that is not functional until the free drug is released at the tumor site by hydrolysis of the bond, thus reducing the nonspecific systemic toxicity of drug conjugates. *In vivo*, hydrolysis can be catalyzed by enzymes or by the pH change in the tumor microenvironment [58].

To illustrate this concept, we have established the design criteria for the ternary nanostructures for tumor-specific targeting.

2.2 Anti-cancer Drug: Paclitaxel

More than 40% active substances being identified through combinatorial screening programs are poorly soluble in water [76]. Conventional and most current formulations of such drugs are frequently plagued with problems such as poor and inconsistent bioavailability. The widely used attempt at enhancing solubility is to generate a salt. For nonionizable compounds, micronization, soft-gel technology, cosolvents, surfactants or complexing agents have been used [17, 77]. Since it is faster and more cost effective to redesign the molecule than to develop a new one, a broadly based technology applicable to poorly water soluble drugs could make a tremendous impact.

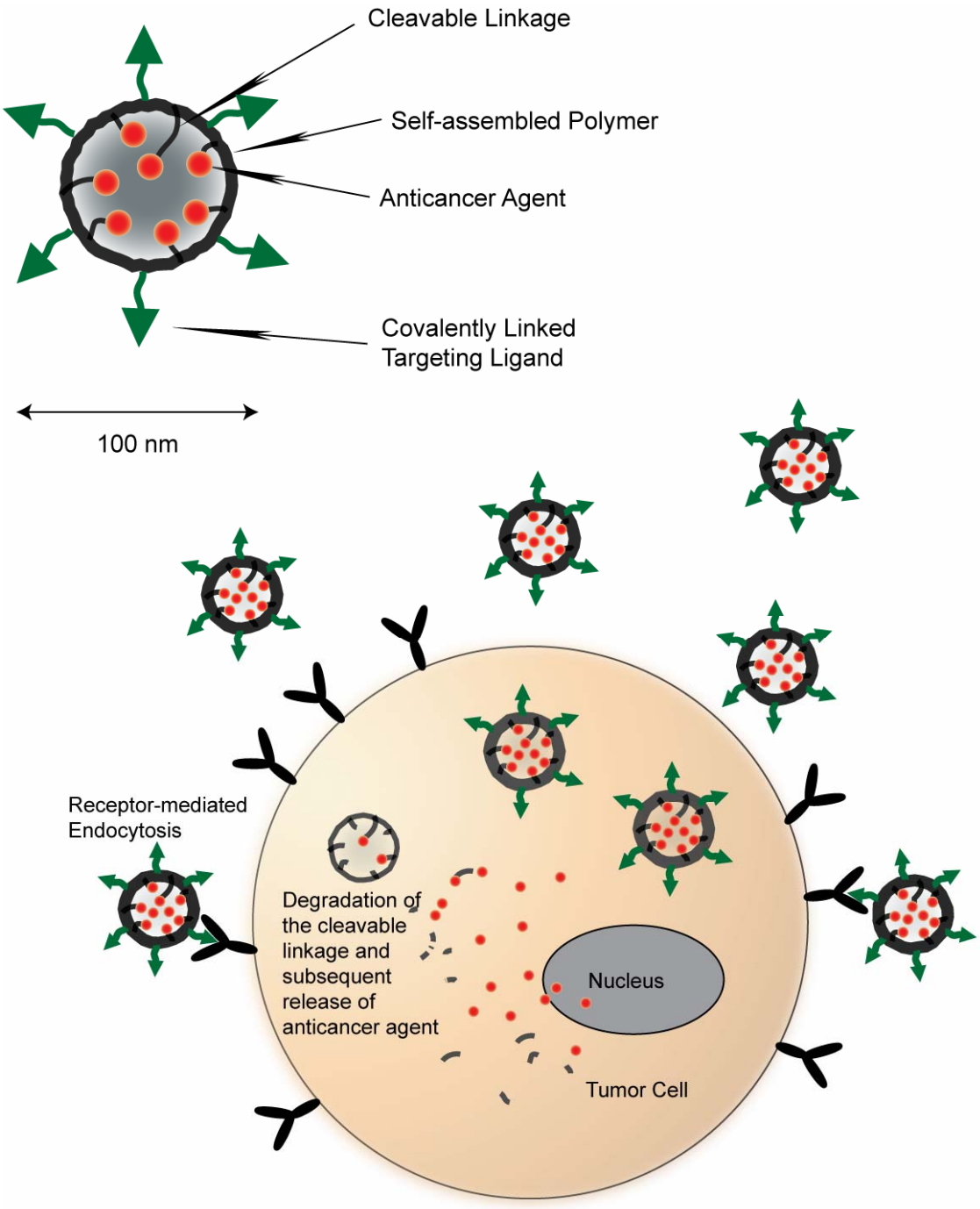

Figure 2.1: Schematics of the Ternary Nanostructure. The conjugate is comprised of an anti-cancer drug, a polymeric carrier and a targeting moiety. The covalent linkage transforms the anti-cancer drug into a prodrug. In its aqueous formulation, the drug self-assembles into nanoparticles that accumulate at the tumor site via passive targeting (EPR effect) and subsequently endocytosed via the active targeting mechanism. Inside the tumor cell, the linkage is degraded and drug released in its active form.

The need to develop formulations for administration of poorly soluble drugs has lead to the application of knowledge of chemistry to drug delivery science leading to the concept of prodrug [78].

Paclitaxel is the most widely used chemotherapeutic agent currently in clinical use. The drug is a microtubule-stabilizing agent that promotes tubulin polymerization, disrupting cell division and leading to cell death[79]. It displays neoplastic activity against primary epithelial ovarian carcinoma, breast, colon, and lung cancers. Because it is poorly soluble in aqueous solution, the formulation available currently is Chremophor EL (polyethoxylated castor oil) and ethanol[80]. Conversion into water soluble prodrug is an attractive option available for delivering paclitaxel which could be further refined by the application of novel drug carriers.

In a new formulation approach used in Abraxane™, recently approved by the FDA to treat metastatic breast cancer, paclitaxel was conjugated to albumin nanoparticles.[81, 82] The new formulation effectively circumvents side effects of the highly toxic Chremophor EL that include hypersensitivity reactions, nephrotoxicity, and neurotoxicity [80, 83]. Besides albumin, studies of paclitaxel conjugate with synthetic polymers such as poly(ethylene glycol) (PEG) and poly N-(2-hydroxypropyl)methacrylamide (HPMA) have been carried out by different research groups. However, these polymer-paclitaxel conjugates are still not tumor-specific and could potentially exert systemic side effects associated with paclitaxel, if not the polymer carrier.

Chemically, paclitaxel has three hydroxyl groups available for covalent linkage at C1, C7, and C2' positions (Figure 2.2). Extensive structure activity relationship

(SAR) studies have shown that a free hydroxyl group at the C2' position is crucial for microtubule binding [84-86] and may play a role as a hydrogen bond donor [87].

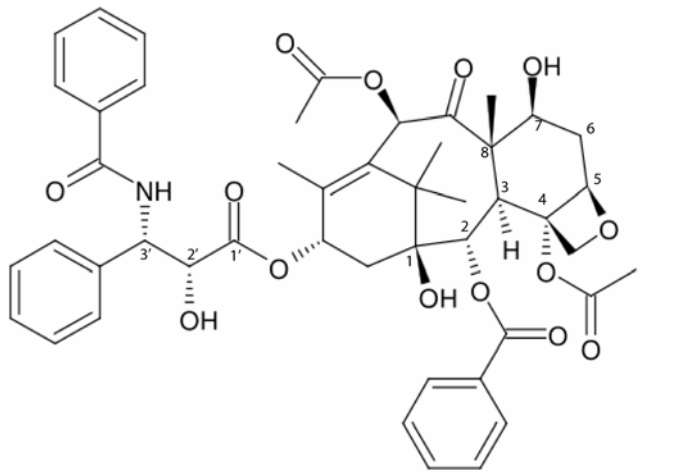

Figure 2.2: Structure of Paclitaxel. The free hydroxyl group at the C2' position is important for paclitaxel potency.

We surmised that paclitaxel with its poor water solubility, non-specificity, and well-documented side effects upon systemic administration would benefit from our ternary nanostructure approach. Since we were to covalently link the three constituents, the presence of derivatizable functional groups on paclitaxel and the polymer of choice were important considerations.

2.3 Polymeric Carriers

N-(2-hydroxypropyl)methylacrylamide

N-(2-hydroxypropyl)methacrylamide (HPMA) copolymers have been studied for drug delivery and other applications for several decades [88]. Homopolymers of HPMA

are hydrophilic, uncharged, and have a low affinity for cell membranes although many functional groups can be incorporated into the polymer backbone such as charged groups [89], targeting moieties [88] and drugs.

HPMA copolymers are generally highly biocompatible but not biodegradable [88] in the main chain, a trait shared with PEG. Therefore, to ensure clearance from the body, an optimal HPMA copolymer molecular weight (~30kDa [78]) must be chosen. Many of the anti-cancer drug conjugates that have entered the clinical stage development use HPMA copolymer as carrier (Table 1.1).

To incorporate active targeting, HPMA copolymer conjugates have been designed to contain saccharides [90], antibodies [91], proteins and peptides [92] as targeting ligands. Only one conjugate, HPMA copolymer–doxorubicin–galactosamine, has progressed into clinical trial [93].

Notable is the rather disappointing outcome of phase I evaluations of HPMA copolymer-paclitaxel conjugates in which paclitaxel is linked to the HPMA copolymer via an ester bond. HPMA copolymer–paclitaxel showed paclitaxel-like dose-limiting toxicity [94]. In addition to these published findings, the low drug loading (10 % wt) and the non-biodegradable nature of HPMA copolymer were factored into our decision to exclude HPMA copolymer as a carrier candidate for our ternary nanostructures.

Poly-l-glutamic Acid

Poly-l-glutamic acid (PG) is composed of naturally occurring l-glutamic acid linked together through amide bonds. The free γ-carboxyl group in each repeating unit of l-glutamic acid is negatively charged at a neutral pH, which renders the polymer water-soluble. The carboxyl groups can be modified for drug conjugation [95].

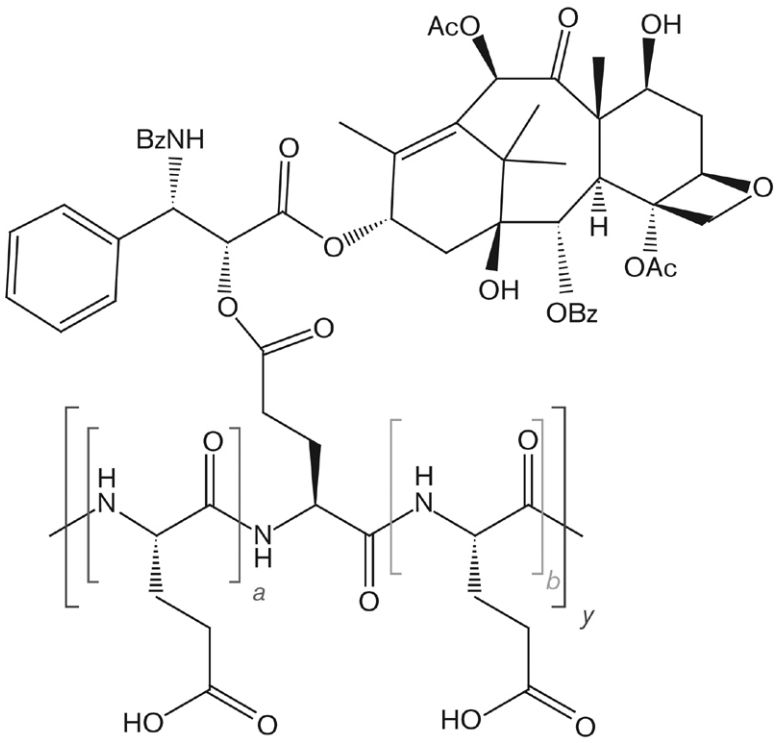

Figure 2.3: Structure of PG-paclitaxel. Paclitaxel is bound to PG at the 2′ position via an ester linkage.

Unlike HPMA copolymers, the PG polymer chain is biodegradable. In contrast to the low loading level of HPMA copolymer-paclitaxel, that of PG-paclitaxel is high (37 % wt). Previous studies report PG-paclitaxel conjugates where paclitaxel is bound to PG at the C2′ position via an ester linkage and the conjugate is found to be highly water-soluble [11, 95, 96]. The hydrolytic release of paclitaxel is slow (up to 14% over 24 h). The release is greatly accelerated after endocytic uptake which exposes the conjugate to lysosomal cathepsin B [95]. EPR-mediated tumor targeting and the greater efficacy of PG–paclitaxel is observed in many preclinical tumor models, and it has an improved safety profile due to both decreased normal tissue exposure and improved drug solubility [96, 97].

Heavy reliance on EPR effect for the PG-paclitaxel for cancer targeting results in non-specific binding of the conjugates with proteins or enzymes [98]. The inclusion of a targeting moiety to induce specific receptor-mediated interactions of PG–drug conjugates with the tumor cell holds great potential in enhancing its efficacy.

Heparin

Heparin, a natural polysaccharide joined by glycosidic linkages, has been used in the clinic as an anticoagulant for more than 50 years. The array of sulfate, hydroxyl and carboxyl groups is known to be responsible for this activity [99, 100]. However, heparin is a complex polysaccharide with diverse properties that are unrelated to its anticoagulant activity [101].

Heparin can associate with growth factors such as vascular endothelial growth factors (VEGF) and basic fibroblast growth factors (bFGF) [102-105]. This interaction between heparin and growth factors is mediated by the physicochemical properties of heparin, which are imparted by its sulfation pattern, charge distribution, overall charge density, and molecular size. Heparin can affect tumor progression via its involvement in a number of physiological processes like angiogenesis and metastasis by binding with angiogenic growth factors and inhibition of heparinases that degrade basement membranes [106-108].

Chemically modified heparins with reduced or no anticoagulant activity retain their ability to effectively inhibit angiogenesis, metastasis and tumor growth [109-111]. Recently, heparin-based nanoparticles or micelles, chemically modified with cationic polymers [112, 113], polysaccharides [114] or deoxycholic acid [115-117] have been developed as drug carriers.

These inherent anti-cancer properties of heparin could potentially work in synergy with paclitaxel once it reaches the tumor site, making the biologically active polysaccharide a promising carrier candidate for our ternary nanostructures.

2.4 Targeting Ligand: Folic Acid

For specific targeting, the differences between cancerous cells and normal cells, which include uncontrolled proliferation, insensitivity to negative growth regulation and anti-growth signals, angiogenesis, and metastasis can be exploited. There is a growing body of knowledge of unique cancer markers thanks to recent advances in proteomics and genomics. They form the basis of complex interactions between bioconjugated nanoparticles and cancer cells. Carrier design and targeting strategies may vary according to the type, developmental stage, and location of cancer.

A variety of ligands, such as antibodies, growth factors, or cytokines, have been explored to facilitate the uptake of carriers inside target cells [118-120]. Among them, folic acid (FA) has been utilized for tumor targeting of anticancer drugs via folate receptor (FR)-mediated endocytosis [121-124](Figure 2.4). FR is known to be abundantly expressed in a large fraction of human ovary, mammary gland, colon, lung, prostate, and brain tumors, but only minimally distributed in normal tissues. Therefore, FR serves as an excellent tumor marker as well as a functional tumor-specific receptor[125-128].

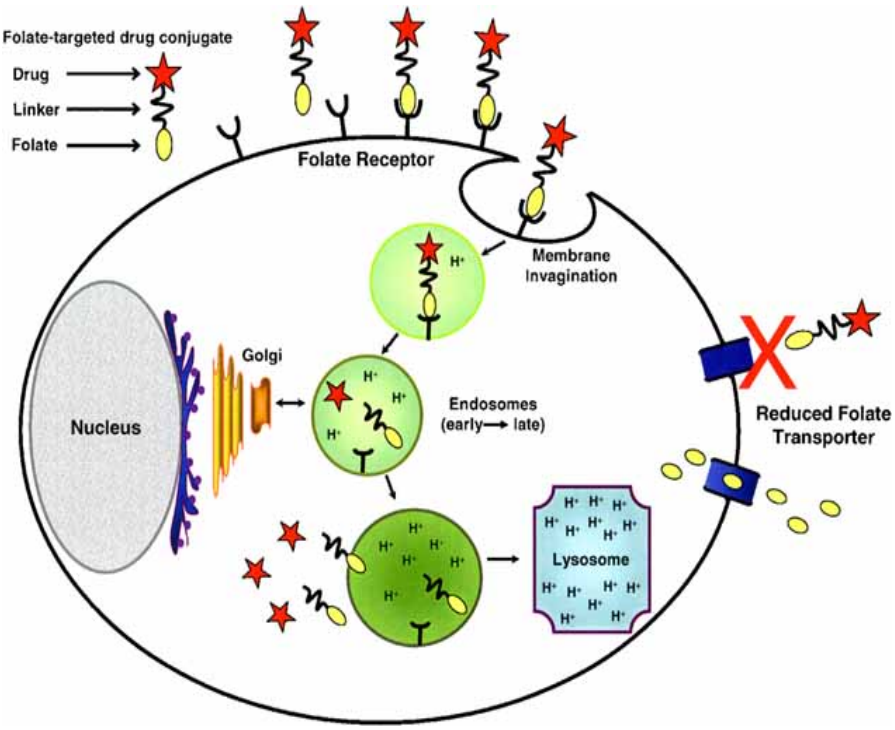

Figure 2.4: Receptor-mediated Endocytosis of Folate Conjugates. Folate-targeted conjugates bind to cell surface folate receptors (FRs) with nanomolar affinity. After binding, the cell membrane invaginates and pinches off to form an endosome. As the endosomal compartment acidifies, the folate conjugate and its drug may be released from the receptor into the cytosol. Although the reduced folate carrier is thought to be present in virtually all cells, folate-conjugates are not substrates, and therefore, are taken up only by cells expressing a functional folate receptor. (Journal of Pharmaceutical Sciences; Hilgenbrink, A.R. and Low, P.S.; Copyright 2005; Reprinted with permission of Wiley-Liss, Inc. a subsidiary of John Wiley & Sons, Inc.)[124]

To date, all FA-drug conjugates that have been reported in the literature have been developed as anti-cancer agents [129-133]. Direct conjugation of the drug by attachment to the α or γ carboxyl group of FA had limited success as FA derivatization diminished the potency of the parent drug. Folate targeted liposomes loaded with doxorubicin [34, 134-137] showed effective targeting, inhibition of tumor growth, and prolonged survival in mice. Quintana et al. conjugated methotrexate (MTX) to FA-dendrimers through a non-biodegradable amide linkage and a hydrolyzable ester linkage[133]. The ester-containing dendrimer designed to release the MTX drug in the

endosome after FR mediated entry into the cell was 4-fold more efficient at inducing a cytotoxic response in KB cells than was free MTX.

Both successful and failed folate-drug conjugates provide useful information on features required for a successful formulation that could make a clinical impact. Firstly, it is important to attach the drug to FA in a manner that retains the affinity to FR. This can be assured by the use of a polymeric carrier, preventing intramolecular interactions between folate and its therapeutic cargo. Secondly, in order for some drugs to be active, they must be released inside the cell in unmodified form. This can be achieved by inserting a cleavable bond immediately prior to the attached drug. A variety of cleavable linkers, including ester bonds, disulfide bonds, pH-sensitive linkers, and enzymatically cleavable bonds, have either been tested or proposed. Finally, a highly potent drug must be selected. Many human cancer cells express up to 10^7 FR/cell. However, even delivery of 10^7 drugs/cell may be inadequate for compounds with IC_{50} values $>10^{-8}$ M.

Our choice of components satisfies the above-mentioned criteria for effective folate targeting. The novelty of the approach is highlighted by the use of heparin whose nascent anti-tumor and anti-angiogenic properties enables it to act not only as a polymeric carrier, but as a therapeutic component as well.

In spite of the technological advances, many challenges and opportunities remain before the full potential of folate targeted chemotherapeutics can be realized. No two FA-drug conjugates will distribute identically among all of the tissues in the body. In addition, although many conjugates have repeatedly demonstrated activity without toxicity in mice, similar confirmation is needed in other animals models, and ultimately, in patients. Furthermore, since tumors are heterogeneous, multiple drug combinations

that include one or more FA-targeted agents may be needed to completely eradicate a tumor. This point may actually be very relevant to the clinic, especially if the FA-drug conjugate adds potency without toxicity.

CHAPTER 3

SYNTHESIS AND CHARACTERIZATION OF POLYMER-PACLITAXEL-FA TERNARY NANOSTRUCTURES

3.1 Introduction

Based on the design criteria described in chapter 2, we set out to synthesize the ternary nanostructures. The synthesis would modify poly-l-glutamic acid (PG) and heparin suitable for passive targeting and active targeting via the folate receptor. The polymer and folic acid (FA) were linked through a stable amide bond. Paclitaxel was joined to the polymeric carrier via a labile ester bond. First, we prepared heparin-paclitaxel-FA conjugates. There were three main challenges in this task: 1) To retain the inherent anti-cancer properties of heparin while suppressing its known side effects such as thrombocytopenia or bleeding; 2) to optimize the number of active FA attached to heparin; and 3) to examine the suitability and position of the ester bond for the proposed prodrug design. The outcome gave us some feedback on how to streamline the synthesis procedure and considerations in synthesizing PG-paclitaxel-FA.

The goals of the process were: 1) To produce an optimized nanostructures capable of specifically targeting tumor cells and releasing drugs by the cleavage of the ester linkage that is stable in serum containing conditions; 2) to characterize the physiochemical features of the conjugates; and 3) to develop a robust and scalable process in order to prepare materials for further evaluation in animal studies.

We describe here the methods to synthesize ternary nanostructures of heparin-paclitaxel-FA and PG-paclitaxel-FA. These conjugates were well characterized by various analytical tools, measuring the product purity, chemical identity, degree of modification of the polymer backbone, paclitaxel loading and release under different conditions. Tumor-specific uptake was assessed *in vitro* by analyzing cytotoxicity.

3.2 Materials and Methods

Materials

All reagents were obtained from commercial sources. Heparin sodium was from Celsus Laboratories, Inc. (Cincinnati, OH). Poly-l-glutamic acid sodium salt with a nominal molecular weight 42,000 Da was ordered from Sigma. Paclitaxel was purchased from Polymed Therapeutics, Inc. (Houston, TX). Folic acid (FA), dicyclohexylcarbodiimide (DCC), ethylene diamine, N-hydroxysuccinimide (NHS), pyridine, dimethyl sulfoxide (DMSO), acetonitrile, methanol, formamide, anhydrous diethyl ether, methylene chloride, human antithrombin III, bovine factor Xa, bovine factor Xa chromogenic substrate, acetic acid, and MTT-based toxicology assay kit were purchased from Sigma-Aldrich (St. Louis, MO). Tubulin polymerization assay kit was from Cytoskeleton, Inc. (Denver, CO).

KB (human nasopharyngeal epidermoid carcinoma cells), A549 (human lung carcinoma cells) and MCF-10A (human mammary epithelial cells) were purchased from American Type Culture Collection. Penicillin-streptomycin, fetal bovine serum (FBS), Ham's F12K medium with 2 mM L-glutamine, MEGM, cholera toxin and 0.25% (w/v)

trypsin-0.03% (w/v) EDTA solution were from American Type Culture Collection (Manassas, VA). FA-deficient RPMI 1640 medium was from Invitrogen.

Synthesis of Heparin-paclitaxel-FA

Preparation of Aminated FA

To aminate FA, FA (1 mmol) dissolved in 30 mL DMSO was reacted with DCC (1.2 mmol) and NHS (2 mmol) at 60 °C for 8 hours. FA-NHS was obtained by filtering the precipitated DCU and precipitation by adding 100 mL of 30 % acetone in ethyl ether with stirring. The yellow precipitate was collected on sintered glass and washed with acetone and ether and was used immediately in the next step of synthesis.

The resulting FA-NHS was mixed with ethylene diamine (10 mmol) plus 200 μL pyridine and allowed to react at room temperature overnight. The reaction was confirmed by TLC analysis (silica gel plate, 2-propanol/chloroform, 70:30 v/v %). The crude product was precipitated by addition of excess acetonitrile, filtered and washed three times with diethyl ether before drying under vacuum.

Unreacted FA and aminated FA were separated by ion-exchange chromatography. The column (200mm ×10 mm) was packed by swollen DEAE Sephadex A-25 in 0.5 M potassium tetraborate solution (pH 7.0). After dissolving in deionized water, the product (0.03 mg/mL) was loaded into the column. The linear ionic gradient of ammonium bicarbonate solution (pH 7.8, 10 to 30 mM) was applied. The FA-NH-$(CH_2)_2$-NH_2 solution was fractionally collected after continuous TLC analysis as mentioned above. It is also possible to separate the unreacted FA and aminated FA via Gel Permeation Chromatography (GPC).

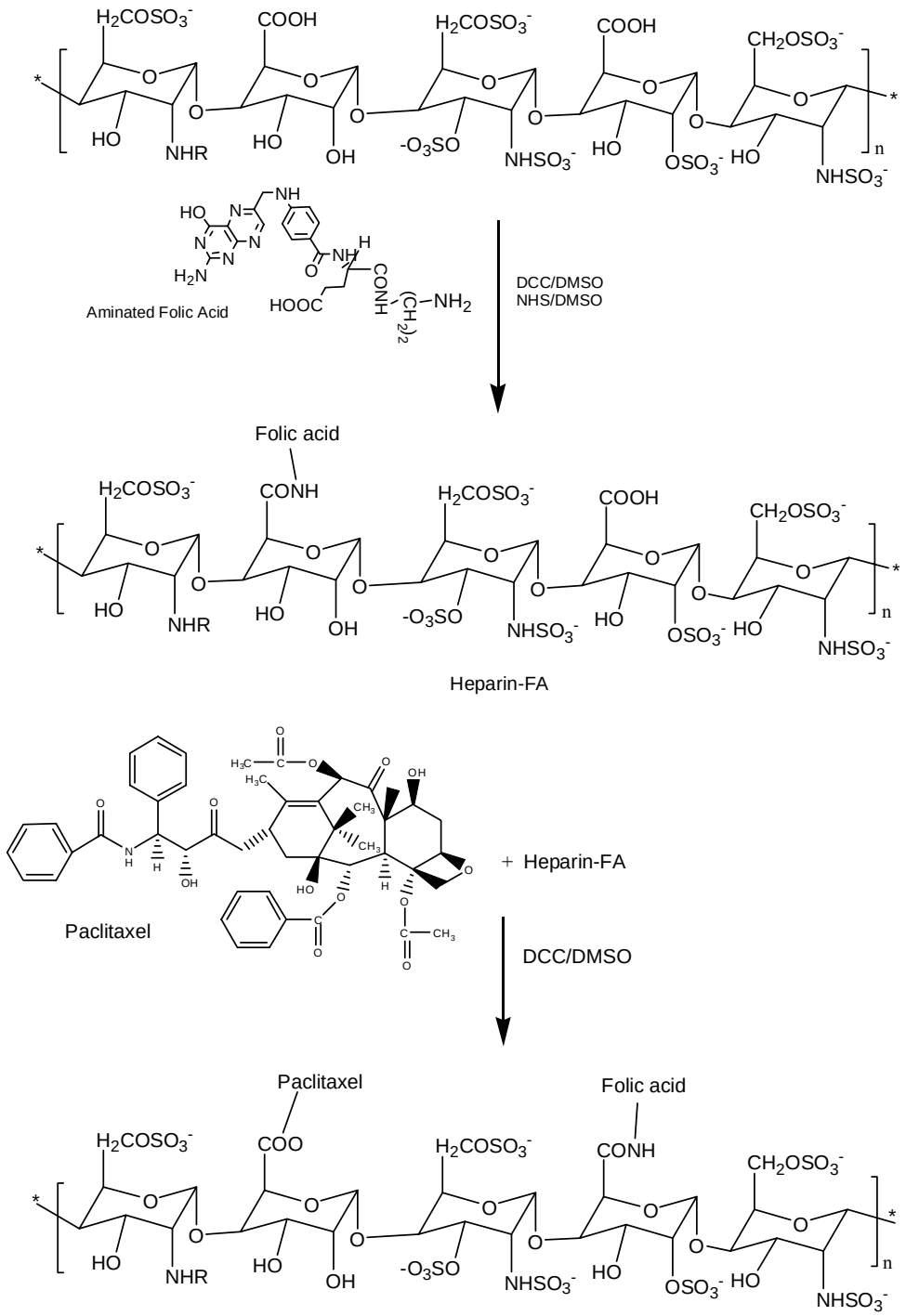

Figure 3.1: Synthesis of Heparin-paclitaxel-FA. Heparin-FA conjugates were prepared by postmodification of the carboxyl group of FA as shown. The coupling was achieved by amide bonds between carboxyl groups of heparin and amine groups of aminated FA. Paclitaxel was linked to heparin-FA via dicyclohexylcarbodiimide (DCC) mediated reaction of hydroxyl groups of paclitaxel and the carboxyl groups of heparin to form an ester bond.

The γ mono-aminated FA [γ, FA-NH-$(CH_2)_2$-NH_2] was separated from the α isomer by HPLC on a preparative C-18 reversed phase column (250mm × 21mm) using a linear gradient (eluant A, water with 0.05% TFA at pH 3.5; eluant B, acetonitrile; gradient 0 to 15% B over 20 minutes at a flow rate of 10 mL/min). The respective elution times for γ mono-aminated FA and α mono-aminated FA were 7.0 and 12.5 min.

Values for *^{1}H-NMR* of aminated FA (400MHz, DMSO) were: δ1.1 [s, C7-H of FA, 1H], 4.28-4.16 [m, α-CH_2 of Glutamate of FA, 1H], 6.64 [d, 3', 5'-H of FA, 2H], 7.64 [d, 2', 6'-H of FA, 2H], 8.1-8.17 [H of CONH].

Values for *^{1}H-NMR* of γ mono-aminated FA were: (300MHz, DMSO-d_6)/CF_3CO_2D~10/1 v/v) were δ8.75 [s, 1H of C7-H], 7.66 [d, 2H, Ar], 6.63 [d, 2H, Ar], 4.57 [s, 2H, C9-H_2], 4.34 [dd, 1H, C19-H]. 3.22-3.15 [m, 2H, C25- H_2], 2.80 [m, 2H, C26- H_2], 2.16 [m, 2H, C22- H_2], 2.15-1.85 [m, 2H, C21- H_2].

Preparation of Heparin-paclitaxel-FA

Heparin (1 mmol) was activated using DCC (20 mmol) and NHS (40 mmol) in formamide at 4 °C overnight. Dicyclohexylurea (DCU) was removed by filtration and then heparin-NHS was obtained by recrystallization. The activated heparin-NHS (1 mmol) and aminated FA (10 mmol) were reacted at room temperature for 1 day. Unreacted aminated FA was removed by dialysis (MWCO 2000) against 0.1M sodium bicarbonate buffer. The elevated pH of the dialysis buffer facilitated hydrolysis of the activated ester. The resultant heparin-FA was dialysed against water for 2 days and lyophilized.

A solution of paclitaxel (15 mmol) in DMSO was added to FA-heparin in foramide. DCC (15 mmol) in DMSO were subsequently added dropwise and stirred on ice. When addition of DCC was complete, the reaction was allowed to proceed for 6 hours at room temperature. After the reaction, filtration, recystallization and dialysis against water for 48 hours followed. Yellow powder was obtained after lyophilization. The reaction was monitored by TLC analysis (silica plate; 2-propanol/chloroform 10:90 v/v %) and *^{1}H-NMR* (400MHz, D_2O). TLC analysis showed complete conversion of paclitaxel (R_f =0.66) to the conjugate (R_f =0). The spots of heparin, paclitaxel, heparin-FA and heparin-paclitael-FA were used to estimate purity of the final product.

Values for *^{1}H-NMR* of paclitaxel (400MHz, $CDCl_3$) were: ($CDCl_3$) were: δ1.11 [s, $^{17}CH_3$], 1.20 [s,$^{16}CH_3$], 1.69 [s, $^{19}CH_3$], 1.97 [s, $^{18}CH_3$], 2.2 [m, OAc], 2.4 [m, OAc], 3.78 [d, ^{3}CH], 4.17 [d, $^{20}CH_2$], 4.27 [H-α, PG], 4.3 [d, $^{20}CH_2$], 4.39 [dd, ^{7}CH], 4.96 [d, ^{5}CH], 4.78 and 5.63 [d, $^{2'}$CH], 5.67 [d, ^{2}CH], 5.98 [dd, $^{3'}$CH], 6.22 [t, ^{13}CH], 6.27 [s, ^{10}CH], 7.09 [d, NH], 7.25 [s, 3'-Ph], 7.4 [m, 3'-NBz], 7.5 [m, 2-OBz], 7.73 [d, 3'-NBz], 8.1 [d, 2-OBz].

Values for *^{1}H-NMR* of heparin (400MHz, D_2O) were: δ5.38 [H1 of glucosamine residue (A)], δ5.04 [H1 of iduronic acid residue(I)], δ4.84 [I-5], 4.36-4.23 [A-6], 4.12-4.40 [I-3], 4.08 [I-4], 4.02 [A-5], 3.78 [I-2], 3.71 [A-4], 3.65-3.69 [A-3], 3.24 [A-2].

Values of *^{1}H-NMR* of heparin-paclitaxel-FA (400MHz, D_2O) were: δ1.11-2.4 [CH_3 or OAc of paclitaxel], 3.24-5.38 [A or I of heparin], 7.5-7.64 [2-OBz and NBz of paclitaxel], 7.64 [H of FA, 2H], 8.1-8.45 [CONH between heparin and FA] and 5.6 [COO between heparin and paclitaxel].

Heparin Crosslinking

To probe the heparin crosslinking following the conjugation scheme in Figure 3.1, two controls were constructed. Heparin (0.5 mmol) and heparin-FA (0.5 mmol) was each dissolved in formamide and activated by adding a DMSO solution of DCC (10 mmol) and reacting overnight. Purification of heparin-DCC and heparin-FA-DCC was carried out by dialysis, under the same conditions as heparin-paclitaxel-FA conjugates. Unreacted DCC precipitated out from the resultant aqueous solution and was removed by centrifugation followed by filtering through a sintered glass funnel. The filtrate was lyophilized to obtain a white powder. Values for *^{1}H-NMR* were (400MHz, D_2O) essentially the same as the ones previously determined for heparin and heparin-FA. Both DCC-treated compounds and their respective starting materials were subjected to GPC analysis.

Synthesis of Heparin-paclitaxel

A solution of paclitaxel (25 mmol) in DMSO was added to heparin in formamide. DCC (25 mmol) in DMSO were subsequently added dropwise and stirred on ice. When addition of DCC was complete, the reaction was allowed to proceed for 6 hours at room temperature. After the reaction, filtration and dialysis against water for 48 hours followed. White powder was obtained after lyophilization. The reaction was monitored by TLC analysis (silica plate; 2-propanol/chloroform 10:90 v/v %) and *^{1}H-NMR* (400MHz, D_2O). TLC analysis showed complete conversion of paclitaxel (R_f =0.66) to the conjugate (R_f=0).

Synthesis of Site-specific Heparin-paclitaxel-FA

Protection of 2'-OH (Compound 1, Figure 3.2)

Paclitaxel (1g, 1.17 mmol) and pyridine (9.5 mL) were dissolved in 50 mL methylene chloride. At room temperature, a total of 10.2 mL of benzyl chloroformate was added in 6 equal aliquots at 10 minute intervals. The reaction was monitored via TLC (silica gel plate, EtOAc/haxane, 50:50 v/v %) until there was almost no remaining starting material (R_f=0); two additional bands at R_f =0.5 for the product and R_f =0.7 for benzylchloroformate were also observed. The reaction was quenched with 10 mL aqueous NH_4Cl. After dilution with 100 mL ethyl acetate, the reaction mixture was washed twice with 10 mL NH_4Cl, four times with 100 mL copper sulfate and 50 mL NaCl. The organic layer was combined, dried with Na_2SO_4, concentrated and purified by flash chromatography (silica, ethyl acetate (EtOAc)/hexane, 50:50 v/v %) by extraction of R_f =0.5 band. The eluent was collected and dried to yield a white powder of 2'-carboxybenzoyltaxol (840mg).

Protection of 7-OH (Compound 2, Figure 3.2)

2'-carboxybenzoyltaxol (structure) was heated at 60˚C in 20 mL CH_3CN/CH_2Cl_2 (50:50 v/v %) for 40 min. Meanwhile, imidazole (2 g, 30 mmol) and chlorotriethylsilane (4.3 mL, 32 mmol) were also heated at 60 °C in CH_3CN/CH_2Cl_2 (50:50, 15 mL) and both solutions were mixed quickly and stirred at 60 °C for 1.5 h. The organic layer was separated, dried and concentrated under reduced pressure. The crude product was purified by flash chromatography (silica, heptane/EtOAc, 60:40 v/v %) to obtain an amorphous white solid.

Deprotection of 2'-OH (Compound 3, Figure 3.2)

A solution of compound 2 in methanol at room temperature under argon was treated with 10 % palladium on carbon and placed under hydrogen. After 2 hours, the mixture was filtered to remove the catalyst and evaporated to dryness under vacuum to obtain a white powder.

Preparation of heparin-paclitaxel-FA conjugated at the C2' position of paclitaxel (Compound 4, Figure 3.2)

Heparin-FA was prepared as outlined and conjugated to compound 3 via DCC coupling as described above. The silyl protective group at C7 was removed by adding dropwise HF/pyridine at 0˚C to the solution of compound 3 in pyridine/acetonitrile. The mixture was stirred at 0˚C for 3 hours. The reaction was quenched with saturated aqueous sodium hydrogen carbonate solution. After workup, the extract was purified via dialysis against water for 2 days and lyophilized.

Protection of 2'-OH (Compound 5, Figure 3.2)

To a well-stirred solution of paclitaxel (1 g, 1.17 mmol) and imidazole (920 mg, 13.5 mmol) in CH_2Cl_2 (24 mL) at room temperature was added chlorotriethylsilane (0.3 mL, 2 mmol) slowly under a nitrogen atmosphere. After stirring the reaction mixture for 30 min, the reaction was quenched with water (30 mL), and the organic layer was separated, dried and concentrated under reduced pressure. The crude product was purified by flash chromatography (silica, heptane/EtOAc, 60:40 v/v %; R_f = 0.58) to obtain a white powder of 2′-triethylsilyloxypaclitaxel (850mg).

Values for *^{1}H-NMR* (400 MHz, $CDCl_3$) were: δ 0.37–0.49 (m, 6H, $SiCH_2CH_3$), 0.80 (t, J=7.9, 9H, $SiCH_2CH_3$), 1.12 (s, 3H, H16), 1.23 (s, 3H, H17), 1.67 (s, 3H, H18),

1.71–1.74 (m, 1H, H6b), 1.92 (s, 3H, H19), 2.11–2.19 (m, 2H, H14), 2.23 (s, 3H, C10-CH_3CO), 2.32–2.55 (m, H6a), 2.54 (s, 3H, C4-CH_3CO), 3.80 (d, J=7.0, 1H, H3), 4.21 (d, J=8.5, 1H, H20), 4.30 (d, J=8.5, 1H, H20), 4.41 (dd, J=10.6, 6.6, 1H, H7), 4.67 (d, J=1.9, 1H, H2′), 4.96 (d, J=8.0, 1H, H5), 5.67–5.70 (m, 2H, H3′ and H2), 6.25 (t, J=8.8, 1H, H13), 6.28 (s, 1H, H10), 7.09 (d, J=8.6, 1H, NH), 7.31–7.58 (m, 11H, ArH), 7.64 (d, J=8.0, 2H, ArH), 8.13 (d, J=8.0, 2H, ArH).

Preparation of heparin-paclitaxel-FA conjugated at C7 position of paclitaxel (Compound 6, Figure 3.2)

Heparin-FA was prepared as outlined and conjugated to compound 5 via DCC coupling as described above. The silyl protective group at C2' was removed by adding dropwise HF/pyridine at 0˚C to the solution of compound 6 in pyridine/acetonitrile. The mixture was stirred at 0˚C for 3 hours. The reaction was quenched with saturated aqueous sodium hydrogen carbonate solution. After workup, the extract was purified via dialysis against water for 2 days and lyophilized.

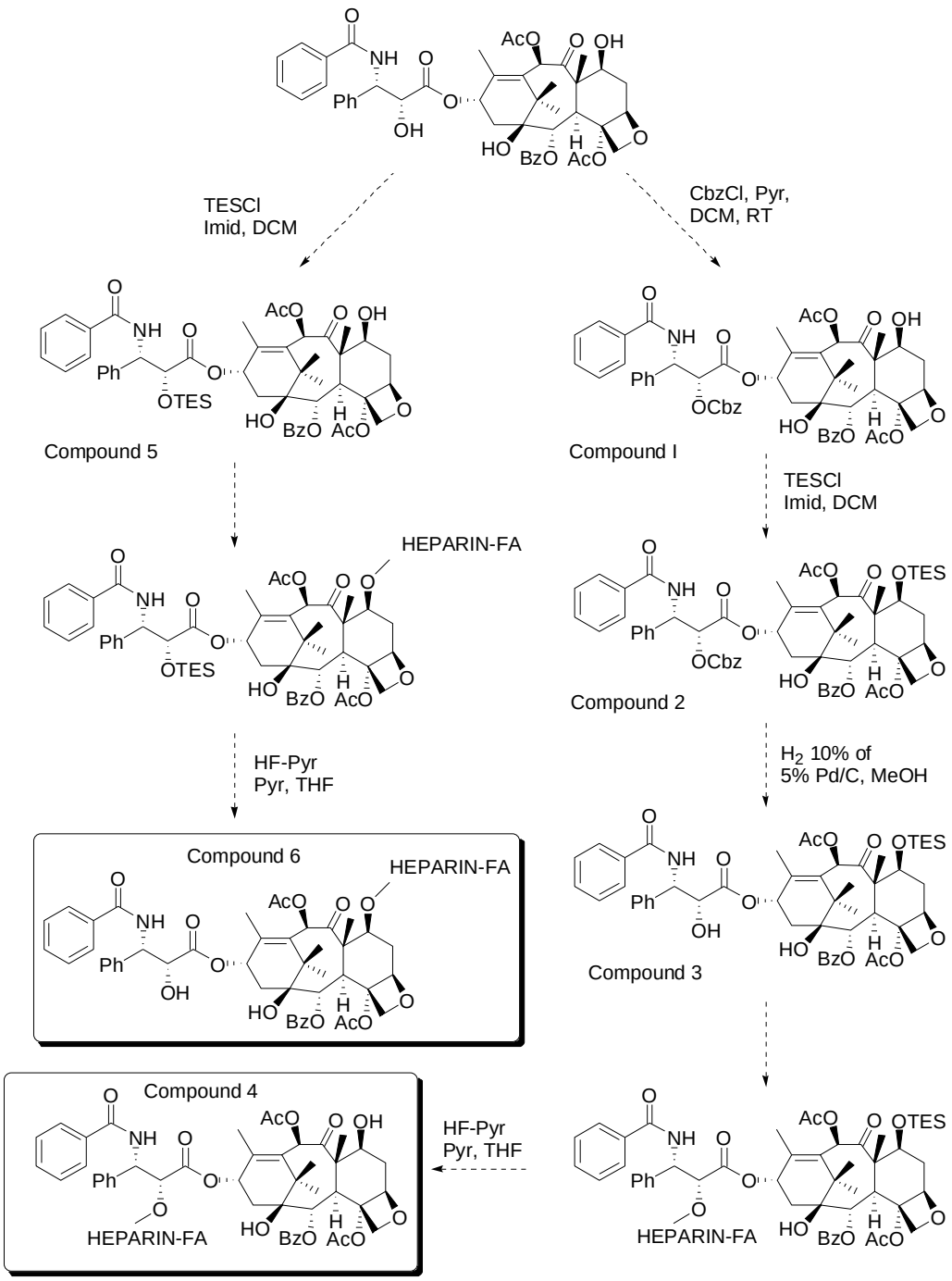

Figure 3.2: Site-specific C2' and C7 Conjugation of Paclitaxel and FA on Heparin.

Synthesis of PG-paclitaxel-FA

PG sodium salt was dissolved in water. To this solution, 0.75 M HCl was added slowly to bring the pH down to 3.3. After dialysis against water for 2 days, the white powder was collected via lyophilization. The desalted PG (1 mmol) was activated by reacting with DCC (10 mmol) and NHS (12 mmol) in formamide at 4 ˚C overnight. Aminated folate was synthesized using the procedure outlined above. Activated PG-NHS (1 mmol) and aminated folate (10 mmol) were reacted at room temperature for 24 hours. The unreacted NH_2- folate was removed by dialysis (MWCO 2000). The final product (95% yield) was obtained by lyophilization.

FA-PG conjugate (1 mmol) was dissolved in formamide. Paclitaxel (20 mmol) and DCC (20 mmol) in DMSO were added to the solution and reacted overnight at room temperature. After the reaction, recystallization and filtration were done to remove the unreacted DCC. For further purification, this product was precipitated by adding excess acetonitrile. After filtration, the yellow powder was dried in vacuum. The reaction was confirmed by TLC analysis (silica plate; eluent, 2-propanol/chloroform 10:90 vol %) and ^{1}H-NMR (400 MHz, in D_2O).

Values for *^{1}H-NMR* of PG-paclitaxel-FA (400MHz, D_2O) were: δ 1.11 [s, ^{17}CH3], 1.20 [s,^{16}CH3], 1.69 [s, $^{19}CH_3$], 1.97 [s, $^{18}CH_3$], 2.2 [m, OAc], 2.4 [m, OAc], 3.78 [d, ^{3}CH], 4.17 [d, $^{20}CH_2$], 4.27 [H-α, PG], 4.3 [d, $^{20}CH_2$], 4.39 [dd, ^{7}CH], 4.96 [d, ^{5}CH], 4.78 and 5.63 [d, $^{2'}$CH], 5.6 [COO between PG and Paclitaxel], 5.67 [d, ^{2}CH], 5.98 [dd, $^{3'}$CH], 6.22 [t, ^{13}CH], 6.27[s, ^{10}CH], δ6.64[d, 3', 5'-H of FA, ^{2}H], 7.09 [d, NH], 7.25 [s, 3'-Ph], 7.4 [m, 3'-NBz], 7.5 [m, 2-OBz], 7.73 [d, 3'-NBz], 8.1 [d, 2-OBz], δ8.1-8.45 [CONH between PG and FA].

Synthesis of PG-paclitaxel

A solution of paclitaxel (20 mmol) in DMSO was added to PG in formamide. DCC (20 mmol) in DMSO were subsequently added dropwise and stirred on ice. When addition of DCC was complete, the reaction was allowed to proceed for 6 hours at room temperature. After the reaction, filtration and dialysis against water for 48 hours followed. White powder was obtained after lyophilization.

Synthesis of Fluorescently Tagged Polymer-paclitaxel-FA Conjugates

Oregon Green® 488 labeled paclitaxel (Figure 3.3) was used in place of paclitaxel. The same procedure for synthesizing heparin-paclitaxel-FA and PG-paclitaxel-FA was used. The feeding mole ratio of polymer: labeled paclitaxel: aminated FA was 1:2:10. The conjugate was purified by centrifugation, dialysis and lyophilization.

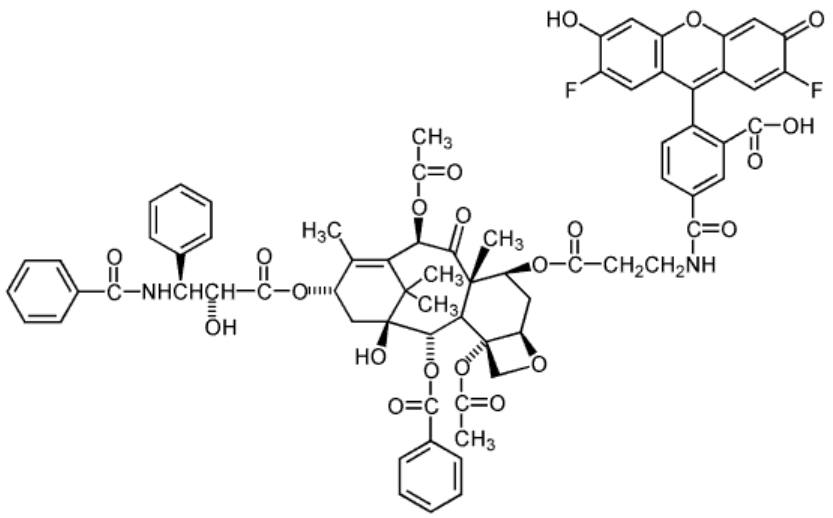

Figure 3.3: Structure of Oregon Green® 488 Labeled Paclitaxel (Flutax-2).

IR Spectroscopy

The IR spectra of heparin, paclitaxel, heparin-paclitaxel-FA, PG, PG-paclitaxel and PG-paclitaxel-FA were acquired on a Fourier transform infrared spectroscopy (FT-IR) using a Perkin Elmer system 2000 spectrometer and the samples were analyzed as KBr pellets.

Morphology and Size Distribution

Nanoparticle size and size distribution were determined by laser light scattering with particle size analyzer (90 Plus, Brookhaven Instruments). Dried nanoparticles were suspended in filtered deionized water and sonicated to prevent particle aggregation and to form uniform dispersion. Triplicate measurements were run at settings of wavelength 656 nm, viscosity 0.89 cp, and refractive index 1.33. Morphology of the formulated nanoparticles was observed by TEM (H-600, Hitachi, Japan) operating at an acceleration voltage of 80 kV. The aqueous dispersion of the particles was drop-cast onto a carbon coated copper grid and grid was air dried at room temperature before loading into the microscope. Samples for the size measurements were prepared by dispersing small amounts of the heparin-paclitaxel-FA and PG-paclitaxel-FA powder in deionized water and treating in an ultrasonic bath for 1 min.

Paclitaxel Extraction from Heparin-paclitaxel-FA

200 mg of heparin-paclitaxel-FA was dissolved in 20 mL water. Dichloromethane was added to the aqueous solution to extract the free paclitaxel from the conjugate. After workup, the extracted paclitaxel was obtained by distilling off the

dichloromethane. The amount of released paclitaxel was analyzed by UV spectroscopy and HPLC.

Values for *^{1}H-NMR* of the extracted paclitaxel (400MHz, $CDCl_3$) were: δ1.13 [s, $^{17}CH_3$], 1.25 [s,$^{16}CH_3$], 1.70 [s, $^{19}CH_3$], 1.95 [s, $^{18}CH_3$], 2.2 [m, OAc], 2.4 [m, OAc], 3.80 [d, ^{3}CH], 4.14 [d, $^{20}CH_2$], 4.22 [H-α, PG], 4.3 [d, $^{20}CH_2$], 4.41 [dd, ^{7}CH], 4.96 [d, ^{5}CH], 4.75 and 5.63 [d, $^{2'}$CH], 5.66 [d, ^{2}CH], 5.98 [dd, $^{3'}$CH], 6.20 [t, ^{13}CH], 6.25 [s, ^{10}CH], 7.12 [d, NH], 7.25 [s, 3'-Ph], 7.4 [m, 3'-NBz], 7.5 [m, 2-OBz], 7.75 [d, 3'-NBz], 8.1 [d, 2-OBz]. Melting point of the extracted paclitaxel was 211-215°C.

To facilitate the release of paclitaxel from the heparin-paclitaxel-FA conjugates in the aqueous layer, heparin was degraded by treating with NO under acidic condition. The aqueous layer was treated with a pH 4 buffer (0.12 M sodium citrate) and the resulting solution was aliquoted. Five 2 mL aliquots were pregassed with argon and bubbled for 1 minute with a slow stream of NO gas at room temperature in a fume hood. No yellow color, characteristic of NO_2 formation, was observed. Assuming that the NO gas was saturated, the concentration of NO was estimated to be approx. 2 mM (based on a solubility of 5.7 cm^3/100 mL at 20 °C). After 10 min at room temperature, the solution was neutralized with saturated $NaHCO_3$. The solution was left at room temperature overnight. Degradation of heparin by NO was confirmed by analyzing the NO treated and untreated solutions utilizing the GPC method described above. The precipitated paclitaxel from the treated group was extracted with dichloromethane and worked up. The amount of released paclitaxel was analyzed by UV spectroscopy and HPLC. Values for *^{1}H-NMR* of the extracted paclitaxel (400MHz, $CDCl_3$) were: δ1.08 [s, $^{17}CH_3$], 1.15 [s,$^{16}CH_3$], 1.65 [s, $^{19}CH_3$], 1.91 [s, $^{18}CH_3$], 2.2 [m, OAc], 2.4 [m, OAc], 3.80 [d, ^{3}CH],

4.17 [d, $^{20}CH_2$], 4.16 [H-α, PG], 4.3 [d, $^{20}CH_2$], 4.41 [dd, ^{7}CH], 4.96 [d, ^{5}CH], 4.75 and 5.63 [d, $^{2'}CH$], 5.66 [d, ^{2}CH], 5.98 [dd, $^{3'}CH$], 6.20 [t, ^{13}CH], 6.25 [s, ^{10}CH], 7.12 [d, NH], 7.21 [s, 3'-Ph], 7.4 [m, 3'-NBz], 7.5 [m, 2-OBz], 7.70 [d, 3'-NBz], 7.8 [d, 2-OBz]. Melting point of the extracted paclitaxel was 212-216°C.

UV Spectroscopy

UV spectroscopy method based on standard curve was used to determine FA and paclitaxel content. The absorption spectra were recorded on a Shimadzu UV-2401PC scanning spectrophotometer operating at a slit width of 1.0nm. Paclitaxel, FA, heparin, heparin-FA, heparin-paclitaxel-FA, PG, PG-FA and PG-paclitaxel were dispersed each in methanol. A standard curve was generated with known concentrations of paclitaxel (λ = 228 nm and 273 nm in methanol) and FA (λ = 280 nm, in methanol). The molar extinction coefficients determined from the standard curves were: 29500 $M^{-1}cm^{-1}$ (λ = 228 nm, paclitaxel in methanol), 1650 $M^{-1}cm^{-1}$ (λ = 273 nm, paclitaxel in methanol), and 27200 $M^{-1}cm^{-1}$ (λ = 280 nm, FA in methanol).

GPC Analytical Method

The HPLC-GPC system (Waters 2695 separation module) was equipped with a tandem column system, auto sampler, RI detector (Waters 410 differential refractometer), UV/Vis detector (Waters 2487 dual wavelength absorbance detector) and a data station. The UV and RI detector were linked in series, with the outlet end of the columns attached to the UV detector. Narrow-range calibrators (Choay Laboratories) of 15 oligosaccharide fractions (22500, 17300, 14800, 12900, 10100, 8650, 7540, 6150, 5360, 5000, 4000, 3410, 2440, 1880, 1300 Da) from native heparin

were used to generate a log MW versus retention time calibration curve. Each calibrator was dissolved in 0.5 M Na_2SO_4 to give a final concentration of 10 mg/mL. A 20 μL sample was injected and the system was run at a flow rate of 0.5 mL/min. All analyses were carried out at room temperature. The run time for each sample was set at 75 minutes. Each of these fractions had a narrow MW distribution with dispersities less than 1.1, making it applicable for the MW determination of heparin and its conjugates.

HPLC Analytical Method

Reversed phase analytical assay was devised to monitor paclitaxel yield and purity. The HPLC system (Waters 2695 separation module) was equipped with a C18 column (Waters Nova-Pak, 3.9mm x 50 mm, 4 μm), auto sampler, UV/Vis detector (Waters 2487 dual wavelength absorbance detector) and a data station. The eluent (methanol: 0.02 M ammonium acetate: acetonitrile = 1:5:4) was run at a flow rate of 1.0 mL/min while monitoring at 228 nm. Peak areas were quantitated and compared with standard curves to determine paclitaxel concentrations.

HPLC Monitoring of CPG-mediated Cleavage

The HPLC system (Waters 2695 separation module) was set up with a Phenomenex Prodigy C8 (4.6 mm × 50 mm) column auto sampler, UV/Vis detector (Waters 2487 dual wavelength absorbance detector) and a data station. The method was run at a flow rate of 1 mL/min while monitoring at 285 nm. For analysis of polymer-paclitaxel-FA conjugates, the system was used in isocratic mode, with methanol/10 mM sodium phosphate at pH 7.0 (92:8 v/v). The retention times of heparin-paclitaxel-FA and PG-paclitaxel-FA were 6.2 and 8.5 min, respectively. The enzymatic cleavage of pteroate from the FA moiety of the conjugates could be followed by the decrease in the

total conjugate peak area. A solution of polymer-paclitaxel-FA (0.1 mg/mL) was prepared in 150 mM Tris buffer (pH 7.3). A 10 μL aliquot of this solution was injected into the HPLC system to obtain the time zero peak integration. Enzyme carboxypeptidase G (CPG, Sigma, 1 unit) was added to the polymer-paclitaxel-FA solution. The resulting solution was incubated at 30 ˚C, and 10 μL aliquots were injected into the HPLC system at different time points. The rate of enzymatic hydrolysis was initially fast. After 3.5 hours incubation, the rate slowed down. Additional 1 unit aliquots of CPG were added to the reaction mixture at 4, 12 and 24 hour time points. Data were collected for up to 72 hours. Prolonged incubation times beyond 48 hours did not change the size of the conjugate peak once it diminished to 35% of the initial integration value, indicating that 65% of the heparin-paclitaxel-FA was γ-carboxyl-linked. The run performed with PG-paclitaxel-FA as a substrate showed that 40% of the FA residues in this conjugate were γ-carboxyl-linked.

FXa Chromogenic Assay for Heparin Activity

Bioactivity of heparin in heparin-paclitaxel-FA conjugate was determined by factor Xa (FXa) chromogenic assay. Heparin standards, and plasma samples containing heparin-paclitaxel-FA (25 μL) were mixed with 200 μL of antithrombin III solution (0.1 IU/mL), in which antithrombin III concentration was higher than heparin concentration. After incubating the solution at 37°C for 2 min, 200 μL of FXa (4 nanokatals/mL) was added. The solution was incubated an additional minute. FXa substrate (200 μL, 0.8 μmol/mL) was then added and incubated at 37°C for 5 minutes. The reaction was terminated by adding 200 μL 50% acetic acid. The absorbance of the final solution recorded at 405 nm had a linear relationship with the concentration of heparin in the

range of 0 to 0.8 IU/mL. The bioactivity of heparin-paclitaxel-FA was determined based on the standard curve.

Bioactivity of Paclitaxel

To measure paclitaxel activity, tubulin polymerization was quantified in G-PEM buffer (1 mM GTP, 80 mM PIPES, 1 mM EGTA, 0.5 mM magnesium chloride; pH 6.8) at a tubulin concentration of 1 mg/mL (10 μM) in the presence of nanoparticles (10 μM). The baseline was fixed with the solution at 4 °C. The spectrophotometer was zeroed at 340 nm with the blank at 4 °C. Paclitaxel, polymer-paclitaxel-FA conjugates, and polymer-paclitaxel conjugates were then quickly mixed into the tubulin solution to a final concentration of 10 μM and the absorbance was continually monitored over 80 minutes. These samples were placed in quartz cuvettes and incubated at 32°C and absorbance of the solution was measured at 340 nm.

Release Profile

The release profile of paclitaxel from the polymer-paclitaxel-FA conjugates was gathered at both higher and lower pH to mimic the conditions found in cellular endosomes and cytoplasm as well as in human serum to gauge the susceptibility of the ester bond.

100 μL of equimolar paclitaxel solutions (10^{-2} mM paclitaxel equivalent concentration) of heparin-paclitaxel-FA, PG-paclitaxel-FA and free paclitaxel were dispersed in PBS (pH 7.4) added to 1 mL of in PBS (pH 7.4), sodium citrate (pH 3), sodium citrate (pH 5), sodium bicarbonate (pH 8.3), and human plasma. The samples were kept at 37 °C under mild stirring. At scheduled times, 100 μL volumes were taken

and added to 50 μL of 40 μg/mL N-octylbenzamide solution in acetonitrile (internal standard). The samples were added to 1 mL of acetonitrile and centrifuged at 12,000 rpm for 3 min at 4 °C. The precipitate was washed with 0.5 mL of acetonitrile and centrifuged. The acetonitrile volumes were pooled and the organic solvent was removed under vacuum. The residue was dissolved in 200 μL of methanol: 0.02 M ammonium acetate: acetonitrile = 1:5:4 mixture and analyzed by HPLC using the method described above. The reliability and accuracy of the method has been previously verified by other groups. It allows for 98% paclitaxel recovery. Each experiment was repeated in triplicate.

Cell Culture

All cells were cultured at 37°C in a humidified atmosphere containing 5% CO_2. KB cells were cultured in 5% CO_2 in FA deficient medium RPMI 1640 with 10% fetal calf serum. A549 cells were maintained at 37°C in Ham's F12K medium with 2 mM L-glutamine adjusted to contain 1.5 g/L sodium bicarbonate with 10%. MCF-10A cells were cultured in medium MEGM (Mammary epithelial growth medium, serum-free) supplemented with cholera toxin.

FACS Analysis for Folate Receptor Expression

5 μg/mL primary antibody (anti-Folate-binding Protein MAb (Mov18/ZEL) was added to the cells (0.5×10^6) in 200 μL PBS 2 % bovine serum albumin, and the mixture was incubated for 20 min at room temperature. Fluorescein isothiocyanate (FITC)-conjugated secondary antibody (Invitrogen) was added after washing. After 20 min incubation at room temperature shielded from light, the antibody binding was

measured. The samples were analyzed with a FACScan (Becton Dickinson) using FlowJo software. The fluorescence index (FI) was calculated as the ratio between mean fluorescence intensity in the presence and absence of primary antibody.

Cytotoxicity Assay

Cells (4×10^4 cells/mL) were harvested by incubating in 0.25% trypsin-0.03% EDTA solution and seeded in a 96-well plate. MTT assay kit was used to measure cytotoxicity of polymer-paclitaxel-FA and paclitaxel on KB, A549 and MCF-10A cells by incubating at 37°C for 48 hours at different concentrations of the each compound in quadruplicate. The optical density was measured at 570 nm with 630 nm as the reference wavelength. The absorbance of each well was read in a microplate reader at 570 nm of wavelength, which was subtracted by the background absorbance measured at 690 nm. The concentration of the agent causing 50 % cell death (IC_{50}) was calculated.

Tumor-specific Uptake

Cellular uptake and intracellular distribution of fluorescently tagged polymer-paclitaxel-FA conjugates was visualized using confocal laser scanning microscopy (Zeiss LSM510, Germany) with KB cells grown on a Lab-Tek® II chamber slide (Nalge Nunc, Napevillem, IL). Oregon Green® 488-paclitaxel conjugate was used in the synthesis steps described above. The concentration of tagged polymer-paclitaxel-FA conjugates was 1 μg/mL in RPMI-1640 medium. After 1 hr incubation, the medium containing the conjugates was aspirated from the wells. The cells were then washed three times with PBS buffer (pH 7.4). Cells were then fixed with 200 μL 4 % formaldehyde in phosphate buffer saline. The samples were observed as quickly as

possible. The tissue sections or cells were scanned initially under conventional fluorescence microscope with an FITC filter. The FITC labeled areas were then scanned with the confocal microscope (excitation/emission wavelengths: 488 nm and 510 nm). The objective lens magnification is listed for each image.

Quantification of florescence uptake was done by flow cytometry. Treated cells were washed three times with PBS and treated with 0.25% trypsin-0.03% EDTA solution. Cells were resuspended in their respective medium, spun down, washed, and resuspended in cold PBS. The mean fluorescence intensity was determined by FACS analysis.

3.3 Results and Discussion

Synthesis of Heparin-paclitaxel-FA and PG-paclitaxel-FA

Following the scheme depicted in Figure 3.1, we successfully synthesized heparin-paclitaxel-FA conjugates. Once the procedure was optimized, PG-paclitaxel-FA was produced following the same coupling scheme after desalting PG-sodium salt. The conjugation was achieved by amide bonds formed by the coupling between carboxyl groups of the polymer and amine groups of aminated FA.

Folic acid has two carboxyl groups (Figure 3.4), and in order to couple only one EDA to one folic acid, care must be taken to activate only one ester group per folic acid molecule prior to coupling. Thus, complete solubilization of the folic acid is imperative prior to the addition of 1 equivalent of the coupling reagents (NHS and DCC). Folic acid has a low solubility in most organic solvents, and the only solvent in which folic acid is completely soluble is DMSO. Unfortunately, when the coupling reaction was carried out in DMSO, it was impossible to isolate the product from the reaction mixture. Thus, we

decided to separate the ester activation and the coupling step, and we first prepared and isolated the N-hydroxysuccinimide activated FA derivative, which precipitates readily from DMSO, when a mixture of acetone/ether mixture is added. The activated ester was immediately reacted with EDA. The excess of unreacted FA was easily removed by ion-exchange chromatography or gel permeation chromatography (GPC).

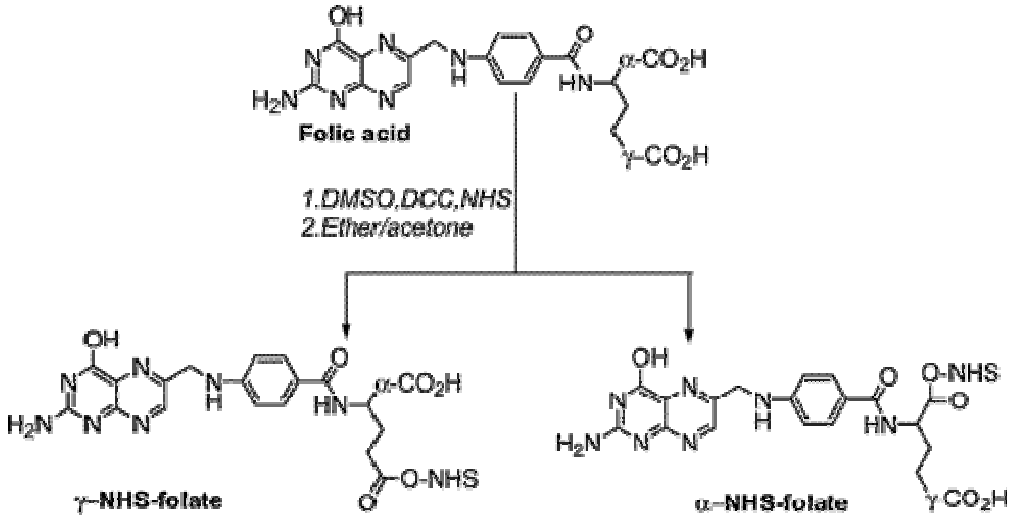

Figure 3.4: Preparation of Activated Folic Acid, FA-NHS. The reaction yields two isomers, γ-NHS-folate and α-NHS-folate. Only folate conjugates linked at the γ –carboxyl of FA retain strong binding affinity to folate receptors.

The procedure for FA amination outlined in the methods section produces a mixture of α mono-aminated FA [α FA-NH-$(CH_2)_2$-NH_2] and γ mono-aminated FA [γ, FA-NH-$(CH_2)_2$-NH_2]. The presence of peaks at δ4.27ppm in the ^{1}*H-NMR* spectrum data confirmed that primarily the γ-carboxyl group in folic acid reacted with ethylene diamine. This result agrees with other groups' findings that γ-carboxyl group is more reactive than the α-carboxyl group in folic acid. [96, 138]

Wang et al. demonstrated that only those folate conjugates containing the adduct attached at the gamma-carboxyl of folic acid retrain the ability to bind to cell surface folate receptors with the same affinity as free FA [139]. Therefore, it was important to determine the percentage of the γ-isomer in the FA-conjugates. For this purpose, we used the carboxypeptidase G HPLC assay [136] that is based on the ability of CPG to cleave the glutamic residue of FA only if its γ -carboxyl is unconjugated. In view of the fact that 35% and 40% of the heparin-paclitaxel-FA and PG-paclitaxel-FA were respectively enzymatically cleaved by CPG we assume that γ -isomer fraction for each conjugates were 65% and 60%. This was in general agreement with the yield of γ -carboxyl isolated by preparative HPLC (58%).

The presence of amide bonds coupling of FA to the polymers was confirmed by the presence of signals at δ6.75-8.77 ppm in the ^{1}H-NMR spectrum and by an absorbance at λ = 280 nm in the UV/Vis spectrum of the heparin-FA.

Paclitaxel was coupled to the polymer via DCC mediated reaction of hydroxyl groups of paclitaxel and the carboxyl groups of the polymers to form an ester linkage. The presence of the C=O of the ester group signals at 1732 cm^{-1} in the FT-IR spectrum, and an absorbance at λ= 227 nm indicated successful binding of paclitaxel to heparin-FA. In PG-paclitaxel-FA, the FT-IR confirmation came from the decrease of peak intensity at 3280-3400 cm^{-1}. In both cases, the ester linkage was confirmed by the presence of signals at δ5.6 ppm in the ^{1}H-NMR spectrum.

UV/Vis spectrum is not a definite indicator of covalent binding. The ester bonds that appear on FT-IR spectrum may be the result of the ester bond formation between the –OH and –COOH of heparin. Therefore, a control experiment to confirm if this was

the case was conducted by subjecting heparin and heparin-FA to the same synthesis reaction conditions.

Heparin consists of sulfated polysaccharide chains with broad molecular size dispersion. The MW of these chains ranges from 3 to 25 kDa. To reliably measure the MW of heparin preparations by GPC, we employed heparin-like molecules to calibrate columns [140, 141]. The method has been shown to be applicable to low-molecular weight heparins, as well as unfractionated high molecular weight heparins. The results (Table 3.1) indicate some crosslinking does occur amongst heparins when its carboxyl groups are subjected to DCC activation. The lower polydispersity and less than expected MW increase in DCC-treated heparin-FA and heparin-paclitaxel-FA conjugates may be due to the polydispersity and microheterogenicity of the unmodified heparin, and the fact that less carboxyl groups are available to undergo intermolecular heparin esterification once the functional groups engage in formation of an amide bond to anchor FA to heparin.

Table 3.1: GPC Analyses of Heparin and Heparin Conjugates

Sample	Molecular Weight (kDa)		Dispersity
	Number Average	Weight Average	
Heparin (starting material)	10.9	14.5	1.33
Heparin-FA	13.5	17.3	1.28
Heparin (DCC-treated)	15.1	22.9	1.52
Heparin-FA (DCC-treated)	18.0	23.4	1.30
Heparin-paclitaxel-FA	24.3	32.6	1.34

Both C2' proton and C7 proton overlapped with the peaks of heparin. Paclitaxel possess three hydroxyl groups, namely, C1, C2' and C7, which differ from each other in their reactivities towards moieties possessing acid functional groups (Figure 2.2). The C2'-OH group of paclitaxel is more chemically reactive relative to tertiary C1-OH and more hindered secondary C7-OH group [142]. Although we confirmed with FT-IR spectroscopy the presence of ester bond in the final product FT-IR spectroscopy, the specific site of esterification on paclitaxel molecule remained unidentified. Cavallaro et al. found that succinylation of taxol takes place preferentially at the position 2'-OH position under mild conditions. [143, 144] Li et al. reported esterification of PG and paclitaxel occurs on both C2' and C7 positions [96]. Both C2' and C7 ester prodrugs of paclitaxel have been reported to retain their cytotoxic activity on cell lines [143, 145].

Since the C2′ hydroxyl group is more important than the C7 hydroxyl group as determined by structure activity relationship (SAR) studies [84-86], we expected that conjugation at the C2′ position would render the conjugate inactive whereas conjugation at the C7 site allows the conjugate to retain at least part of its activity. To test this, site-specific conjugation on C2' and C7 positions to heparin was carried out according to the scheme in Figure 3.2. In cytotoxicity tests, however, the C2' and C7 conjugates did not show statistically significant difference. It is known that hydrolysis of ester-linked polymeric prodrugs is sensitive to the electron withdrawing and donating substituents close to the reaction center [146] as well as the hydration of the polymeric drug. Since the physical environment is similar, the rate of hydrolysis of both C2' and C7 heparin-paclitaxel-FA conjugates may be in fact comparable, leading to similar cytotoxicity.

Using the molar extinction coefficients 29500 $M^{-1}cm^{-1}$ (λ = 228 nm, paclitaxel in methanol), 1650 $M^{-1}cm^{-1}$ (λ = 273 nm, paclitaxel in methanol), and 27200 $M^{-1}cm^{-1}$ (λ = 280 nm, FA in methanol), it was determined by UV spectroscopy that the paclitaxel loading of heparin-paclitaxel-FA was 22 % wt (molar feeding ratio 1:15:10) and PG-paclitaxel-FA 25 % wt (molar feeding ratio 1:20:20). Since heparin crosslinking does occur, leading to a reduced number of available carboxyl groups that paclitaxel can bind to, the question of how to account for the paclitaxel content was raised. In other words, how is paclitaxel incorporated in the heparin-paclitaxel-FA nanostructure, i.e., is it via covalent binding to heparin and/or entrapment in the hydrophobic core?

Titration had been attempted first. However, the approach and the results were dismissed because of the high dependency on the chemical environment surrounding a weak acid that rendered the outcome inconclusive. Instead, we extracted the entrapped paclitaxel using dichloromethane from heparin-paclitaxel-FA. The heparin-paclitaxel-FA remaining in the aqueous phase was subjected to NO gas treatment under pH 4 to degrade the heparin[147]. GPC analysis of both heparin and heparin-paclitaxel-FA marked a nearly complete loss of main heparin peak and appearance of smaller peaks, confirming heparin degradation. The pH 4 was chosen to prevent degradation of paclitaxel, which is most stable at pH 3-5[148]. Exposure to NO gas does not adversely affect paclitaxel[149]. The liberated paclitaxel was then recovered by extraction with dichloromethane. The distinctly different melting points of DCC (34-35°C), NHS (95-98°C), paclitaxel (213-216°C) and DCU (232-233°C) were taken advantage of to ascertain the purity of the isolated paclitaxel. Heparin and folic acid do not have a distinct melting point and undergo gradual decomposition above 250°C. In this manner,

it was determined that 40 % of the total loaded paclitaxel was entrapped in its free form in the hydrophobic core of the self-assembled nanostructure. As described by Kataoka and his coworkers [150] in their work with doxorubicin, the covalently bound paclitaxel increases the hydrophobicity of the inner core of the self-assembled nanostructure to facilitate incorporation of the free paclitaxel.

Water solubility of the conjugates was 50 mg/mL for heparin-paclitaxel-FA and 78 mg/mL for PG-paclitaxel-FA. The markedly increased water solubility compared with free paclitaxel allow the ternary conjugates be administrated via vehicles that do not have harmful side effects.

Morphology and Size

In aqueous solution, heparin-paclitaxel-FA spontaneously assembled into nanostructures with a diameter 102±2 nm, PG-paclitaxel-FA had a larger diameter, 285±10 nm as determined by dynamic light scattering (DLS) (Figure 3.5).

TEM images (Figure 3.6) revealed that above the critical micelle concentration (CMC) of 43.9 μg/mL, the amphiphilic ternary conjugates of heparin-paclitaxel-FA self-assemble into nanoparticles. PG-paclitaxel-FA showed a decreased diameter size of 200 nm under the TEM microscope (not shown), which may be attributed to the larger hydrodynamic volume of the PG polymer that has a larger molecular weight and better solubility in water than heparin.

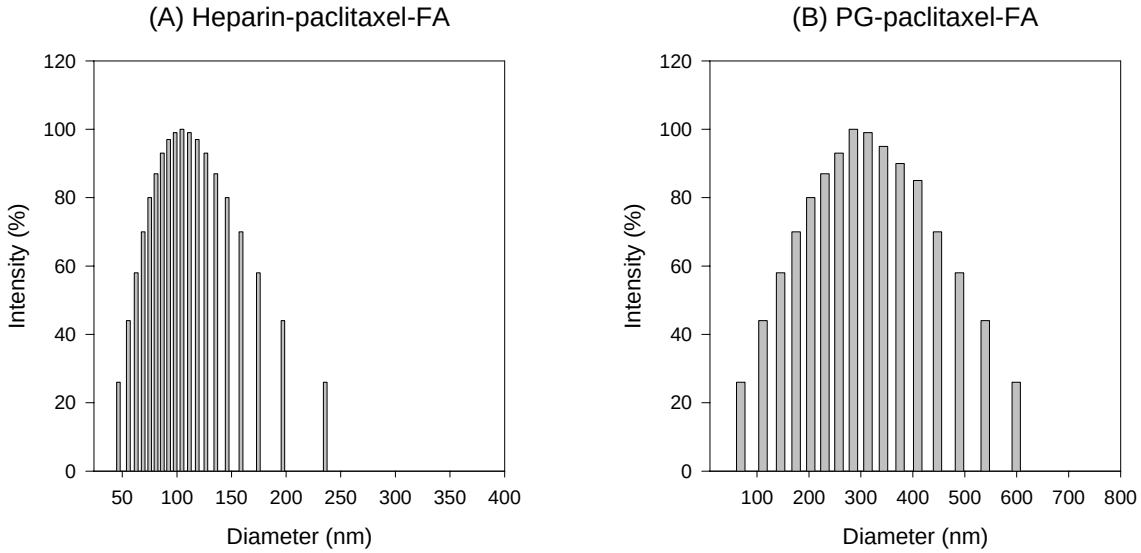

Figure 3.5: Size Distribution of the Ternary Conjugates. DLS measurement shows that the mean diameter of heparin-paclitaxel-FA nanoparticles is 102 nm and that of PG-paclitaxel-FA is 285 nm. The nanoparticles have the optimal size for targeting via the EPR effect.

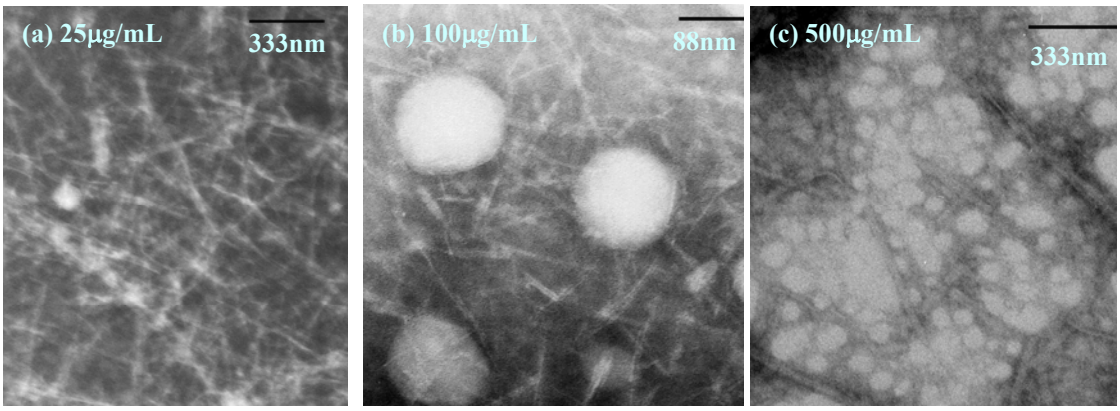

Figure 3.6: TEM Micrograph of Heparin-paclitaxel-FA Conjugates. Above the critical micelle concentration (CMC) of 43.9 μg/mL, the amphiphilic structure spontaneously self-assembles into nanoparticles.

Bioactivity of the Ternary Nanostructures

Anti-coagulant Activity of Heparin

Chromogenic assay results indicate that modifying the carboxyl group of heparin diminishes its affinity to factor Xa by more than 60% (Figure 3.7). This agrees with previous findings by Lee et al [151].

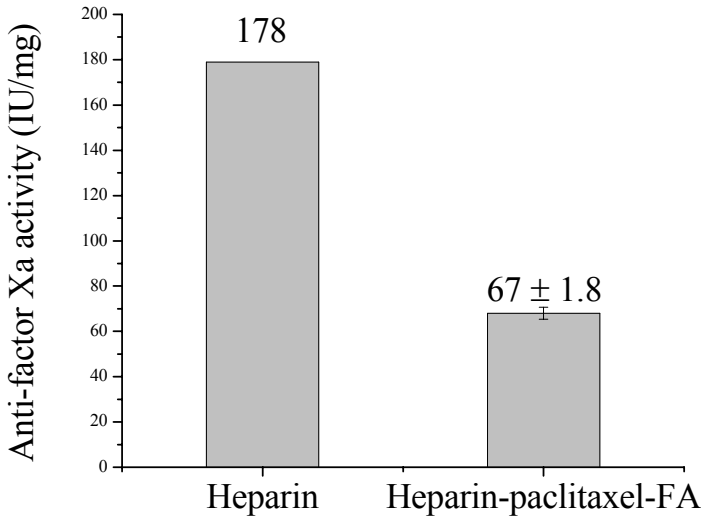

Figure 3.7: Anti-coagulation Factor Xa Activity of Heparin and Paclitaxel-heparin-FA. The bioactivities of heparin and paclitaxel-heparin-FA conjugate were measured by factor Xa chromogenic assay. Our data showed that the relative bioactivity of paclitaxel-heparin-FA was reduced to 38% of the unmodified heparin, suggesting that the conjugated heparin may pose a lower risk of bleeding than the unconjugated heparin when administered *in vivo*.

The reduced anticoagulant activity is advantageous because: 1) By bypassing the coagulation cascade, more heparin-paclitaxel-FA conjugates gain access to the tumor site; 2) conjugation to anticancer drug and FA reduces the negative charges of heparin, decreasing side effects such as heparin induced thrombocytopenia or bleeding that arise from the charge and molecular size of heparin; and 3) through the intact sulfate group, the conjugated heparin retains its ability to bind with angiogenic factors and its anti-

heparanase activity. Lapierre et al. [152] reported when both carboxyl groups and sulfate groups of heparin are altered, heparin completely loses its heparanase-inhibitory activity

Bioactivity of Paclitaxel

Paclitaxel binds to microtubules and inhibits their depolymerization into tubulin. Addition of paclitaxel to a solution of tubulin in an assembly buffer caused a clear increase in absorbance due to the increase in light scattering that resulted from the polymerization of tubulin into microtubules (Figure 3.8). The ability of paclitaxel to induce microtubule assembly dramatically decreased after esterification of the hydroxyl group of paclitaxel. Since the hydroxyl group at C2' of paclitaxel is vital for its efficacy, this is an indirect indication that indeed most of the ester linkages formed at the generally more reactive C2' position.

Increased incubation time triggered the release of paclitaxel in its active form. The elevation is gradual, pointing to a controlled release as the ester bonds are cleaved from the conjugate.

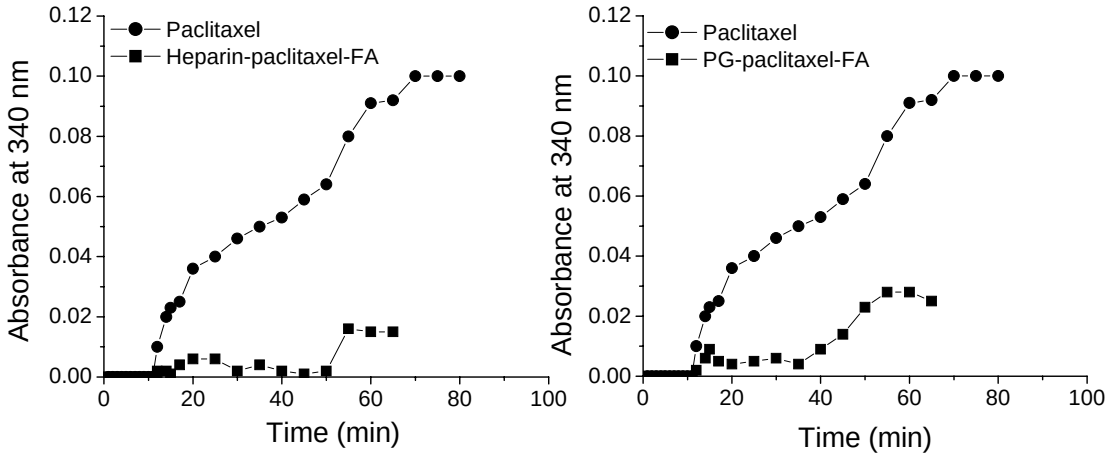

Figure 3.8: Bioactivity of Paclitaxel in the Conjugates. Heparin-paclitaxel-FA and PG-paclitaxel-FA show a substantial decrease in the ability to induce tubulin polymerization. Over time, paclitaxel is released from the conjugates and show bioactivity.

Release Profile and Stability

In our conjugates, amide bonds were used to couple of FA to the polymers. The kinetics and mechanism of nonenzymatic hydrolysis of amides have been thoroughly studied [153]. Amide bonds are very resistant to aqueous hydrolysis at physiological pH and to enzymatic to enzymatic hydrolysis by esterases.

Paclitaxel degradation profiles at pH 3, 5, 7.4, 8.3 and human plasma are depicted in Figure 3.9. This confirms that paclitaxel undergoes pH-dependent degradation as reported in the literature [148]. Dordunoo et al. published a U-shaped pH-dependent hydrolysis profile of paclitaxel which showed that the drug has maximum stability in the pH range of 3-5 [148]. Kearns et al. have conducted a detailed study on the hydrolytic products of paclitaxel [154]. Similar degradation profiles at pH 7.4 and human plasma suggest that paclitaxel degradation occurs via non-enzymatic mechanisms that would involve neutral or ionic species of paclitaxel catalyzed by H^+, H_2O or OH^-.

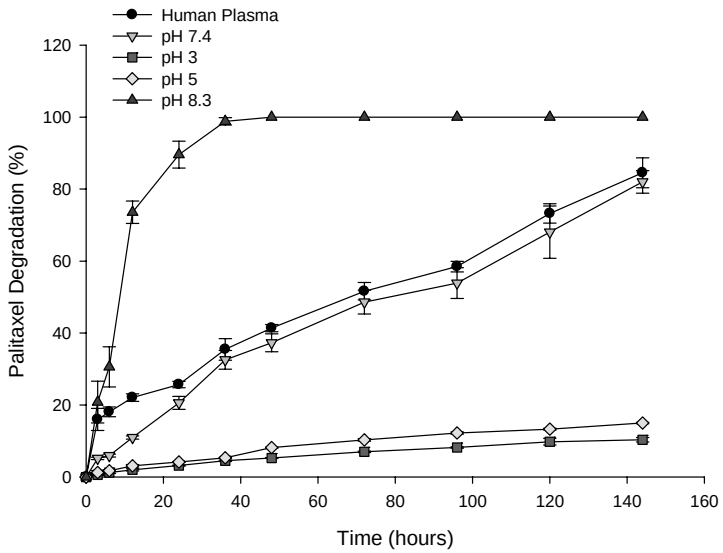

Figure 3.9: Degradation Profile of Paclitaxel. Paclitaxel degradation profiles at pH 3, 5, 7.4, 8.3 and human plasma were monitored. In agreement with previous studies, the drug is stable at pH 3-5. Similarity of profiles in pH 7.4 and human plasma suggest non-enzymatic degradation.

Release profile from the polymer-paclitaxel-FA conjugates are shown in Figure 3.10. Four of the five different conditions that were used in monitoring paclitaxel degradation were used in this study. The pH range was deliberately chosen to mimic the environment the conjugates would be subjected to *in vitro* and *in vivo*. We wanted to determine whether the ester linkage between the polymer and the drug would be prematurely cleaved by esterases in the plasma while being systemically transported to the tumor site through the blood stream.

The fast release of paclitaxel from the ternary conjugates can be attributed to a possible biphasic release. 40% of the loaded paclitaxel in heparin-paclitaxel-FA is entrapped and not covalently bound. The entrapped free paclitaxel is released first by diffusion and dissolution of crosslinked heparin, followed by the covalently bound paclitaxel as the ester bond undergoes hydrolysis.

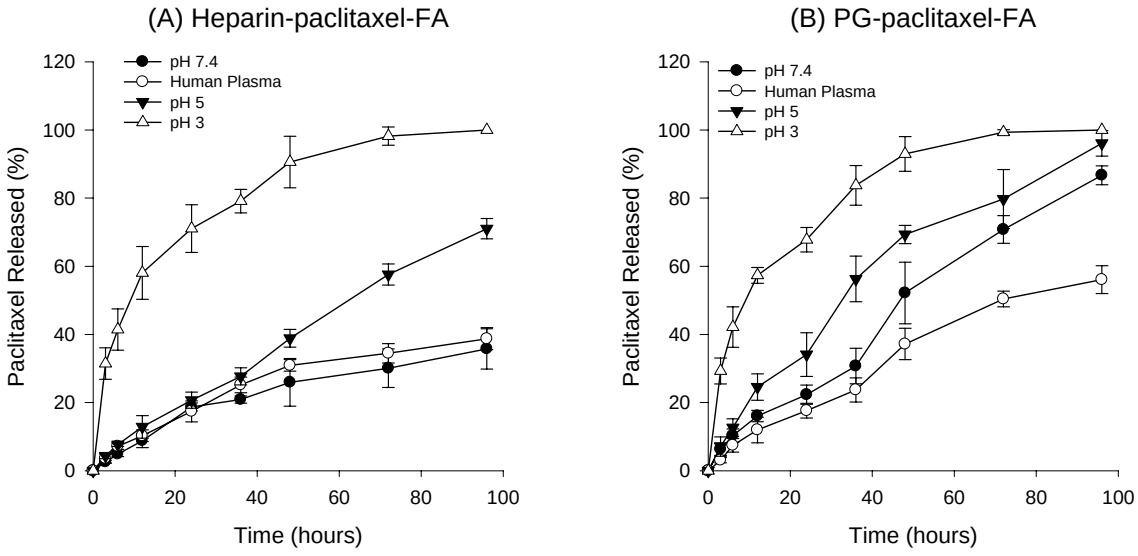

Figure 3.10: Release Profiles of Heparin-paclitaxel-FA and PG-paclitaxel-FA. Paclitaxel release at pH 3, 5, 7.4 and human plasma from the conjugates were monitored. Data was analyzed using HPLC.

Both conjugates underwent fastest paclitaxel release at pH 3 (nearly 60% within the first 12 hours) and showed pH-dependent hydrolysis. PG-paclitaxel-FA seemed more susceptible to the pH change and sensitive to the presence of enzymes in human plasma. The strong pH dependence of PG hydrolysis is widely known. The pH-dependent hydrolysis of PG is not limited to cathepsin B, but also observed with other enzymes, such as chymotrypsin, elastase, ficin and subtilisin. There is a plausible explanation for the release mechanism of paclitaxel from its ester linkage from PG-paclitaxel once it enters the cell (Figure 3.11). The proposed two-step, proteolytic/autoesterolytic pathway for endosomal degradation of PG-paclitaxel first involves cleavage of PG backbone amide linkages by an endosomal protease(s) of restricted specificity. An autocatalytic ester cleavage in the paclitaxel/glutamic acid heterodimer follows, liberating paclitaxel [155].

Negatively charged molecules are poor substrates for carboxylate esterases, which explains why heparin-palictaxel-FA undergoes less then 35% degradation in human plasma. As depicted in Figure 3.10, paclitaxel is most stable at pH 3-5 and degrades faster at pH 7.4. The fact that heparin-paclitaxel-FA releases the drug quickly at the endosomic pH while remaining relatively stable at physiological pH attests to its potential enhanced effectiveness *in vitro* and *in vivo* with less side effects.

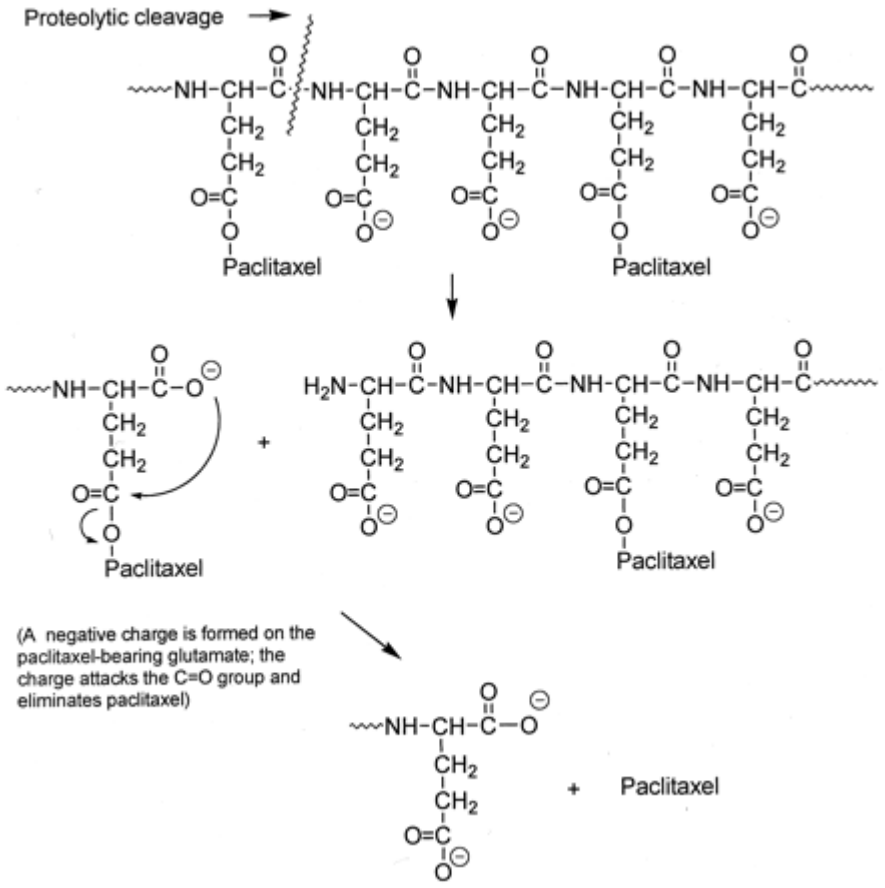

Figure 3.11: Release Mechanism of Paclitaxel from PG-paclitaxel. The proposed two-step mechanism involves both enzymatic degradation of the backbone by proteases and non-enzymatic degradation through autocatalysis (Adapted from [155]).

Tumor-specific Cytotoxcity and Uptake

To verify the enhanced selectivity through active targeting, we first confirmed the folate receptor (FR) expression of KB (human nasopharyngeal epidermoid carcinoma cells) cell line which overexpresses folate receptor, MCF-10A (normal human mammary epithelial cells) that have a small number of folate receptors, and A549 (human lung carcinoma cells) cell lines that lack detectable folate receptor expression [156].

MTT assay showed that heparin or PG by themselves were not cytotoxic (data not shown). Normal breast cells (MCF10A) with minimal folate receptor expression were not greatly affected by the treatment with heparin-paclitaxel-FA conjugates, while showing marked susceptibility to equivalent concentrations of paclitaxel and FA (Figure 3.12 (A). The significantly low viability of KB cells treated with heparin-paclitaxel-FA indicated specific uptake via folate receptor mediated endocytosis (Figure 3.12 (B).

Visual confirmation was set up with confocal microscopy using fluorescently tagged heparin-paclitaxel-FA conjugates (Figure 3.13). Oregon Green 488–paclitaxel conjugate was used to synthesize heparin-paclitaxel-FA conjugates. Clearly, tagged heparin-paclitaxel-FA conjugates selectively accumulate in KB cells, whereas heparin-paclitaxel conjugates that do not have the built-in targeting component do not specifically associate with KB cells both in the presence and absence of FA that compete against the conjugates for available folate receptors. The diminished uptake in the presence of FA is indicative of FR-mediated pathway. In folate receptor-deficient A549 cells, no uptake of heparin-paclitaxel-FA conjugates was observed. FACS analysis were in agreement with the micrograph. Uptake of heparin-paclitaxel-FA conjugates by KB cells was ~60 times greater than that of heparin-paclitaxel.

(A) MCF10A

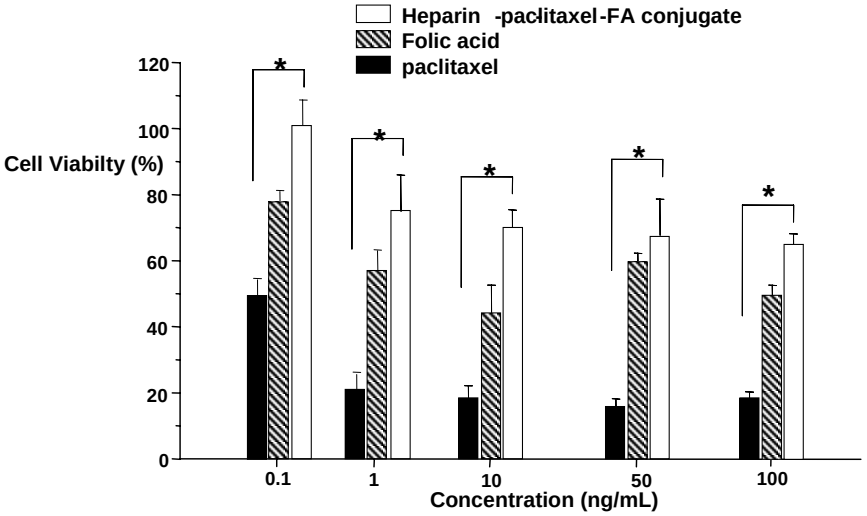

(B) KB

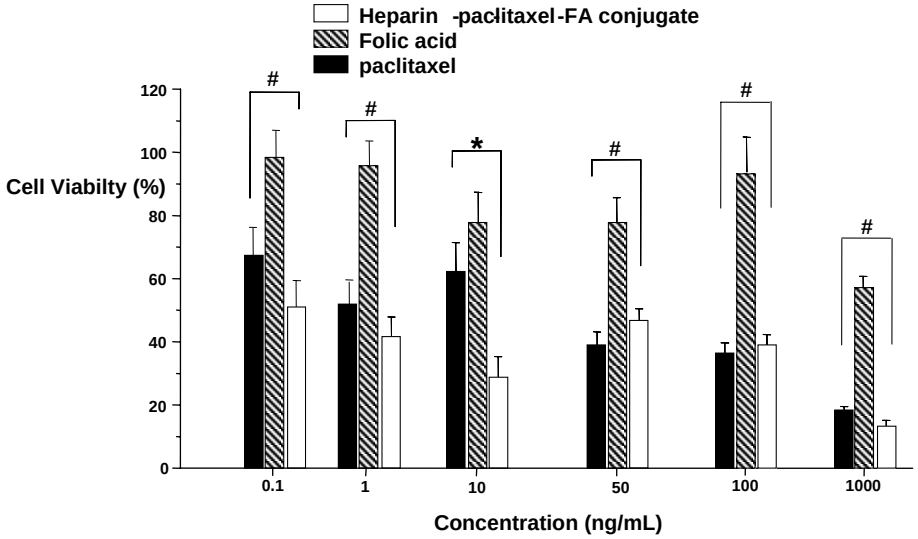

Figure 3.12: Selective Cytotoxicity of Heparin-Paclitaxel-FA in Tumor Cells. (A) MCF-10A cells and (B) KB cells after 48 hours treatment with paclitaxel, FA and heparin-paclitaxel-FA after (n=4). * and # represent $p < 0.001$ and $p < 0.01$, respectively. The selective toxicity indicates the conjugates are preferably taken up by tumor cells overpressing the folate receptor.

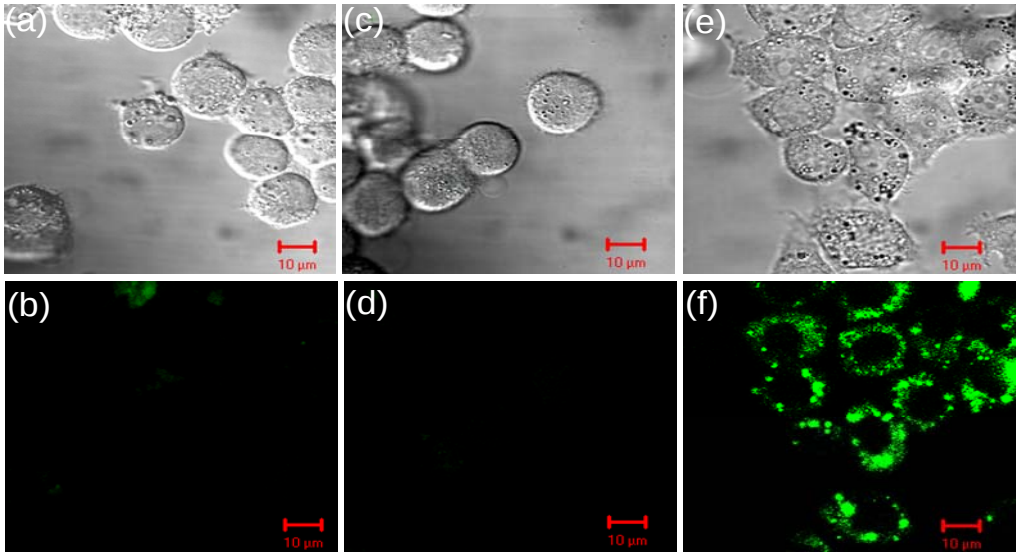

Figure 3.13: Cell Surface Distribution of the Heparin-paclitaxel-FA Conjugates. KB cells treated with heparin-paclitaxel conjugates (a) and (b), heparin-paclitaxel mixed physically with FA (1µg/mL) (c) and (d), and heparin-paclitaxel-FA conjugates (e) and (f). After 60 min incubation at 4˚C to prevent endocytosis, the cells were observed under the microscope as optical (top row) and confocal (bottom row) images. The fluorescence signal was observed in only heparin-paclitaxel-FA treated cells. Paclitaxel used for this experiment was tagged with Oregon Green 488.

Normal breast cell viability was virtually unaffected by PG-paclitaxel-FA in contrast to paclitaxel alone. In KB cells, PG-paclitaxel-FA seemed to be more potent than paclitaxel alone, but the difference was not statistically significant. This stands within reason since in the cell culture monolayer in vitro system, the rate of diffusion may be faster than the rate of endocytosis, resulting in a similar or even lower IC_{50} of paclitaxel than the conjugates. Less cytotoxicity *in vitro* may not translate to the loss in anti-tumor efficacy *in vivo.*

The capability of remaining stable in the systemic circulation, as well as the sensitivity of the conjugates to folate receptors suggest that the polymer-paclitaxel-FA conjugates can actively target the tumor tissue and potentially have localized drug release. We predict that these qualities will improve both the circulation half life of the conjugate and the percentage dose accumulated in the tumor tissue. While these effects can bring about improvement in anti-tumor efficacy *in vivo* but cannot be measured in cell culture assays, further investigation in animal models is warranted.

CHAPTER 4

IN VIVO EFFICACY OF POLYMER-PACLITAXEL-FA TERNARY NANOSTRUCTURES: TUMOR AND VACULATURE TARGETING

4.1 Introduction

We have developed and characterized ternary nanostructures of polymer-paclitaxel-FA that are stable under physiological conditions, specifically target folate-receptor positive tumor cells, and are capable of releasing bioactive paclitaxel hydrolysis of the ester linkage.

Although *in vitro* models provide convenient settings for experimentation, with well defined and controllable variables, they lack the complexity of the actual disease environment. Furthermore, we intended our design to favorably alter the pharmacokinetics and biodistribution of the chemotherapeutics. These potential benefits can only be observed in an *in vivo* model, in which tissues are interconnected and mechanisms are in place for drug clearance and metabolism. Experienced investigators in the field have emphasized that *in vivo* but not *in vitro* results are useful as basic indicators of any clinical potential. For example, as briefly mentioned in chapter 2, Abraxane™ is the first and only FDA-approved nanotherapeutic binary drug. *In vitro* studies of Abraxane™ did not show an advantage in tumor cell inhibition than its nonconjugated counterpart. However, the drug showed significantly improved efficacy

in vivo and in clinical trials as compared with free paclitaxel, underlining *in vivo* examination of nanotherapeutic drugs may provide more accurate evaluation for their potential efficacies.

The goals of our *in vivo* studies were: 1) To assess the anti-tumor and anti-angiogenic efficacy of the polymer-paclitaxel-FA ternary nanostructures and compare the results to paclitaxel administered using the standard Bristol-Myer Squibb method (cremophor EL: ethanol = 50:50 v/v, followed by further dilution with saline) and the binary drug Abraxane™ and 2) to evaluate systemic toxicity and potential side effects in normal tissues. To accomplish these purposes, we performed experiments in human tumor xenograft mouse models.

4.2 Materials and Methods

Materials

Paclitaxel was purchased from Polymed Therapeutics, Inc. (Houston, TX). Abraxane™ was bought from Abraxis Oncology (Los Angeles, CA). Heparin-paclitaxel-FA, heparin-paclitaxel, PG-paclitaxel-FA and PG-paclitaxel were synthesized and purified as described in chapter 3. human tumor cell line KB (human nasopharyngeal epidermoid carcinoma) were grown from seed vials purchased from American Type Culture Collection (Manassas, VA) grown and maintained in folate-free medium obtained from Invitrogen (Carlsbad, CA), as described in chapter 3. The cells were tested negative for murine pathogens and mycoplasma prior to being used in the animal studies.

Animal Models

Crl:NU/NU-*nu*BR female nude mice aged 4-6 weeks (about 20-25 g body weight) were obtained from Charles River Laboratory (Wilmington, MA). The mice were maintainted on a folate-free chow purchased from Dyets Inc (Bethlehem, PA). Animal studies were conducted in accordance with an approved protocol by the Institutional Animal Care and Use Committee (IACUC) at Emory University. $1\sim2 \times 10^6$ KB cells were suspended in 100 μL PBS and injected subcutaneously at the mid-dorsal level to induce tumors.

Three rounds of *in vivo* experiments were conducted. All mice received weekly intravenous (i.v.) injections via the tail vein after the tumor reached the desired volume. Tumors appeared in about 10–14 days. The mice were randomly divided into groups. Tumor volume was determined by measuring three orthogonal tumor diameters and applying the following formula[157]: Volume (mm^3) = $\pi/6 \times$ larger diameter (mm) × [smaller diameter(mm)] ^{2}. Mice were sacrificed when they became moribund due to the tumor or when they sustained over 20% weight loss. To check systemic toxicity, the body weight of the mice was monitored. Upon conclusion of the experiment, all mice were sacrificed and the tissues were collected.

Anti-Tumor Efficacy of PG-paclitaxel-FA and Heparin-paclitaxel-FA

Treatment was initiated after the tumor was allowed to grow to about 100 mm^3. Mice were divided into six experimental groups with six mice in each group. Each group was intravenously injected with saline as control, paclitaxel (80 mg/kg), PG-paclitaxel-FA (80 mg/kg paclitaxel equivalent) and PG-paclitaxel (80 mg/kg paclitaxel equivalent) with FA (20 mg/kg), heparin-paclitaxel-FA (80 mg/kg) and heparin-

paclitaxel (80 mg/kg paclitaxel equivalent) with FA (20 mg/kg). The experiment was terminated on day 30, after four weekly injections.

Comparison of Ternary and Binary Nanostructures

Mice bearing tumors of 100 mm^3 volume were divided into nine experimental groups with six mice in each group. Each group was intravenously injected weekly with i.v. injections of saline, paclitaxel (80 mg/kg), three different dosages of heparin-paclitaxel-FA (40, 80, 120 mg/kg paclitaxel equivalent), heparin, heparin-paclitaxel (80 mg/kg paclitaxel equivalent), heparin-paclitaxel (80 mg/kg paclitaxel equivalent) with 20 mg/ kg FA, and Abraxane™ (80 mg/kg paclitaxel equivalent) respectively. Survival data were presented in a Kaplan–Meier plot.

Dosage Response to Heparin-paclitaxel-FA

Mice bearing tumors of 300 mm^3 volume were divided into four experimental groups with four mice in each group. Each group was intravenously injected with saline and three different dosages of heparin-paclitaxel-FA (40, 80, 120 mg/kg paclitaxel equivalent). The experiment was terminated on day 30, after four weekly injections.

Histology and Immunohistochemistry

H&E

Excised tumors were embedded in Optimal Cutting Temperature (OCT) compound (Miles, Elkhart, IN) and snap-frozen in liquid nitrogen. Tissue sections of 5 μm were prepared on glass slides. For H&E staining, the sections were rehydrated through a series of graded ethanol (100%, 90% and 70%) and water before staining with hematoxylin and eosin.

Ki-67

To quantify cell proliferation, Ki-67 expression was measured. Snap-frozen tumors were sectioned and processed with mouse anti-human Ki-67 (Clone MIB-1, DakoCytomation, Cat# M7240). Horse Anti-Mouse IgG was used as the secondary antibody. The sections were than incubated with HRP-Streptavidin, washed, and incubated in DAB peroxidase substrate solution. Counterstaining was done with hematoxylin.

α-tubulin

To visualize the effect of and paclitaxel and paclitaxel released from the conjugates, pieces of tumor from each animal were fixed in PHEMO buffer containing 3.7% formaldehyde, 0.05% glutaraldehyde, 0.5% Triton X-100 for 1–2 hr at room temperature. Following fixation, tumor pieces were stored in 4% paraformaldehyde in 0.1% sodium cacodylate at 4°C for up to a month before further processing. Fixed tumor sections were embedded in low-melting agarose (Sigma) and 50 μm sections were obtained by vibratome sectioning at low speed (Vibratome Series 1000 Sectioning System). Sections were then processed for immunofluorescence with rat anti-α-tubulin antibodies (Chemicon MAB1864). Alexa Fluor 568 goat anti-rat antibody (Molecular Probes A11077) was used as the secondary antibody. Sytox Green (Invitrogen) was used for DNA counterstaining.

PECAM-1

To quantify the anti-angiogenic effect of the treatments, snap-frozen tumors embedded in O.C.T. were sectioned and stained for endothelial specific marker CD31 (PECAM-1) using rat anti-mouse PECAM-1(Santa Cruz Biotechnology Inc., Santa

Cruz, CA) followed by FITC X (RRX)-labeled goat anti-rat IgG (Jackson ImmunoResearch Laboratories Inc, West Grove, PA). The nuclei were counterstained with Hoechst 33258 (Sigma) to identify areas of cell invasion. The green colored PECAM-1 positive areas were measured and normalized by the total cellular area determined by blue nuclear counterstaining.

Fluorescent Angiography

Mice were sacrificed and perfused with 10 mL heparinized saline (10 IU/mL) injected through the left ventricle. To identify capillaries with the capacity to be perfused through the circulatory system, we infused 0.1 μm Fluospheres (Molecular Probes) diluted 20-fold in heparinized saline. The tumor in-growth subcutaneous muscle group was dissected and tissue was examined as a whole mount specimen.

Statistical Analysis

Differences in mean tumor shrinkage between the treatment cohorts were assessed using the Student t-test and Mann-Whitney test for comparison of two treatments, and F-test and Kruskal-Wallis test in a one-way analysis of variance (ANOVA) for comparison of multiple treatments. Since multiple hypotheses were tested, differences were considered significant if the corresponding p-value is less than 0.01. Statistical power was estimated by testing differences in the mean tumor shrinkage between two treatment groups. Based on prior experience, the standard deviation of tumor shrinkage varies from 50% to 80% of the mean value. To protect against a type 1 error differences are considered significant if p is less than 0.01.

4.3 Results and Discussion

Animal Study Design

To ascertain the anti-tumor effect of the ternary nanostructures *in vivo*, we used subcutaneous tumor models in Crl:NU/NU-*nu*BR female nude mice. These types of rodent models are most common in literature and can be readily set up.

Since it was determined in the cell studies that free folic acid can compete with the conjugates for the folate receptors (chapter 2), it was important to construct the model so the interference would be minimal. It has been shown that nutritional folate status influences the efficacy and toxicity of chemotherapeutic agents [158]. The physiologic range of human folate plasma is about 20 nM that of mice is 160 nM. As reported by other researchers, in mice, the change in diet makes significant difference in the plasma folate level [137, 159, 160]. To ensure the results of this study be relevant to humans with respect to serum folate level, KB cells were cultured in a folate-free medium and the mice were kept on a folate-free diet.

Normal human dosage of paclitaxel is 135~175 mg/m^2 [161]and that of Abraxane is 260 mg/m^2 [162]. Conversion from mg/m^2 to mg/kg is based on the empirical correlation [163]

$$surface\_area\_(m^2) = \frac{K \times W^{2/3}}{100}$$

K is a species-specific factor and W is body weight in kilograms. K value of 9 is used for rats and mice and 10.6 for a 70-kg human. Therefore, a paclitaxel dose of 150 mg/m2 for human is equivalent to 975 μg for a 20g mouse and 260 mg for a 70-kg

human. Calculation of paclitaxel equivalent of polymer-paclitaxel-FA and polymer-paclitaxel was based on the paclitaxel content determined by HPLC analysis (chapter 2).

Treatment began after the tumor volume had reached at least $100mm^3$. This experimental protocol is intended to mimic the clinical situation when treatment begins after a tumor has already been established in a patient. Since all the polymer-paclitaxel and polymer-paclitaxel-FA conjugates we synthesized had greatly enhanced water solubility, the conjugates were suspended in 200 μL saline for administration. For paclitaxel, standard Cremophor EL-ethanol formula was used. The anti-tumor and anti-angiogenic efficacy was measured by monitoring the tumor volume after treatment, and by histological and immunochemical means.

Anti-tumor Efficacy of Ternary Nanostructures

All the polymer conjugates, binary (PG-paclitaxel and heparin-paclitaxel) and ternary (PG-paclitaxel-FA and heparin-paclitaxel-FA) nanostructures were better tumor inhibitors than paclitaxel alone. This was the case even though the available paclitaxel at the tumor site is presumably less because uptake of binary polymer-paclitaxel conjugates is limited compared with their ternary counterparts as they compete with FA for available FR receptors. The polymers are allowing the binary conjugates to remain longer in the circulation and protecting paclitaxel from degradation in the physiologic environment. The fact that added FA diminishes their anti-tumor effect delineates that active targeting via FR is indeed how the ternary nanostructures are taken up by the tumor cell.

The groups treated with heparin-paclitaxel-FA conjugates showed superior potency in tumor suppression. After four injections, tumor size in this group had

reduced from 100 mm^3 to 60 mm^3. The inhibition of tumor growth statistically significant ($p < 0.001$) compared to the control group (Figure 4.1 (C).

The body weight of mice was used as an indicator of systemic toxicity. No weight loss resulted from the treatment with PG-paclitaxel-FA and heparin-paclitaxel-FA conjugates (Figure 4.1 (B) and (D) with mice attaining healthy growth towards the end of the 30 day study. Groups treated with free paclitaxel sustained drastic weight loss. Clear identifiable sources of toxicity may be the standard Bistol-Myer Squibb formulation of used to administer paclitaxel which consisted of Cremophor EL and ethanol, which is known to cause severe side effects [80].

As discussed previously in chapter 2, the anticoagulation activity of heparin was a potential concern. However, in agreement with our findings that paclitaxel-heparin-FA had only one third of the anticoagulation activity of heparin (Figure 3.7), no visible side effects associated with heparin were observed.

The marked difference in tumor growth inhibition observed amongst groups treated with PG-paclitaxel-FA and heparin-palitaxel-FA may be attributed to the larger hydrodynamic diameter of PG-paclitaxel-FA conjugates in aqueous solution (285 nm for PG-paclitaxel-FA, 102 nm for heparin-paclitaxel-FA, Figure 3.5), indicating less effective passive targeting via EPR effect, thus less accumulated particles at the tumor site.

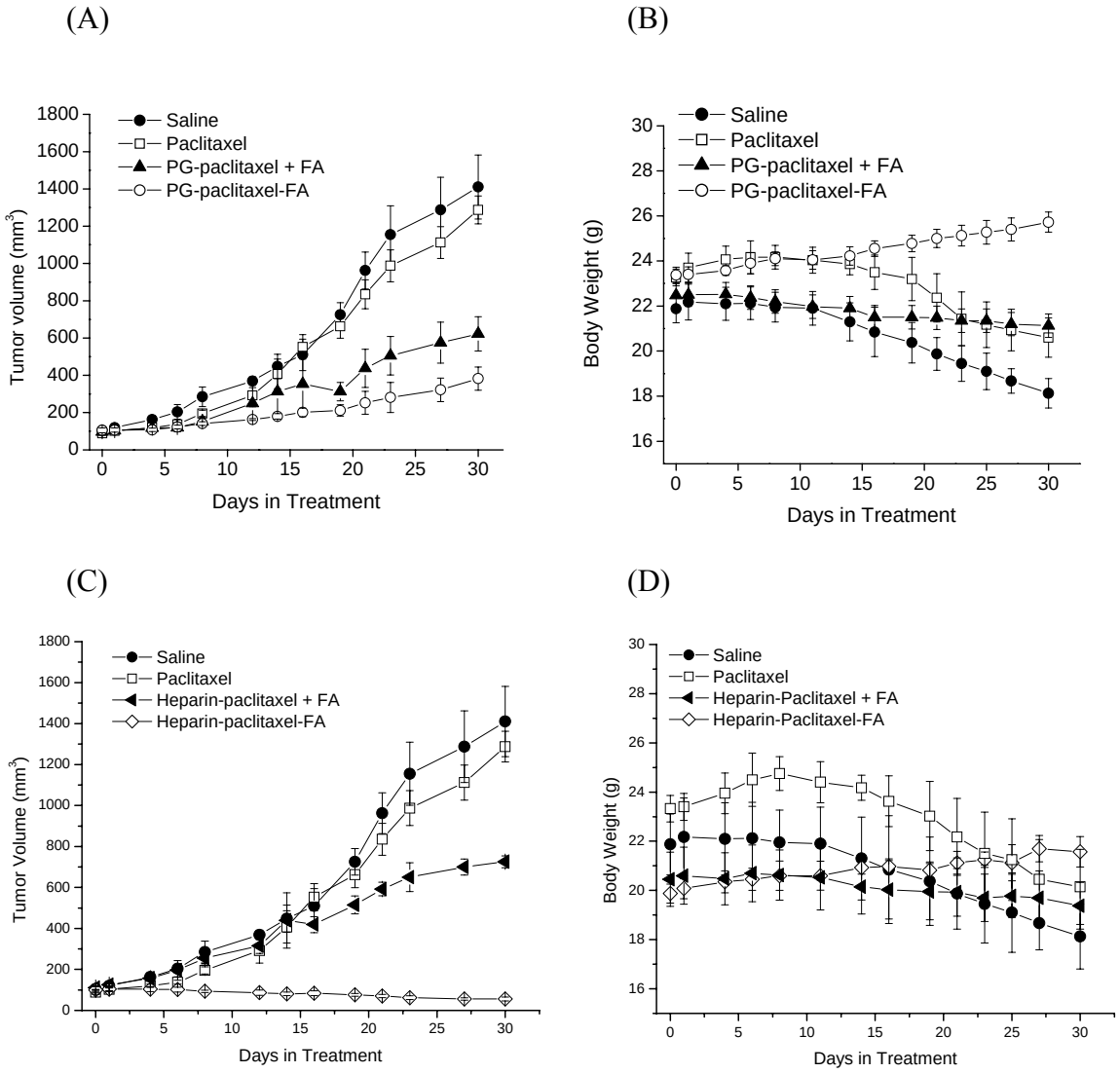

Figure 4.1: Anti-tumor Efficacy of Ternary Nanostructures. Tumor progression and body weight in KB tumor bearing mice with different treatments: saline (●), paclitaxel (□), PG-paclitaxel mixed with 20 mg/kg FA (▲), PG-paclitaxel-FA (○), heparin-paclitaxel mixed with 20 mg/kg free FA (◀) and heparin-paclitaxel-FA (◇). Equivalent dosage of paclitaxel at 80 mg/kg of mouse body weight was used for each i.v. injection.

The anti-tumor effect from the ternary nanostructures was also assessed by measuring the proliferative index using Ki-67 stain, a marker for dividing cells. The tumor sections from the saline control and free paclitaxel treated group had a much higher proliferative index than the conjugate treated group (Figure 4.2), which is in agreement with the tumor progression data. Two-tailed t-test results between the control group and ternary conjugates were $p = 0.0005$ (PG-paclitaxel-FA) and $p = 0.0003$ (heparin-paclitaxel-FA). The reduced proliferative index reflects the pharmacological action of paclitaxel which hinders proliferation by polymerizing tubulin disrupts cell division and leads to cell death.

Histochemical examination for apoptosis and necrosis was done by H& E staining. The deep purplish-blue color of hematoxylin stain signals live cells, whereas the orange-pink color of eosin counterstain indicates nonspecific absorption by dead cells. The groups treated with ternary nanostructures produced tumor cells with signs of apoptosis including cell shrinkage and chromatin condensation (Figure 4.3). The effect was especially pronounced in tumors treated with heparin-paclitaxel-FA where very different colors in KB cells were observed, showing a vast majority of apoptotic cells.

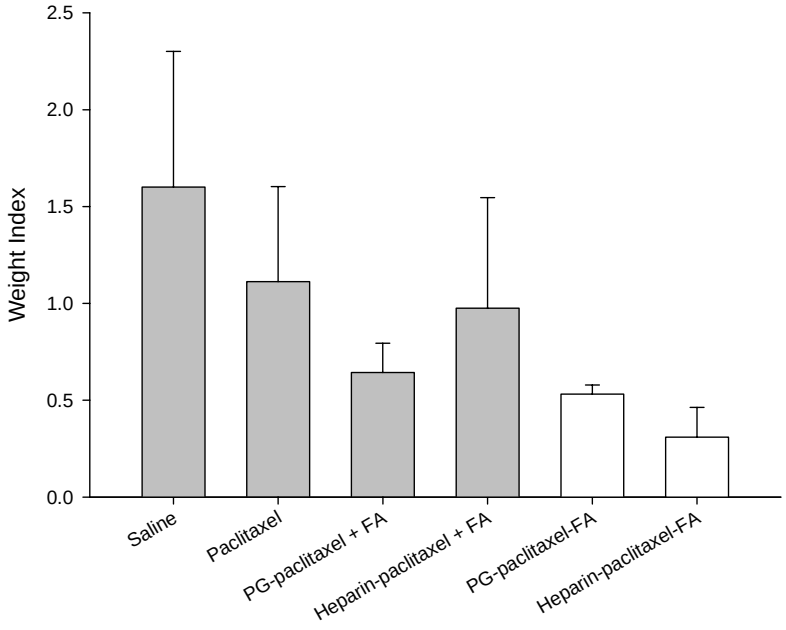

Figure 4.2: Comparison of Proliferative Indices. Indices were determined based on Ki-67 staining of tumor sections. PG-paclitaxel + FA: PG-paclitaxel mixed with 20 mg/kg FA; heparin-paclitaxel + FA: heparin-paclitaxel mixed with 20 mg/kg FA. All treatments were 80 mg/kg paclitaxel equivalent.

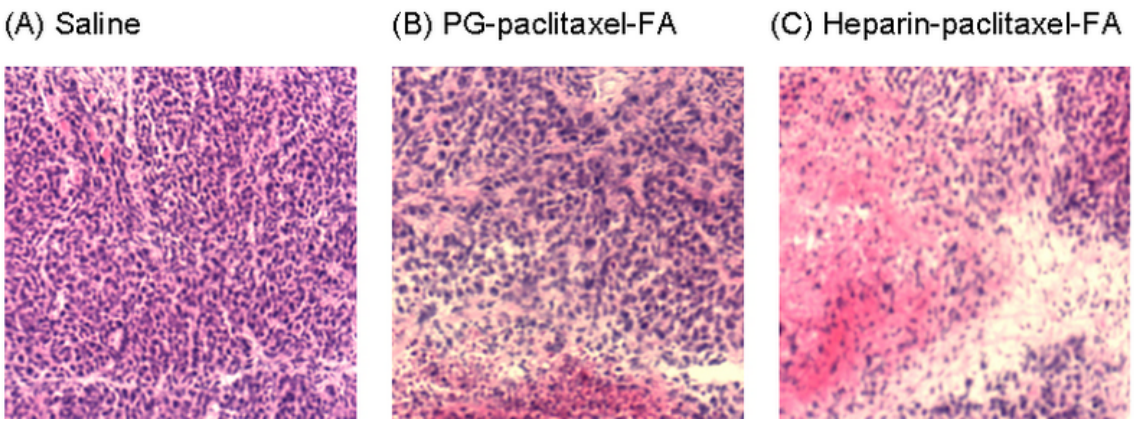

Figure 4.3: Histological Examination of H&E Stained Tumor Sections.

To ascertain whether the anti-tumor effect was from the paclitaxel released from the ternary nanostructures, tubulin integrity was examined by anti-α-tubulin staining by following a procedure described by Mabjeesh et al[164]. Tumors from the control group had well-organized microtubules with clearly defined intricate structures (Figure 4.4 (A). Tumors from the group treated with free paclitaxel (Figure 4.4 (B) had a small number of microtubules displaying microtubule bundling but still had signs of normalcy, such as the presence of multi-polar spindles. The classical paclitaxel effect was most apparent in tumors from the heparin-paclitaxel-FA group (Figure 4.4 (C). The phenotype indicated an effect similar to that of low-dose paclitaxel effect that suppresses microtubule dynamics and leads to aberrant mitotic arrest. Some mitotic figures appeared normal, but the lagging chromosomes at the spindle poles indicated that the dynamics of microtubules were compromised. These cells stay arrested in mitosis and eventually undergo apoptosis.

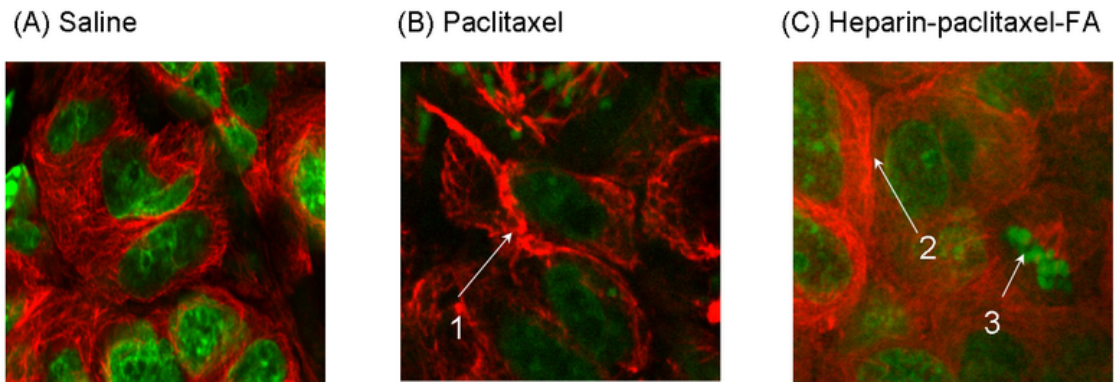

Figure 4.4: Anti-α-tubulin Staining of Tumor Tissues. The group with no treatment (A) maintained the structural integrity of microtubules. Arrow 1 in paclitaxel-treated group (B) points to microtubule bundling. Heparin-paclitaxel-FA groups (C) show microtubule bundling (arrow 2) and aberrant arrest of chromosomes (arrow 3).

Anti-angiogenic Efficacy of Ternary Nanostructures

All tumor cells depend on a viable vasculature for growth and survival [165-168]. Tumor cells interact with host factors in the microenvironment to induce growth and the expansion of vasculature [165, 166]. Antivascular therapy can destroy tumor cells that require oxygen and nutrients for survival. It is important, however, to target tumor-associated endothelial cells rather than all endothelial cells. Endothelial cells in normal tissues rarely divide, whereas 2-3% of endothelial cells in cancer divide daily [169]. These dividing endothelial cells should be sensitive to anticycling drugs such as paclitaxel. The anti-angiogenic activity of paclitaxel has been reported by several researchers [170-173] at doses as low as 0.1–100 pM in endothelial cell cultures.

Fluorescent angiography revealed extensive vasculature surrounding the tumor treated with paclitaxel alone (Figure 4.5(A). In sharp contrast, blood vessles around the tumors treated with heparin-paclitaxel-FA were almost invisible. Tumors treated with PG-paclitaxel-FA (Figure 4.5(C) also showed far less vasculature compared to those treated with paclitaxel alone. Immunohistochenical staining against the endothelial marker PECAM-1 allowed us to quantify the anti-angiogenic extent. In the specimen examined, heparin-paclitaxel-FA treatment produced only 7% positive PECAM-1 area, in contrast to that of paclitaxel (44%). Again, the most significant decrease of tumor vasculature was observed in tumors treated with the heparin-paclitaxel-FA conjugates (Figure 4.6).

Since PG-paclitaxel-FA exhibits less anti-tumor and anti-angiogenic effects compared with heparin-paclitaxel-FA, it is very likely the nascent anti-tumor property of heparin that enables its interaction with vascular endothelial growth factors (VEGF) and

basic fibroblast growth factors (bFGF) [102-105] contributes to a synergistic effect with paclitaxel on the tumor and its vasculature. This data lead us to conclude that the marked anti-angiogenic activity contributes to the highly effective potency of heparin-paclitaxel-FA in inhibiting tumor growth and inducing rapid tumor shrinkage.

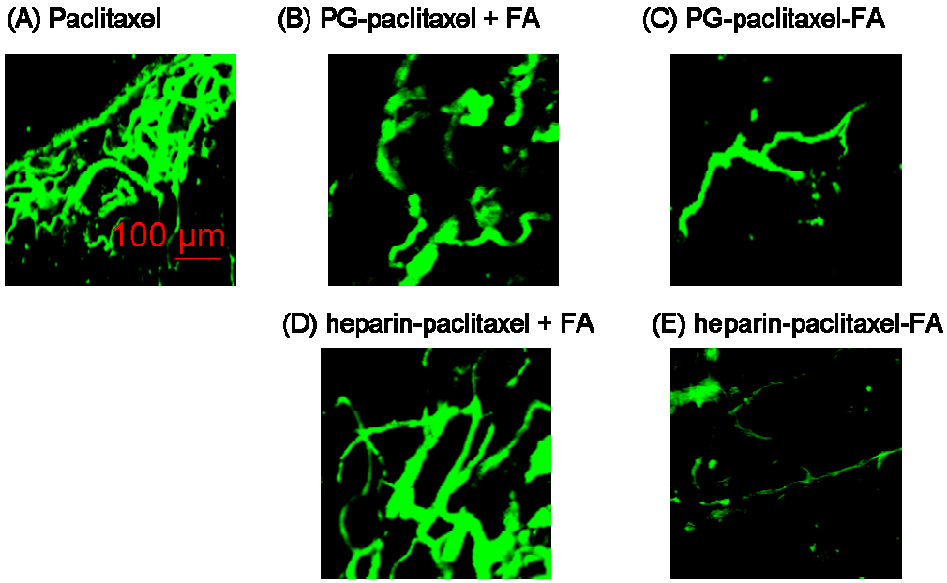

Figure 4.5: Anti-angiogenic Effect of Ternary Nanostructures. Fluorescent angiography showed that heparin-paclitaxel-FA and PG-pclitaxel-FA were highly effective in targeting and inhibiting tumor vasculature growth.

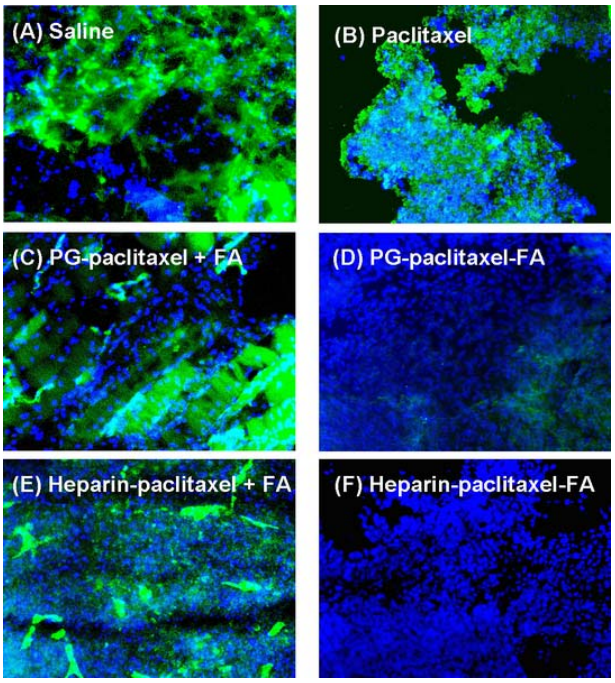

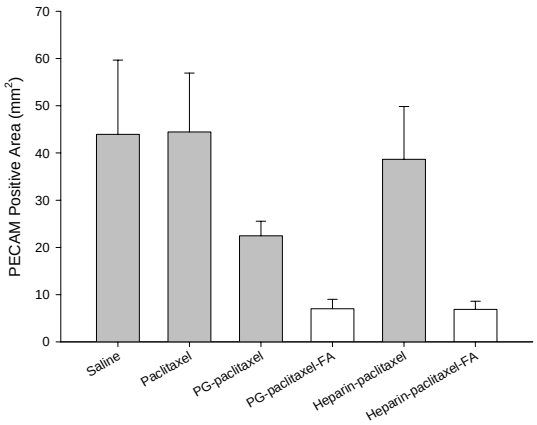

Figure 4.6: Quantification of Anti-angiogenic Effect of Ternary Nanostructures.

.

Comparison of Ternary and Binary Nanostructures

The anti-tumor efficacy of actively targeted the ternary heparin-paclitaxel-FA conjugates and passively targeted binary conjugates (heparin-paclitaxel and Abraxane™), was tested. Six mice (n=6) in each group were treated weekly with i.v. injections of saline, paclitaxel (80 mg/kg), three different dosages of heparin-paclitaxel-FA (40, 80, 120 mg/kg paclitaxel equivalent), heparin, heparin-paclitaxel (80 mg/kg paclitaxel equivalent), heparin-paclitaxel (80 mg/kg paclitaxel equivalent) with 20 mg/ kg FA, and Abraxane™ (80 mg/kg paclitaxel equivalent) respectively.

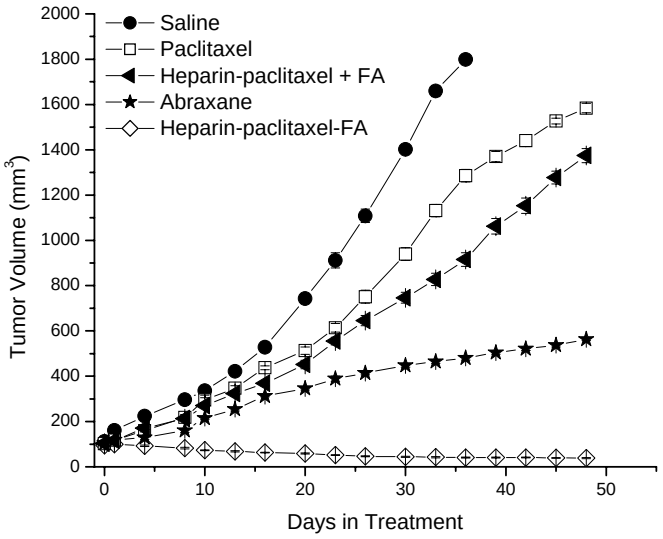

Figure 4.7: Anti-tumor Effect of Ternary and Binary Nanostructures. Groups treated with ternary heparin-paclitaxel-FA conjugates underwent over 50% tumor shrinkage. Abraxane and heparin-paclitaxel failed to contain tumor progression. All treatments shown on the curve here are 80 mg/kg paclitaxel equivalent.

Mice treated with heparin did not show apparent tumor regression (data not shown), despite known anti-tumor properties associated with heparin. In fact, minor signs of bleeding and thrombocytopenia started to show as the study progressed with the

heparin treated group. This is due to the preferable binding to factor Xa by the unmodified heparin that triggers the anticoagulant cascade.

While both binary conjugates of heparin-paclitaxel and Abraxane were more effective than paclitaxel alone, they could not contain tumor growth. The most dramatic effect was seen in the heparin-palitaxel-FA ternary conjugates where tumor volume was reduced from 95 mm^3 to 39 mm^3 over the course of the treatment (Figure 4.7).

In aqueous solution, both Abraxane™ and heparin-paclitaxel-FA form nanostructures of about size 100 nm, which enables them to accumulate at the tumor site via the EPR effect. The difference in anti-tumor efficacy, then, is best explained by the effective active targeting via the folate receptor. This reasoning is supported by the finding that when binary heparin-paclitaxel is subjected to compete with FA (group treated with heparin-paclitaxel + 20 mg/kg FA), the outcome is far less tumor inhibition compared with Abraxane™ treatment.

Survival of mice in response to the above treatment was determined. The results are presented in a Kaplan–Meier plot (Figure 4.8). The treatment/control ratio (T/C) based on mean survival time for each treatment group is presented in Table 4.1. The mice treated with heparin-paclitaxel-FA showed a 128% greater treatment/control ratio (T/C) value than those that received paclitaxel ($p < 0.01$). Both heparin-paclitaxel-FA and Abraxane™ were significantly more effective in prolonging mouse survival ($p < 0.01$) than free paclitaxel.

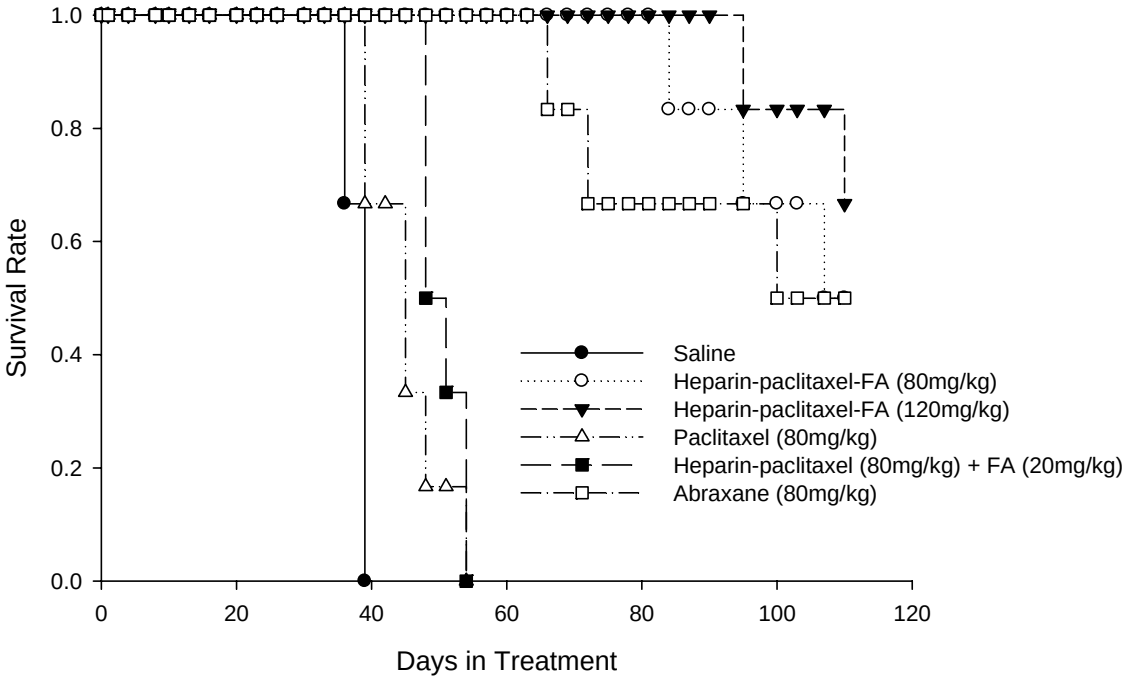

Figure 4.8: Effect of Ternary and Binary Nanostructures on the Survival of Tumor-bearing Nude Mice. Animal survival was recorded starting from the day of initial treatment, which was 18 days after KB tumor cell injection. All mg/kg are paclitaxel equivalent.

Table 4.1: Effect of Treatments on the Survival of Tumor-bearing Nude Mice

	Treatment/Control ratio (T/C) value
Saline	84.4
Heparin-paclitaxel-FA (80mg/kg)	228.2
Heparin-paclitaxel-FA (120mg/kg)	237.8
Paclitaxel (80mg/kg)	100 Survival time of mice treated with paclitaxel was defined as 100.
Heparin-paclitaxel (80mg/kg) + FA (20mg/kg)	112.2
Abraxane™	210.4

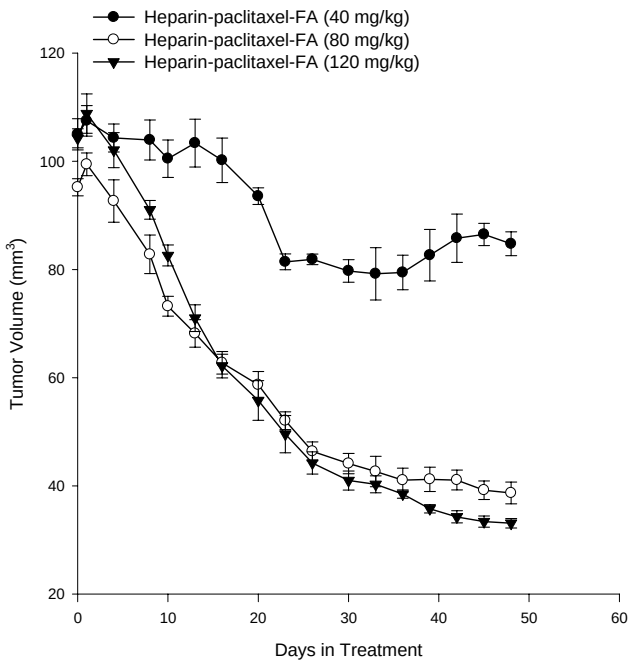

Figure 4.9: Dose Response to Ternary Nanostructures. The rate of tumor regression was proportional to dosage of heparin-paclitaxel-FA. The starting tumor volume was 100 mm^3. All numbers in dosage are paclitaxel equivalent.

Mice treated with 120 mg/kg of heparin-paclitaxel-FA conjugates showed rapid tumor regression where tumor size was reduced from 105 mm^3 to 33 mm^3 (Figure 4.9). This was a 5-fold difference compared with 40 mg/kg dosage ($p<0.01$). At the starting tumor volume of 300 mm^3, the tumor size dramatically diminished from 313 mm^3 to 20 mm^3 in 30 days at the 120 mg/kg dosage (Figure 4.10). Stable weight of the mice treated with heparin-paclitaxel-FA even at 120 mg/kg paclitaxel equivalent, which exceeds the maximum tolerated dosage, was indicative of the lack of systemic toxicity (Figure 4.10). From PECAM-1 quantification (Figure 4.11), the extent of blocking tumor vasculature seemed also proportional to the dosage administered.

To evaluate potential side effects in normal tissues, the excised organs (heart, liver, lung, kidney and spleen) from the mice treated with 120 mg/kg dosage were examined for morphological abnormalities. H&E staining and TEM revealed no

significant damage to the organ tissues (Figure 4.12). Notable point is the seemingly structurally unaffected liver and kidney at this high dosage. Guo et al. showed efficient uptake of folate-conjugated low-molecular-weight radiopharmaceuticals in kidneys and the turmor [174]. The concern for potential nephrotoxicity, however, can be appeased, since studies with FR-targeted liposomes studies [137, 175] report large molecular weight enables liposomes to elude glomerular filtration. The same reasoning is applicable to the ternary heparin-paclitaxel-FA conjugates.

The dosage-dependent anti-tumor effect can be attributed to the higher folate requirements of the tumor cell that enable them to readily take up more ternary conjugates to meet this demand. This agrees with the finding that the folate receptor function is regulated by cellular folate requirements [176].

A recent study showed that pretreatment of tumor histocultures with chemotherapeutic agents that induce tumor cell apoptosis resulted in greater permeability of the tumors to subsequently administered therapeutic agents [177]. This can be related to the dosage dependent efficacy as follows: Paclitaxel-induced necrosis and apoptosis within the tumor mass, which is enhanced by folate receptor dependent cellular uptake, might in turn facilitate the subsequent diffusion of heparin-paclitaxel-FA into the tumor cells. Reduction in viable tumor cells may partially remove the diffusion barrier that prevents efficient intratumoral distribution of the ternary nanostructures.

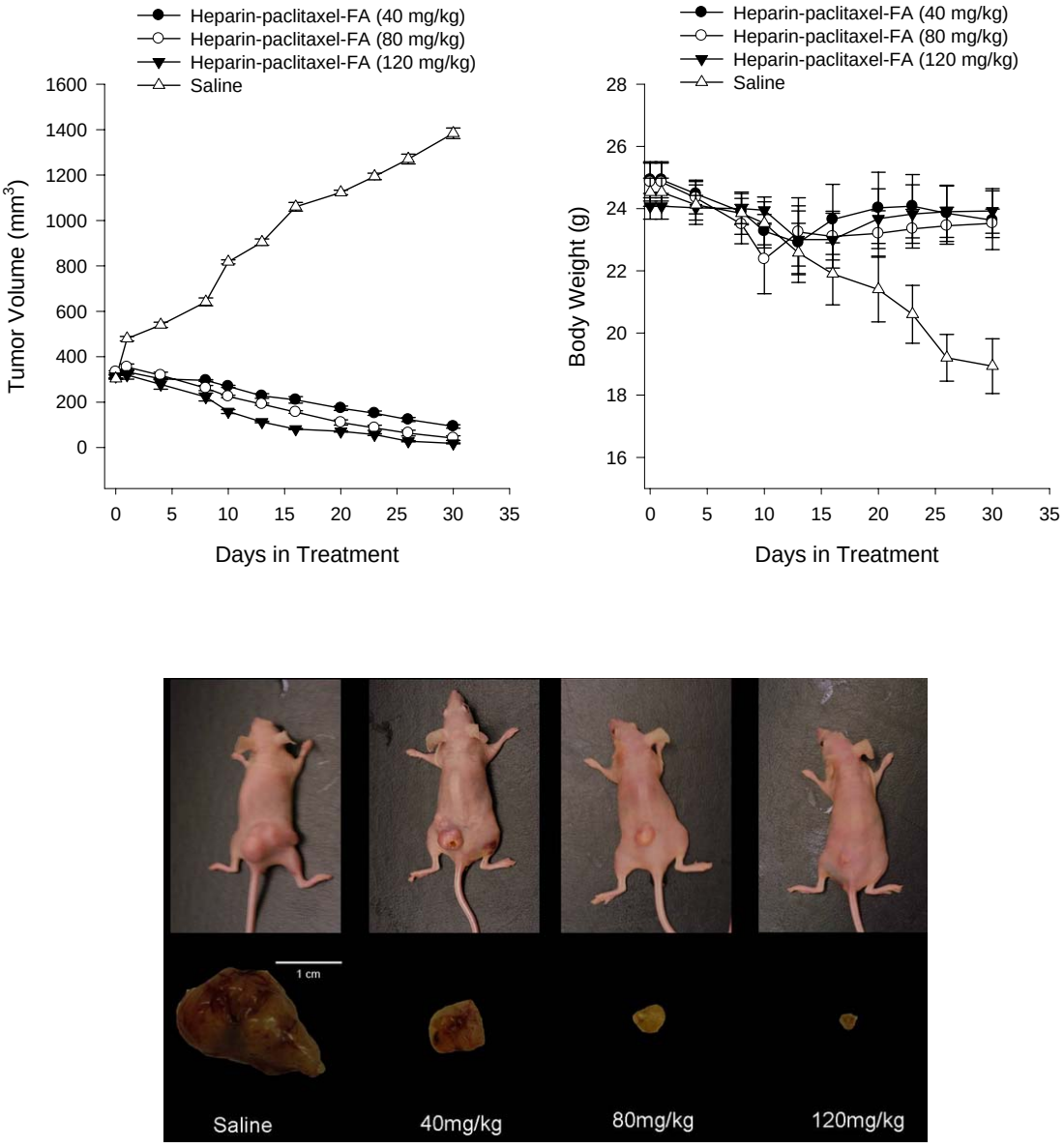

Figure 4.10: Tolerance to Heparin-paclitaxel-FA Treatment. The rate of tumor regression was proportional to dosage. The starting tumor volume was 300 mm^3. The only group that sustained drastic weight loss was the control group. All treated mice remained healthy with eventual weight gain towards to end of the study.

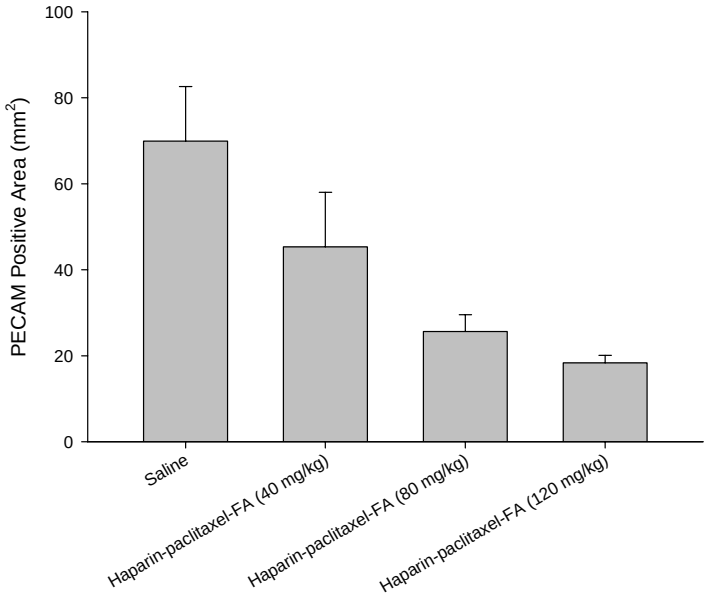

Figure 4.11: Quantification of Dosage-dependent Anti-angiogenic Effect of Heparin-paclitaxel-FA. The starting tumor volume was 300 mm^3.

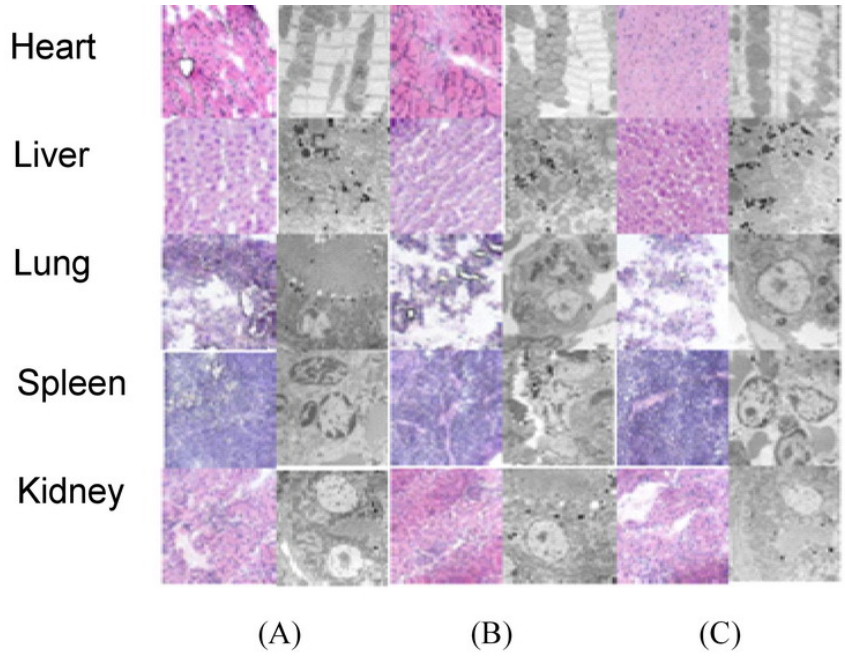

Figure 4.12: Effect of Heparin-paclitaxel-FA on Normal Tissues. Major organs show little abnormalities, indicative of highly effective tumor-specific targeting. Left column are H&E staining and right column are TEM images. (A) No treatment, healthy tumor-free group (B) Treated with 120 mg/kg heparin-paclitaxel-FA, 100mm^3 tumor-bearing group (3) Treated with 120 mg/kg heparin-paclitaxel-FA, 300mm^3 tumor-bearing group.

The dosage-dependent anti-tumor effect has potential implications in overcoming paclitaxel resistance. Goren et al. [34] reported that folate-targeted liposomes loaded with doxorubicin can bypass the multidrug-resistance efflux pump. The emergence of paclitaxel-resistant tumors [72, 73] is limiting the broad anti-tumor spectrum paclitaxel once spanned. Since our ternary conjugates can be efficiently targeted to the folate receptors, thereby circumventing the efflux pump, they could be potentially an effective remedy against paclitaxel resistant tumors.

CHAPTER 5

IN VIVO EFFICACY OF POLYMER-PACLITAXEL-FA TERNARY NANOSTRUCTURES: MULTI DRUG RESISTANCE

5.1 Introduction

Success of paclitaxel chemotherapy is limited primarily by two obstacles; its poor water solubility (1 μg/mL in aqueous solutions) and multidrug resistance (MDR). MDR is often found in many types of human tumors that have relapsed after an initial favorable response to drug therapy. The sensitivity of the MDR tumor cells to antineoplastic agents can decrease significantly, which hinders the efficacy of these drugs in tumor therapy[178]. Mechanisms of MDR to the taxanes have been identified. Classically paclitaxel binds to ß-tubulin to stabilize microtubules. Alterations in the expression patterns of both α- and ß-tubulin can impair this ability[179]. Another mechanism stems from the elevated expression of particular proteins, such as glycoprotein P (Pgp) [180, 181]. In general, Pgp acts as an efflux pump to extrude positively charged xenobiotics, including some anticancer drugs, out of the cell, lowering their intracellular concentrations. In certain cases, up to 100-fold overexpression of Pgp in MDR cells have been observed [182]. There is conclusive evidence to indicate that paclitaxel is a substrate for Pgp and that overexpression of Pgp results in paclitaxel resistance [183-185].

It is well established that the use of paclitaxel in solid tumors can induce the Pgp encoding gene (MDR-1) mediated drug resistance and that MDR-1 overexpressing tumors are often resistant to other drugs that are Pgp substrates. Tsuruo et al. were the first to report that MDR-1 associated drug efflux could be reversed with verapamil or trifluoperazine [186]. Pharmacologic manipulation of MDR-1 function to restore paclitaxel sensitivity has subsequently moved rapidly from the laboratory to the clinic. Several other molecular mechanisms of paclitaxel resistance have also been targeted in an attempt to restore sensitivity.

Gabizon et al. reported because 100 nm nanoparticles can passively extravasate in tumor tissues, increased selectivity of anticancer drug delivery at the tumor site, while markedly reducing drug accumulation and toxicity in many susceptible healthy tissues can be achieved [136, 187]. This increased delivery of anticancer drugs may overcome MDR based only on mass action, provided that the level of drug resistance is of a magnitude comparable to the increase in tumor drug levels [181]. Utilizing a ligand that binds specifically to its receptor on malignant cell may help in reducing dose-limiting cytotoxicity of the drug and also enable the drug to bypass the drug resistance mechanism especially caused by p-glycoprotein overexpression, via internalization through receptor-mediated endocytosis.

We hypothesize our ternary heparin-paclitaxel-FA may be able to overcome drug resistance because they enter cells by FR-mediated endocytosis, not by free diffusion across the cell membrane as is the case for free paclitaxel. Particularly, in the case of Pgp-mediated drug resistance, we expect that the increased intracellular accumulation of conjugated paclitaxel will oversaturate the ability of the cell-surface

pump to bind and pump out the drug. Also, we don't expect this protein to be able to pump out the drug unless it is released from the polymer nanoparticle. As a result, more paclitaxel will be available intracellularly for binding its target tubulin and eliciting its antiproliferative effects. Paclitaxel binds tubulin with a stoichiometry of 1:1 in the commercial cell-free systems; in cells, it takes only one molecule of paclitaxel every few hundred tubulin dimers for the drug to exhibit its antiproliferative activity. Here, the potential of overcoming MDR was examined *in vivo* using our ternary heparin-paclitaxel-FA nanostructures.

5.2 Materials and Methods

Materials

Paclitaxel was purchased from Polymed Therapeutics, Inc. (Houston, TX). Abraxane™ was bought from Abraxis Oncology (Los Angeles, CA). Heparin-paclitaxel-FA, heparin-paclitaxel, PG-paclitaxel-FA and heparin-paclitaxel were synthesized and purified as described in chapter 3. Drug-resistant KB variants KB-8-5, KB-C1, KB-V1 were donated from Dr. Gottesman at the National Cancer Institute. The cells were tested negative for murine pathogens and mycoplasma prior to being used in the animal studies.

FACS Analysis for Pgp and FR Expression

5 μg/mL primary antibody (PgP: Calbiochem, # 517308; FR: Alexis, #804-439-R100) was added to the cells (0.5×10^6) in 200 μL PBS 2 % bovine serum albumin, and the mixture was incubated for 20 min at room temperature. Fluoresceinisothiocyanate

(FITC)-conjugated secondary antibody (Invitrogen) was added after washing. After 20 min incubation at room temperature shielded from light, the antibody binding was measured. The samples were analyzed with a FACScan (Becton Dickinson) using FlowJo software. The fluorescence index (FI) was calculated as the ratio between mean fluorescence intensity in the presence and absence of primary antibody.

Cytotoxicity Assay

Cells (4×10^4 cells/mL) were harvested by incubating in 0.25% trypsin-0.03% EDTA solution and seeded in a 96-well plate. MTT assay kit was used to measure cytotoxicity of heparin-paclitaxel-FA, heparin-paclitaxel and paclitaxel on KB-8-5, KB-C1 and KB-V1 cell lines as described in chapter 3.

Animal Models

Crl:NU/NU-*nu*BR female nude mice aged 4-6 weeks (about 20-25 g body weight) were obtained from Charles River Laboratory (Wilmington, MA). Animal studies were conducted in accordance with an approved protocol by the Institutional Animal Care and Use Committee (IACUC) at Emory University. $1\sim2 \times 10^6$ cells were suspended in 100 μL PBS and injected subcutaneously at the mid-dorsal level to induce tumors.

All mice received weekly intravenous (i.v.) injections via the tail vein after the tumor reached 100 mm^3. The mice were randomly divided into groups. Treatment included control, free paclitaxel, heparin-paclitaxel, and heparin-paclitaxel-FA. Paclitaxel dosage was 40mg/kg for KB-8-5 models and 80 mg/kg for KB-V1 models. The conjugates were scaled accordingly to match paclitaxel equivalent. Tumor volume was determined by measuring three orthogonal tumor diameters and applying the

formula: Volume (mm^3)= $\pi/6 \times$ larger diameter (mm)$\times$ [smaller diameter(mm)] ^{2}, as in previous animal studies described in chapter 4. Mice were sacrificed when they became moribund due to the tumor or when they sustained over 20 % weight loss. To check systemic toxicity, the body weight of the mice was monitored. After 4 treatments, all mice were sacrificed and the tissues were collected.

Histology and Immunohistochemistry

H&E

Excised tumors were embedded in O.C.T. compound (Miles, Elkhart, IN) and snap-frozen in liquid nitrogen. Tissue sections of 5 μm were prepared on glass slides. For H&E staining, the sections were rehydrated through a series of graded ethanol (100%, 90% and 70%) and water before staining with hematoxylin and eosin.

Ki-67

To quantify cell proliferation, Ki-67 expression was measured. Snap-frozen tumors were sectioned and processed with mouse anti-human Ki-67 (Clone MIB-1, DakoCytomation, Cat# M7240). Horse Anti-Mouse IgG was used as the secondary antibody. The sections were than incubated with HRP-Streptavidin, washed, and incubated in DAB peroxidase substrate solution. Counterstaining was done with hematoxylin.

α-tubulin

Pieces of tumor from each animal were fixed in PHEMO buffer containing 3.7% formaldehyde, 0.05% glutaraldehyde, 0.5% Triton X-100 for 1–2 hr at room temperature. Following fixation, tumor pieces were stored in 4% paraformaldehyde in

0.1% sodium cacodylate at 4°C for up to a month before further processing. Fixed tumor sections were embedded in low-melting agarose (Sigma) and 50 μm sections were obtained by vibratome sectioning at low speed (Vibratome Series 1000 Sectioning System). Sections were then processed for immunofluorescence with rat anti-α-tubulin antibodies (Chemicon MAB1864). Alexa Fluor 568 goat anti-rat antibody (Molecular Probes A11077) was used as the secondary antibody. Sytox Green (Invitrogen) was used for DNA counterstaining.

5.3 Results and Discussion

FR-mediated Uptake

Drug-resistant KB cell variants KB-8-5, KB-C1, KB-V1 are known to be 10, 100, or 1000-fold more resistant to paclitaxel than its parental line KB-3-1. The Pgp expression level in drug-resistant KB cells and KB cells was confirmed using flow cytometry (Figure 5.1(A). Measurement of FR expression level revealed similar profiles for all KB cells (Figure 5.1(B).

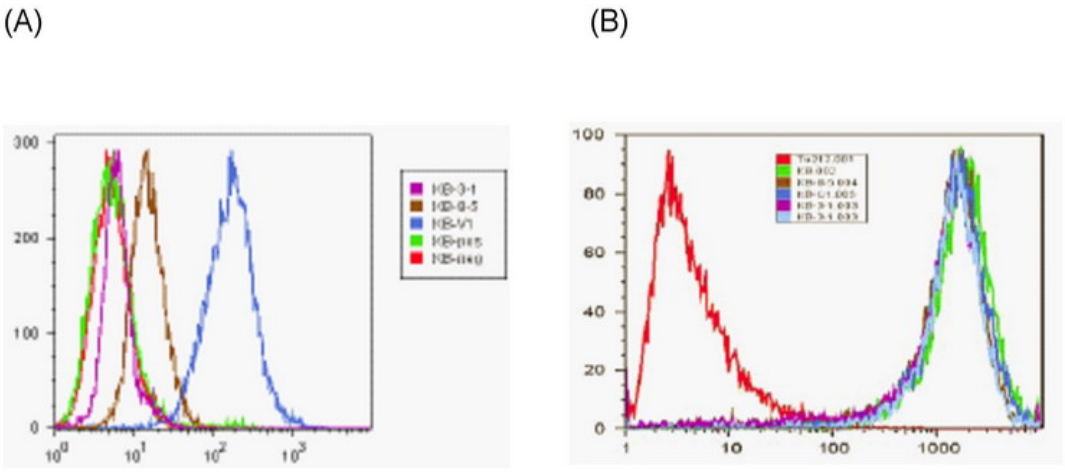

Figure 5.1: Pgp and Folate Receptor Expression. KB, KB-8-5, and KB-V1 cell lines were assayed for their (A) Pgp and (B) FR expression. All KB cell lines had an elevated level of FR expression.

Blocking with FA interfered with the cellular uptake of the fluorescently tagged heparin-paclitaxel-FA ternary conjugates by the KB resistant variants. Also, when FR expression was knocked out with anti-FR siRNA, it significantly hindered uptake of heparin-paclitaxel-FA. All these findings are consistent with FR-dependent, specific uptake of the conjugates observed in previous studies.

Anti-tumor Efficacy in Drug-resistant Tumor Models

The groups treated with heparin-paclitaxel-FA conjugates showed superior potency in suppressing the tumor in drug-resistant KB tumors. However, unlike tumors originated from their parental KB line, no tumor shrinkage was apparent. Heparin-paclitaxel-FA treatment was more effective than paclitaxel both the 10-fold resistant KB-8-5 ($p=0.02$) and the 1000-fold resistant KB-V1 ($p=0.002$) tumors.

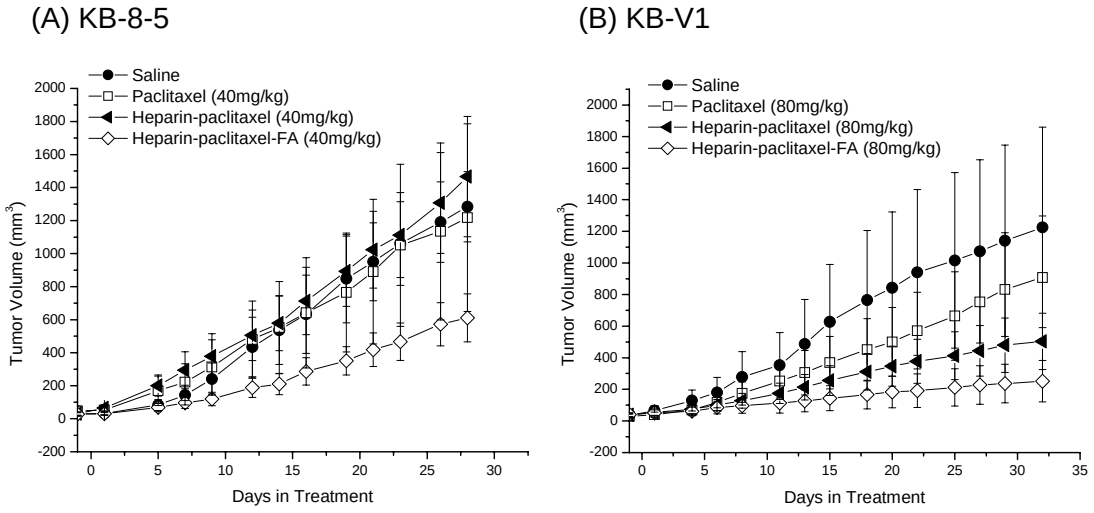

Figure 5.2: Anti-tumor Efficacy of Heparin-paclitaxel-FA in Drug-resistant Tumors. Tumor progression in drug-resistant KB tumor bearing mice with different treatments (A) KB-8-5: 10-fold paclitaxel-resistant, five mice per group; KB-V1: 1000-fold paclitaxel-resistant, six mice per group.

Heparin-paclitaxel-FA treated group had the lowest proliferative index (0.45) compared with that of the untargeted heparin-paclitaxel (0.69), paclitaxel (1.15) and control group (1.68) as determined by Ki-67 staining (Figure 5.3). H&E analysis of tumors from the same group showed a large number of tumor cells with signs of apoptosis including cell shrinkage and chromatin condensation.

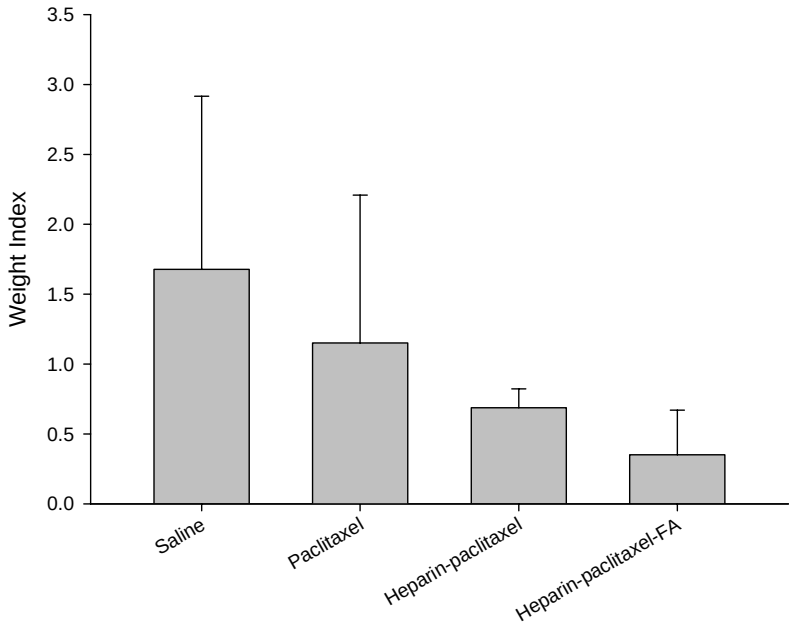

Figure 5.3: Comparison of Proliferative Indices. Indices were determined based on Ki-67 staining of KB-8-5 tumor sections.

To ascertain that whether the anti-tumor effect was caused by paclitaxel released from heparin-paclitaxel-FA, microtubule integrity was examined. Tumors from the control groups (Figure 5.4 (A) maintained a nicely organized microtubule cytoskeleton. Heparin-paclitaxel-FA treatment caused the appearance of multiple cells with aberrant mitotic spindles and occasional bundling of interphase microtubules (Figure 5.4 (B). These hallmark features of taxane-like effect on cells were only observed in this

treatment group. No significant disruption of the microtubule cytoskeleton was observed in groups that received free paclitaxel or heparin-paclitaxel (Figure 5.4(C) and (D). Free paclitaxel treatment occasionally caused a cell to form aberrant mitotic spindles but this activity was much less than that observed with heparin-paclitaxel-FA.

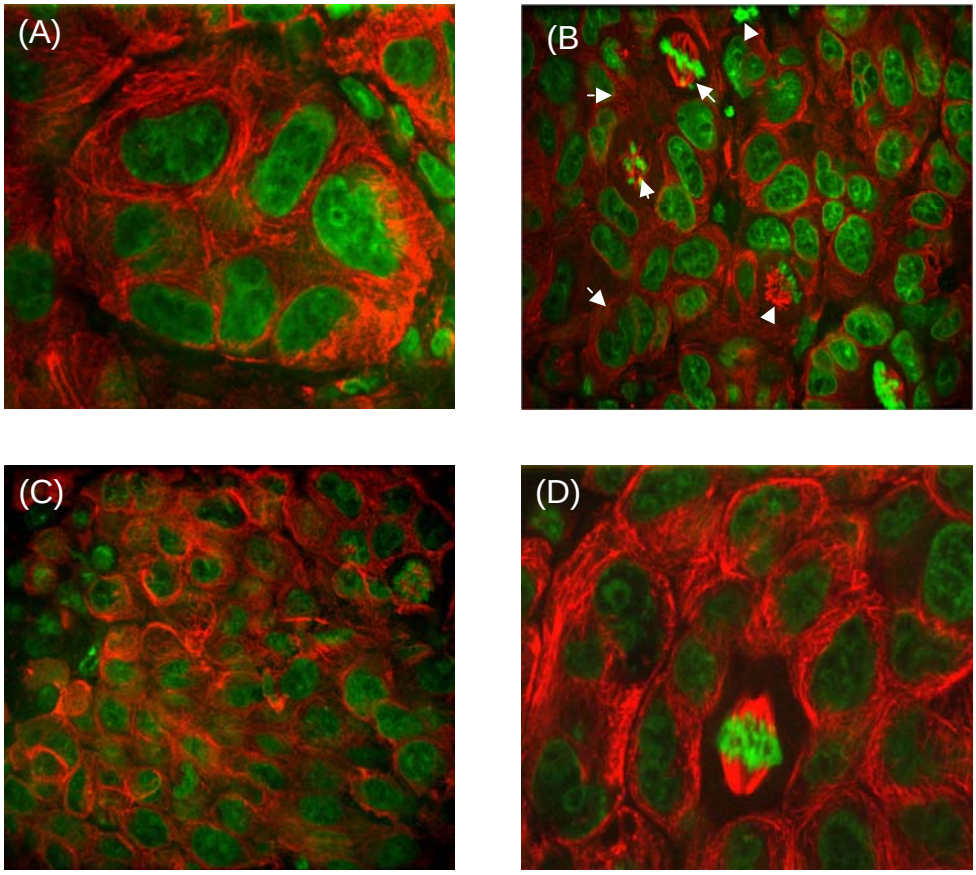

Figure 5.4: Anti-α-tubulin Staining of KB-8-5 Tumor Tissues. (A) Control group; well-preserved microtubule structure. (B) Heparin-paclitaxel-FA; arrows point to characteristic paclitaxel effect such as lagging chromosomes, mitotic arrest and bundling. (C) Paclitaxel; occasional microtubule bundling. (D) Heparin-FA; normal dividing cell and well-organized microtubule cytoskeleton.

So far, the main complications in circumventing MDR have been: 1) Pharmacokinetic interactions between the MDR inhibitor and the anticancer drug, and 2) inhibition of the same transport systems in healthy tissues, causing multiple adverse effects [188]. This situation strengthens the necessity of devising a strategy not only target the malignant cells directly, but also aim at destroying nonmalignant tumor components that are crucial for tumor survival and development. Heparin-paclitaxel-FA with its highly specific tumor uptake and potent anti-tumor and anti-angiogenic properties very well fits the profile of this strategic requirement.

The data presented above show that the heparin-paclitaxel-FA conjugates are effectively targeting paclitaxel to the tumor and releasing the anti-cancer drug to exert its effect. We also examined the tumor sections stained with PECAM-1, but were not able to draw a definite conclusion about the anti-angiogenic effect on KB-8-5 tumor vasculature since comparison of saline treated group against the KB-8-5 the two-tailed t-test resulted in a marginal p value. Further investigation is warranted.

In the previous chapter, we presented marked reduction in KB tumor vasculature resulting from heparin-paclitaxel-FA treatment. Endothelial cells are genetically stable and unlikely to develop MDR [189]. Since the parental KB cells used in the previous study have comparable FR expression levels as the drug-resistant variants, it is not unreasonable to hypothesize that the conjugates that arrive at the tumor site via FR targeting would behave similarly in the KB-8-5 tumor model to exert its anti-angiogenic effect and play a role in overcoming MDR.

CHAPTER 6

SUMMARY AND FUTURE WORK

6.1 Summary

Significant progress has been made in the development of new agents against cancer and new ways of delivering existing and new agents. Yet, the major challenge to target and selectively kill cancer cells while affecting as few healthy cells as possible remains. Nanometer-sized particles have novel optical, electronic, and structural properties that are not available from either individual molecules or bulk solids. When linked with tumor targeting moieties such as tumor-specific ligands or monoclonal antibodies, these nanoparticles can be used to target cancer-specific receptors, tumor biomarkers as well as tumor vasculatures with high affinity and precision. Recently, the use of nanoparticles for drug delivery and targeting has emerged as one of the most exciting and clinically important areas in cancer nanotechnology.

In this work, we tested the hypothesis that our novel ternary biomolecular nanostructures of folic acid, biodegradable polymer (polysaccharide heparin and poly-l-glutamic acid) and paclitaxel will improve the delivery and tumor-specific distribution of the anticancer drug. The design was based on three principles: 1) Passive targeting via EPR effect; 2) active targeting via a tumor-specific ligand; and 3) prodrug that would unleash the anti-cancer agent at the tumor site once specific delivery had been accomplished (chapter 2).

First, self-assembled heparin-paclitaxel-FA and PG-paclitaxel-FA nanostructures were synthesized (chapter 3). Their physicochemical properties were examined and biological efficacy was tested. The conjugates had significantly improved solubility in water, paving the way for cremophor-free formulation. Second, *in vitro* cellular toxicity and targeting ability of the nanostructures were investigated (chapter 3). In KB cancer cell lines with high FR expression, the ternary conjugates were efficiently taken up. In normal cell lines with minimal FR expression level or A549 cancer cells that are FR-negative, no detectable association was found. Competitive assay with FA provided proof that the uptake was indeed via the folate receptor. Third, *in vivo* investigation in human xenograft mice models was carried out (chapter 4). Since the conjugates were highly water soluble, they were suspended in saline for i.v. administration. In the highly FR-positive KB tumor model, ternary nanostructures proficiently inhibited tumor growth without inducing systemic toxicity or side effects. The dramatic tumor shrinkage observed in groups treated with heparin-paclitaxel-FA was on par with the best results reported in the literature found on polymer-drug conjugate investigation. The ternary nanostructures displayed remarkable anti-angiogenic effect on tumor vasculature. Heparin-paclitaxel-FA was also very effective in drug resistant KB tumors, potentially overcoming MDR resistance through FR targeting and tumor vasculature inhibition (chapter 5). Studies using other cancer models are in progress to determine the spectrum of applicability of the ternary nanostructures (appendix A).

6.2 Future Design Improvements

While heparin-paclitaxel-FA in its current form had marked success in inhibition tumor and its vasculature progression, a few improvements in design may be considered.

First, different prodrug linkages that are more stable against serum esterases and more specific tumor environment could be employed. Solid tumors are dynamic heterogeneous structures that typically have significantly lower oxygen tensions than their surrounding normal tissue due to abnormal vasculature. Studies have conclusively identified areas of severe hypoxia in many types of human tumors [190]. Anti-cancer drug mitomycin C [191] and agents such as tirapazamine [192] elicit potency through reductive activation in the hypoxic environment. Vrudhula et al. reported a series of unsymmetrical polar disulfide prodrugs of paclitaxel [193]. The prodrugs had enhanced stability against serum esterases were able to be efficiently activated to induce tumor inhibition *in vivo*.

Alternatively, an enzyme-specific linker could be incorporated. Matrix-metalloproteinases (MMP) are widely studied enzymes which are secreted in elevated levels in many types of human cancers [194-196]. They help the tumor cells to survive and grow by breaking down the extracellular matrix barrier, releasing growth factors to stimulate cell proliferation and releasing angiogenesis factors to promote blood vessel formation [197]. Peptide sequences that are specifically cleaved by MMP-2 and MMP-9 have been extensively studied [198] and found wide application in prodrug development.

Lastly, while little signs of side effects associated with heparin were observed in the animal studies even at doses as high as 120 mg/kg, bleeding and hematoma can be avoided almost completely. To achieve this, we may modify the sulfate functionality of heparin as selective O-desulfation can remove or reduce the residual anticoagulant properties of heparin while retaining their ability to effectively inhibit angiogenesis, metastasis and tumor growth [109-111, 199].

6.3 Cancer Nanotechnology: Perspective

Nanotechnology has become an enabling technology for personalized oncology in which cancer detection, diagnosis, and therapy are tailored to each individual's tumor molecular profile, and also for predictive oncology in which genetic/molecular markers are used to predict disease development, progression, and clinical outcomes. Looking into the future, there are a number of research themes or directions that are particularly promising but require concerted effort for success.

The first direction is the design and development of functional nanoparticles. For cancer and other medical applications, important functions include therapy, imaging, and targeting. With each added function, nanoparticles could be designed to have novel properties and applications. For example, binary nanoparticles with two functions could be developed for molecular imaging, targeted therapy, or for simultaneous imaging and therapy. Bioconjugated quantum dots with both targeting and imaging functions will be used for targeted tumor imaging and molecular profiling applications. Conversely, ternary nanoparticles with three functions could be designed for simultaneous imaging

and therapy with targeting, targeted dual-modality imaging, or for targeted dual-drug therapy. Quaternary nanoparticles with four functions can be conceptualized in the future to have the abilities of tumor targeting, dual-drug therapy and imaging. Carrier design and targeting strategies may vary according to the type, developmental stage, and location of cancer.

The second direction is nanoparticle molecular profiling (nanotyping) for clinical oncology; that is, the use of bioconjugated nanoparticle probes to predict cancer behavior, clinical outcome, treatment response, and individualize therapy. This should start with retrospective studies of archived specimens because the patient outcome is already known for these specimens. The key hypotheses to be tested are that nanotyping a panel of tumor markers will allow more accurate correlations than single tumor markers; and that the combination of nanotyping tumor gene expression and host stroma are both important in defining the aggressive phenotypes of cancer as well as determining the response of early stage disease to treatments such as chemotherapy, radiation, or surgery.

The third important direction is to study nanoparticle distribution, excretion, metabolism, and pharmacodynamics in *in vivo* animal models.

To conclude, there is much synergy between therapy and imaging in cancer nanotechnology. Many of the principles applied in targeted delivery of drugs to tumor and its vasculature may also be utilized to target imaging and diagnostic agents. The ability to design multifunctional nanostructures will have a significant impact on cancer diagnostics, molecular profiling, and the integration of cancer therapy and imaging.

APPENDIX A

IN VIVO EFFICACY OF POLYMER-PACLITAXEL-FA TERNARY NANOSTRUCTURES: PRELIMINARY RESULTS IN METASTATIC PROSTATE CANCER

FR expression was measured by flow cytometry in a host of human prostate cancer cell lines that included LNCaP, C4-2, $ARCaP_E$ and $ARCaP_M$. Among the cell lines tested, $ARCaP_M$ (C2) had the highest level of FR expression (Figure A.1). Pro-apoptotic effects of paclitaxel and heparin-paclitaxel-FA was evaluated by assessing caspase activation and the cleavage of Poly (ADP-ribose) Polymerase (PARP). The results revealed that $ARCaP_M$ cells underwent significant apoptosis upon 48-hour exposure to heparin-paclitaxel-FA due to activation of caspase-3, caspase-8, and caspase-9. Mice with $ARCaP_M$ tumors implanted in the tibia were given weekly i.v. injections of saline, paclitaxel, heparin-paclitaxel, and heparin-paclitaxel-FA for 5 weeks. All paclitaxel dosages were 40 mg/kg. Tumor progression was monitored by X-ray imaging. As can be seen in the X-ray picture of the intratibial site taken after two treatments, heparin-paclitaxel-FA (Figure A.2 (B) was superior to free paclitaxel (Figure A.2 (A) in inhibiting $ARCaP_M$ (C2) tumor growth. Given the highly aggressive nature of $ARCaP_M$, the results may have significant implications in inhibiting metastasis.

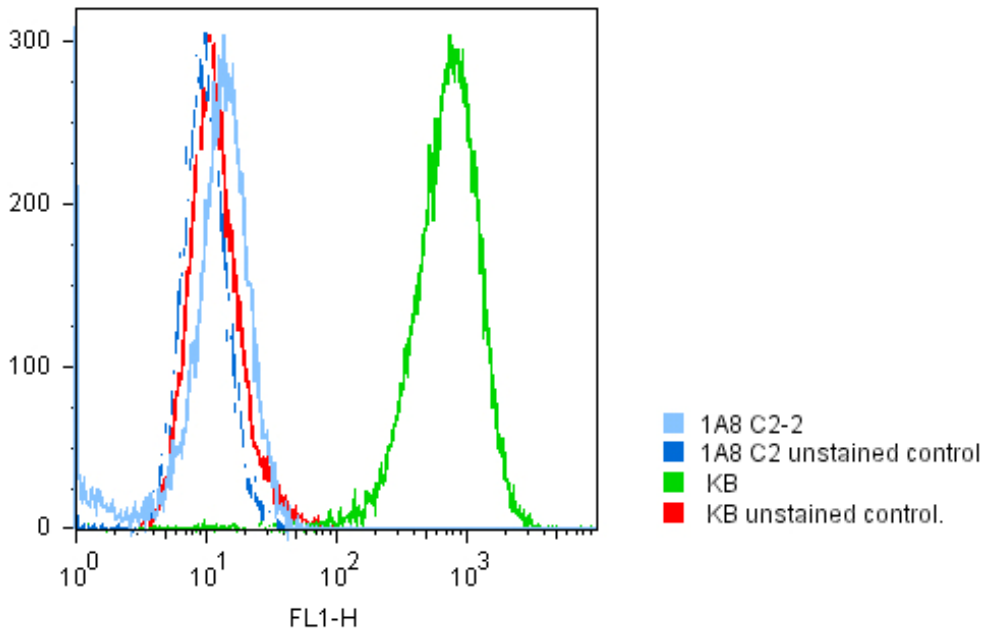

Figure A.1: Folate Receptor Expression Level in ARCaP$_M$.

(A) Paclitaxel

(B) Heparin-paclitaxel-FA

Figure A.2: Inhibition and Regression of Highly Metastatic Prostate Tumors. X-ray pictures taken after two weekly injections. Heparin-paclitaxel-FA treated mice show significantly reduced tumor volume compared with those treated with paclitaxel only.

REFERENCES

1. American Cancer Society, Inc. Cancer Facts and Figures. (2006).

2. Hashida, M. & Takakura, Y. Pharmacokinetics in design of polymeric drug delivery systems. *Journal of Controlled Release* **31**, 163-171 (1994).

3. Yuan, F. et al. Vascular permeability in a human tumor xenograft: molecular size dependence and cutoff size. *Cancer Research* **55**, 3752-6 (1995).

4. Maeda, H., Wu, J., Sawa, T., Matsumura, Y. & Hori, K. Tumor vascular permeability and the EPR effect in macromolecular therapeutics: a review. *Journal of Controlled Release* **65**, 271-84 (2000).

5. Grossfeld, G.D. et al. Thrombospondin-1 expression in patients with pathologic stage T3 prostate cancer undergoing radical prostatectomy: association with p53 alterations, tumor angiogenesis, and tumor progression. *Urology* **59**, 97-102 (2002).

6. Storm, G., Belliot, S., Daemen, T. & Lasic, D. Surface modification of nanoparticles to oppose uptake by the mononuclear phagocyte system. *Advanced Drug Delivery Reviews* **17**, 31-48 (1995).

7. Jain, R.K. Understanding barriers to drug delivery: High resolution in vivo imaging is key. *Clinical Cancer Research* **5**, 1605-1606 (1999).

8. Jain, R.K. Transport of molecules, particles, and cells in solid tumors. *Annual Review of Biomedical Engineering* **1**, 241-63 (1999).

9. Teicher, B.A. Molecular targets and cancer therapeutics: discovery, development and clinical validation. *Drug Resistance Updates* **3**, 67-73 (2000).

10. Teicher, B.A. et al. Treatment regimens including the multitargeted antifolate LY231514 in human tumor xenografts. *Clinical Cancer Research* **6**, 1016-23 (2000).

11. Duncan, R. The dawning era of polymer therapeutics. *Nature Reviews Drug Discovery* **2**, 347-360 (2003).

12. Matsumura, Y. & Maeda, H. A new concept for macromolecular therapeutics in cancer chemotherapy: mechanism of tumoritropic accumulation of proteins and the antitumor agent smancs. *Cancer Research* **46**, 6387-92 (1986).

13. Gref, R. et al. Biodegradable Long-Circulating Polymeric Nanospheres. *Science* **263**, 1600-1603 (1994).

14. Moghimi, S.M. & Hunter, A.C. Poloxamers and poloxamines in nanoparticle engineering and experimental medicine. *Trends in Biotechnology* **18**, 412-420 (2000).

15. Park, E.K., Lee, S.B. & Lee, Y.M. Preparation and characterization of methoxy poly(ethylene glycol)/poly(epsilon-caprolactone) amphiphilic block copolymeric nanospheres for tumor-specific folate-mediated targeting of anticancer drugs. *Biomaterials* **26**, 1053-1061 (2005).

16. Farokhzad, O.C. et al. Nanoparticle-aptamer bioconjugates: a new approach for targeting prostate cancer cells. *Cancer Research* **64**, 7668-72 (2004).

17. Stella, B. et al. Design of folic acid-conjugated nanoparticles for drug targeting. *Journal of Pharmaceutical Sciences* **89**, 1452-1464 (2000).

18. Chari, R.V. Targeted delivery of chemotherapeutics: tumor-activated prodrug therapy. *Advanced Drug Delivery Reviews* **31**, 89-104 (1998).

19. Mansour, A.M. et al. A new approach for the treatment of malignant melanoma: Enhanced antitumor efficacy of an albumin-binding doxorubicin prodrug that is cleaved by matrix metalloproteinase 2. *Cancer Research* **63**, 4062-4066 (2003).

20. Guo, X. & Szoka, F.C. Chemical approaches to triggerable lipid vesicles for drug and gene delivery. *Accounts of Chemical Research* **36**, 335-341 (2003).

21. Bennis, S., Chapey, C., Couvreur, P. & Robert, J. Enhanced cytotoxicity of doxorubicin encapsulated in polyisohexylcyanoacrylate nanospheres against multidrug-resistant tumour cells in culture. *European Journal of Cancer* **30A**, 89-93 (1994).

22. Larsen, A.K., Escargueil, A.E. & Skladanowski, A. Resistance mechanisms associated with altered intracellular distribution of anticancer agents. *Pharmacology and Therapeutics* **85**, 217-229 (2000).

23. Duncan, R. Polymer conjugates as anticancer nanomedicines. *Nature Reviews Cancer* **6**, 688-701 (2006).

24. Graff, C.P. & Wittrup, K.D. Theoretical analysis of antibody targeting of tumor spheroids: importance of dosage for penetration, and affinity for retention. *Cancer Research* **63**, 1288-96 (2003).

25. Jain, R.K. 1995 Whitaker Lecture: delivery of molecules, particles, and cells to solid tumors. *Annals of Biomedical Engineering* **24**, 457-73 (1996).

26. Kannagi, R., Izawa, M., Koike, T., Miyazaki, K. & Kimura, N. Carbohydrate-mediated cell adhesion in cancer metastasis and angiogenesis. *Cancer Science* **95**, 377-384 (2004).

27. Yamazaki, N. et al. Endogenous lectins as targets for drug delivery. *Advanced Drug Delivery Reviews* **43**, 225-244 (2000).

28. Xu, L., Pirollo, K.F. & Chang, E.H. Tumor-targeted p53-gene therapy enhances the efficacy of conventional chemo/radiotherapy. *Journal of Controlled Release* **74**, 115-28 (2001).

29. Wang, S., Lee, R.J., Cauchon, G., Gorenstein, D.G. & Low, P.S. Delivery of antisense oligodeoxyribonucleotides against the human epidermal growth factor receptor into cultured KB cells with liposomes conjugated to folate via polyethylene glycol. *Proceedings of the National Academy of Sciences of the United States of America* **92**, 3318-22 (1995).

30. Shukla, S. et al. Synthesis and biological evaluation of folate receptor-targeted boronated PAMAM dendrimers as potential agents for neutron capture therapy. *Bioconjugate Chemistry* **14**, 158-67 (2003).

31. Moon, W.K. et al. Enhanced tumor detection using a folate receptor-targeted near-infrared fluorochrome conjugate. *Bioconjugate Chemistry* **14**, 539-45 (2003).

32. Leamon, C.P. & Low, P.S. Selective targeting of malignant cells with cytotoxin-folate conjugates. *Journal of Drug Targeting* **2**, 101-12 (1994).

33. Konda, S.D., Aref, M., Wang, S., Brechbiel, M. & Wiener, E.C. Specific targeting of folate-dendrimer MRI contrast agents to the high affinity folate receptor expressed in ovarian tumor xenografts. *Magma* **12**, 104-13 (2001).

34. Goren, D. et al. Nuclear delivery of doxorubicin via folate-targeted liposomes with bypass of multidrug-resistance efflux pump. *Clinical Cancer Research* **6**, 1949-57 (2000).

35. Trail, P.A. et al. Cure of xenografted human carcinomas by BR96-doxorubicin immunoconjugates. *Science* **261**, 212-5 (1993).

36. Tolcher, A.W. et al. Randomized phase II study of BR96-doxorubicin conjugate in patients with metastatic breast cancer. *Journal of Clinical Oncology* **17**, 478-84 (1999).

37. Ajani, J.A., Kelsen, D.P., Haller, D., Hargraves, K. & Healey, D. A multi-institutional phase II study of BMS-182248-01 (BR96-doxorubicin conjugate) administered every 21 days in patients with advanced gastric adenocarcinoma. *Cancer Journal* **6**, 78-81 (2000).

38. Lode, H.N. et al. Targeted therapy with a novel enediyene antibiotic calicheamicin theta(I)1 effectively suppresses growth and dissemination of liver metastases in a syngeneic model of murine neuroblastoma. *Cancer Research* **58**, 2925-8 (1998).

39. Hinman, L.M. et al. Preparation and characterization of monoclonal antibody conjugates of the calicheamicins: a novel and potent family of antitumor antibiotics. *Cancer Research* **53**, 3336-42 (1993).

40. Sievers, E.L. et al. Efficacy and safety of gemtuzumab ozogamicin in patients with CD33-positive acute myeloid leukemia in first relapse. *Journal of Clinical Oncology* **19**, 3244-54 (2001).

41. Liu, C. et al. Eradication of large colon tumor xenografts by targeted delivery of maytansinoids. *Proceedings of the National Academy of Sciences of the United States of America* **93**, 8618-23 (1996).

42. Park, J.W. et al. Anti-HER2 immunoliposomes for targeted therapy of human tumors. *Cancer Letters* **118**, 153-60 (1997).

43. Park, J.W., Hong, K., Kirpotin, D.B., Papahadjopoulos, D. & Benz, C.C. Immunoliposomes for cancer treatment. *Advances in Pharmacology* **40**, 399-435 (1997).

44. Koelemij, R. et al. Bispecific antibodies in cancer therapy, from the laboratory to the clinic. *Journal of Immunotherapy* **22**, 514-24 (1999).

45. Segal, D.M., Weiner, G.J. & Weiner, L.M. Bispecific antibodies in cancer therapy. *Current Opinion in Immunology* **11**, 558-62 (1999).

46. Jain, R.K. Normalization of tumor vasculature: an emerging concept in antiangiogenic therapy. *Science* **307**, 58-62 (2005).

47. Stroh, M. et al. Quantum dots spectrally distinguish multiple species within the tumor milieu in vivo. *Nature Medicine* **11**, 678-682 (2005).

48. Ahmed, S.I., Thomas, A.L. & Steward, W.P. Vascular endothelial growth factor (VEGF) inhibition by small molecules. *Journal of Chemotherapy* **16 Suppl 4**, 59-63 (2004).

49. Chen, Q.R., Zhang, L., Gasper, W. & Mixson, A.J. Targeting tumor angiogenesis with gene therapy. *Molecular Genetics and Metabolism* **74**, 120-7 (2001).

50. Reynolds, A.R., Moein Moghimi, S. & Hodivala-Dilke, K. Nanoparticle-mediated gene delivery to tumour neovasculature. *Trends in Molecular Medicine* **9**, 2-4 (2003).

51. Brooks, P.C. et al. Integrin alpha v beta 3 antagonists promote tumor regression by inducing apoptosis of angiogenic blood vessels. *Cell* **79**, 1157-64 (1994).

52. Cleaver, O. & Melton, D.A. Endothelial signaling during development. *Nature Medicine* **9**, 661-8 (2003).

53. Cheng, S. et al. Design and synthesis of novel cyclic RGD-containing peptides as highly potent and selective integrin alpha IIb beta 3 antagonists. *Journal of Medicinal Chemistry* **37**, 1-8 (1994).

54. Bibby, D.C. et al. Pharmacokinetics and biodistribution of RGD-targeted doxorubicin-loaded nanoparticles in tumor-bearing mice. *International Journal of Pharmaceutics* **293**, 281-90 (2005).

55. Chen, X., Plasencia, C., Hou, Y. & Neamati, N. Synthesis and biological evaluation of dimeric RGD peptide-paclitaxel conjugate as a model for integrin-targeted drug delivery. *Journal of Medicinal Chemistry* **48**, 1098-106 (2005).

56. Ringsdorf, H. Structure and properties of pharmacologically active polymers. *J. Polymer Sci. Polymer Symp.* **51**, 135-153 (1975).

57. Veronese, F.M. & Morpurgo, M. Bioconjugation in pharmaceutical chemistry. *Farmaco* **54**, 497-516 (1999).

58. D'Souza, A.J. & Topp, E.M. Release from polymeric prodrugs: linkages and their degradation. *Journal of Pharmaceutical Sciences* **93**, 1962-79 (2004).

59. Helmlinger, G., Yuan, F., Dellian, M. & Jain, R.K. Interstitial pH and pO2 gradients in solid tumors in vivo: high-resolution measurements reveal a lack of correlation. *Nature Medicine* **3**, 177-82 (1997).

60. Dellian, M., Helmlinger, G., Yuan, F. & Jain, R.K. Fluorescence ratio imaging of interstitial pH in solid tumours: effect of glucose on spatial and temporal gradients. *British Journal of Cancer* **74**, 1206-15 (1996).

61. Huang, S.K., Lee, K.D., Hong, K., Friend, D.S. & Papahadjopoulos, D. Microscopic localization of sterically stabilized liposomes in colon carcinoma-bearing mice. *Cancer Research* **52**, 5135-43 (1992).

62. Ohkuma, S. & Poole, B. Fluorescence probe measurement of the intralysosomal pH in living cells and the perturbation of pH by various agents. *Proceedings of the National Academy of Sciences of the United States of America* **75**, 3327-31 (1978).

63. Tycko, B. & Maxfield, F.R. Rapid acidification of endocytic vesicles containing alpha 2-macroglobulin. *Cell* **28**, 643-51 (1982).

64. Daleke, D.L., Hong, K. & Papahadjopoulos, D. Endocytosis of liposomes by macrophages: binding, acidification and leakage of liposomes monitored by a new fluorescence assay. *Biochimica et Biophysica Acta* **1024**, 352-66 (1990).

65. Cordes, E.H. & Bull, H.G. in Mechanism and catalysis for hydrolysis of acetals, ketals, and ortho esters 581-603 (1974).

66. Rodrigues, P. et al. Synthesis and in vitro efficacy of acid-sensitive poly(ethylene glycol) paclitaxel conjugates. *Bioorganic & Medicinal Chemistry Letters* **13**, 355-60 (2003).

67. Yoo, H.S., Lee, E.A. & Park, T.G. Doxorubicin-conjugated biodegradable polymeric micelles having acid-cleavable linkages. *Journal of Controlled Release* **82**, 17-27 (2002).

68. Ulbrich, K., Etrych, T., Chytil, P., Jelinkova, M. & Rihova, B. HPMA copolymers with pH-controlled release of doxorubicin: in vitro cytotoxicity and in vivo antitumor activity. *Journal of Controlled Release* **87**, 33-47 (2003).

69. Rodrigues, P.C. et al. Acid-sensitive polyethylene glycol conjugates of doxorubicin: preparation, in vitro efficacy and intracellular distribution. *Bioorganic & Medicinal Chemistry* **7**, 2517-24 (1999).

70. Shen, W.C. & Ryser, H.J. cis-Aconityl spacer between daunomycin and macromolecular carriers: a model of pH-sensitive linkage releasing drug from a lysosomotropic conjugate. *Biochemical and Biophysical Research Communications* **102**, 1048-54 (1981).

71. Kong, G., Braun, R.D. & Dewhirst, M.W. Characterization of the effect of hyperthermia on nanoparticle extravasation from tumor vasculature. *Cancer Research* **61**, 3027-32 (2001).

72. Ling, V. Charles F. Kettering Prize. P-glycoprotein and resistance to anticancer drugs. *Cancer* **69**, 2603-9 (1992).

73. Horwitz, S.B. et al. Taxol: mechanisms of action and resistance. *Journal of the National Cancer Institute. Monographs*, 55-61 (1993).

74. Gottesman, M.M. Mechanisms of cancer drug resistance. *Annual Review of Medicine* **53**, 615-27 (2002).

75. Gottesman, M.M., Fojo, T. & Bates, S.E. Multidrug resistance in cancer: role of ATP-dependent transporters. *Nature Reviews Cancer* **2**, 48-58 (2002).

76. Merisko-Liversidge, E., Liversidge, G.G. & Cooper, E.R. Nanosizing: a formulation approach for poorly-water-soluble compounds. *European Journal of Pharmaceutical Sciences* **18**, 113-120 (2003).

77. Fishman, M.L., Cooke, P.H. & Coffin, D.R. Nanostructure of native pectin sugar acid gels visualized by atomic force microscopy. *Biomacromolecules* **5**, 334-341 (2004).

78. Seymour, L.W., Duncan, R., Strohalm, J. & Kopecek, J. Effect of molecular weight (Mw) of N-(2-hydroxypropyl)methacrylamide copolymers on body distribution and rate of excretion after subcutaneous, intraperitoneal, and intravenous administration to rats. *Journal of Biomedical Materials Research* **21**, 1341-58 (1987).

79. Rowinsky, E.K., Cazenave, L.A. & Donehower, R.C. Taxol: a novel investigational antimicrotubule agent. *Journal of the National Cancer Institute* **82**, 1247-59 (1990).

80. Singla, A.K., Garg, A. & Aggarwal, D. Paclitaxel and its formulations. *International Journal of Pharmaceutics* **235**, 179-192 (2002).

81. anonymous. Albumin-bound paclitaxel (Abraxane) for advanced breast cancer. *Medical Letter on Drugs & Therapeutics* **47**, 39-40 (2005).

82. Garber, K. Improved paclitaxel formulation hints at new chemotherapy approach. *Journal of the National Cancer Institute* **96**, 90-91 (2004).

83. Gelderblom, H., Verweij, J., Nooter, K. & Sparreboom, A. Cremophor EL: the drawbacks and advantages of vehicle selection for drug formulation. *European Journal of Cancer* **37**, 1590-1598 (2001).

84. Guenard, D., Gueritte-Voegelein, F., Dubois, J. & Potier, P. Structure-activity relationships of Taxol and Taxotere analogues. *Journal of the National Cancer Institute. Monographs*, 79-82 (1993).

85. Jimenez-Barbero, J. et al. Effect of 2'-OH acetylation on the bioactivity and conformation of 7-O-[N-(4'-fluoresceincarbonyl)-L-alanyl]taxol. A NMR-fluorescence microscopy study. *Bioorganic & Medicinal Chemistry* **6**, 1857-63 (1998).

86. Baloglu, E. et al. Synthesis and biological evaluation of C-3'NH/C-10 and C-2/C-10 modified paclitaxel analogues. *Bioorganic & Medicinal Chemistry* **11**, 1557-68 (2003).

87. Moyna, G. et al. Conformational studies of paclitaxel analogs modified at the C-2' position in hydrophobic and hydrophilic solvent systems. *Journal of Medicinal Chemistry* **40**, 3305-11 (1997).

88. Kopecek, J., Kopeckova, P., Minko, T. & Lu, Z. HPMA copolymer-anticancer drug conjugates: design, activity, and mechanism of action. *European Journal of Pharmaceutics and Biopharmaceutics* **50**, 61-81 (2000).

89. Duncan, R., Cable, H.C., Rejmanova, P., Kopecek, J. & Lloyd, J.B. Tyrosinamide residues enhance pinocytic capture of N-(2-hydroxypropyl)methacrylamide copolymers. *Biochimica et Biophysica Acta* **799**, 1-8 (1984).

90. Seymour, L.W. et al. Hepatic drug targeting: phase I evaluation of polymer-bound doxorubicin. *Journal of Clinical Oncology* **20**, 1668-76 (2002).

91. Ulbrich, K., Etrych, T., Chytil, P., Jelinkova, M. & Rihova, B. Antibody-targeted polymer-doxorubicin conjugates with pH-controlled activation. *Journal of Drug Targeting* **12**, 477-89 (2004).

92. Vasey, P.A. et al. Phase I clinical and pharmacokinetic study of PK1 [N-(2-hydroxypropyl)methacrylamide copolymer doxorubicin]: first member of a new class of chemotherapeutic agents-drug-polymer conjugates. Cancer Research Campaign Phase I/II Committee. *Clinical Cancer Research* **5**, 83-94 (1999).

93. Julyan, P.J. et al. Preliminary clinical study of the distribution of HPMA copolymers bearing doxorubicin and galactosamine. *Journal of Controlled Release* **57**, 281-90 (1999).

94. Meerum Terwogt, J.M. et al. Phase I clinical and pharmacokinetic study of PNU166945, a novel water-soluble polymer-conjugated prodrug of paclitaxel. *Anticancer Drugs* **12**, 315-23 (2001).

95. Li, C. Poly(L-glutamic acid)--anticancer drug conjugates. *Advanced Drug Delivery Reviews* **54**, 695-713 (2002).

96. Li, C. et al. Complete regression of well-established tumors using a novel water-soluble poly(L-glutamic acid)-paclitaxel conjugate. *Cancer Research* **58**, 2404-9 (1998).

97. Singer, J.W. Paclitaxel poliglumex (XYOTAX, CT-2103): a macromolecular taxane. *Journal of Controlled Release* **109**, 120-6 (2005).

98. Tansey, W. et al. Synthesis and characterization of branched poly(L-glutamic acid) as a biodegradable drug carrier. *Journal of Controlled Release* **94**, 39-51 (2004).

99. Sinay, P. Sugars slide into heparin activity.[comment]. *Nature* **398**, 377-8 (1999).

100. Petitou, M. et al. Synthesis of thrombin-inhibiting heparin mimetics without side effects.[see comment]. *Nature* **398**, 417-22 (1999).

101. Lever, R. & Page, C.P. Novel drug development opportunities for heparin. *Nature Reviews. Drug Discovery* **1**, 140-8 (2002).

102. Folkman, J., Weisz, P.B., Joullie, M.M., Li, W.W. & Ewing, W.R. Control of angiogenesis with synthetic heparin substitutes. *Science* **243**, 1490-3 (1989).

103. Salmivirta, M., Lidholt, K. & Lindahl, U. Heparan sulfate: a piece of information. *FASEB Journal* **10**, 1270-9 (1996).

104. Collen, A. et al. Unfractionated and low molecular weight heparin affect fibrin structure and angiogenesis in vitro. *Cancer Research* **60**, 6196-200 (2000).

105. Vlodavsky, I. et al. Mammalian heparanase: gene cloning, expression and function in tumor progression and metastasis.[see comment]. *Nature Medicine* **5**, 793-802 (1999).

106. Smorenburg, S.M. & Van Noorden, C.J. The complex effects of heparins on cancer progression and metastasis in experimental studies. *Pharmacological Reviews* **53**, 93-105 (2001).

107. Borsig, L. et al. Heparin and cancer revisited: mechanistic connections involving platelets, P-selectin, carcinoma mucins, and tumor metastasis. *Proceedings of the National Academy of Sciences of the United States of America* **98**, 3352-7 (2001).

108. Parish, C.R., Freeman, C., Brown, K.J., Francis, D.J. & Cowden, W.B. Identification of sulfated oligosaccharide-based inhibitors of tumor growth and metastasis using novel in vitro assays for angiogenesis and heparanase activity. *Cancer Research* **59**, 3433-41 (1999).

109. Lundin, L. et al. Selectively desulfated heparin inhibits fibroblast growth factor-induced mitogenicity and angiogenesis. *Journal of Biological Chemistry* **275**, 24653-60 (2000).

110. Yoshitomi, Y. et al. Inhibition of experimental lung metastases of Lewis lung carcinoma cells by chemically modified heparin with reduced anticoagulant activity. *Cancer Letters* **207**, 165-74 (2004).

111. Ono, K. et al. Periodate-treated, non-anticoagulant heparin-carrying polystyrene (NAC-HCPS) affects angiogenesis and inhibits subcutaneous induced tumour growth and metastasis to the lung. *British Journal of Cancer* **86**, 1803-12 (2002).

112. Passirani, C., Barratt, G., Devissaguet, J.P. & Labarre, D. Long-circulating nanoparticles bearing heparin or dextran covalently bound to poly(methyl methacrylate). *Pharmaceutical Research* **15**, 1046-50 (1998).

113. Dufresne, M.H. & Leroux, J.C. Study of the micellization behavior of different order amino block copolymers with heparin. *Pharmaceutical Research* **21**, 160-9 (2004).

114. Kwon, S. et al. Physicochemical Characteristics of Self-Assembled Nanoparticles Based on Glycol Chitosan Bearing 5-beta Cholanic Acid. *Langmuir* **19**, 10188-10193 (2003).

115. Park, K. et al. Preparation and characterization of self-assembled nanoparticles of heparin-deoxycholic acid conjugates. *Langmuir* **20**, 11726-31 (2004).

116. Park, K. et al. Heparin-deoxycholic acid chemical conjugate as an anticancer drug carrier and its antitumor activity. *Journal of Controlled Release* **114**, 300-6 (2006).

117. Lee, D.Y. et al. Suppression of angiogenesis and tumor growth by orally active deoxycholic acid-heparin conjugate. *Journal of Controlled Release* (2007).

118. Dubowchik, G.M. & Walker, M.A. Receptor-mediated and enzyme-dependent targeting of cytotoxic anticancer drugs. *Pharmacology & Therapeutics* **83**, 67-123 (1999).

119. Backer, M.V. & Backer, J.M. Targeting endothelial cells overexpressing VEGFR-2: selective toxicity of Shiga-like toxin-VEGF fusion proteins. *Bioconjugate Chemistry* **12**, 1066-73 (2001).

120. Egilmez, N.K. et al. In situ tumor vaccination with interleukin-12-encapsulated biodegradable microspheres: induction of tumor regression and potent antitumor immunity. *Cancer Research* **60**, 3832-7 (2000).

121. Leamon, C.P. & Low, P.S. Delivery of macromolecules into living cells: a method that exploits folate receptor endocytosis. *Proceedings of the National Academy of Sciences of the United States of America* **88**, 5572-6 (1991).

122. Lee, R.J., Wang, S. & Low, P.S. Measurement of endosome pH following folate receptor-mediated endocytosis. *Biochimica et Biophysica Acta* **1312**, 237-42 (1996).

123. Low, P.S. & Antony, A.C. Folate receptor-targeted drugs for cancer and inflammatory diseases. *Advanced Drug Delivery Reviews* **56**, 1055-8 (2004).

124. Hilgenbrink, A.R. & Low, P.S. Folate receptor-mediated drug targeting: from therapeutics to diagnostics. *Journal of Pharmaceutical Sciences* **94**, 2135-46 (2005).

125. Mathias, C.J., Hubers, D., Low, P.S. & Green, M.A. Synthesis of [(99m)Tc]DTPA-folate and its evaluation as a folate-receptor-targeted radiopharmaceutical. *Bioconjugate Chemistry* **11**, 253-7 (2000).

126. Dube, D., Francis, M., Leroux, J.C. & Winnik, F.M. Preparation and tumor cell uptake of poly(N-isopropylacrylamide) folate conjugates. *Bioconjugate Chemistry* **13**, 685-92 (2002).

127. Caliceti, P. et al. Synthesis and physicochemical characterization of folate-cyclodextrin bioconjugate for active drug delivery. *Bioconjugate Chemistry* **14**, 899-908 (2003).

128. Dauty, E., Remy, J.S., Zuber, G. & Behr, J.P. Intracellular delivery of nanometric DNA particles via the folate receptor. *Bioconjugate Chemistry* **13**, 831-9 (2002).

129. Steinberg, G. & Borch, R.F. Synthesis and evaluation of pteroic acid-conjugated nitroheterocyclic phosphoramidates as folate receptor-targeted alkylating agents. *Journal of Medicinal Chemistry* **44**, 69-73 (2001).

130. Leamon, C.P. & Reddy, J.A. Folate-targeted chemotherapy. *Advanced Drug Delivery Reviews* **56**, 1127-41 (2004).

131. Paranjpe, P.V. et al. Tumor-targeted bioconjugate based delivery of camptothecin: design, synthesis and in vitro evaluation. *Journal of Controlled Release* **100**, 275-92 (2004).

132. Lee, J.W., Lu, J.Y., Low, P.S. & Fuchs, P.L. Synthesis and evaluation of taxol-folic acid conjugates as targeted antineoplastics. *Bioorg Med Chem* **10**, 2397-414 (2002).

133. Quintana, A. et al. Design and function of a dendrimer-based therapeutic nanodevice targeted to tumor cells through the folate receptor. *Pharmaceutical Research* **19**, 1310-1316 (2002).

134. Lee, R.J. & Low, P.S. Folate-mediated tumor cell targeting of liposome-entrapped doxorubicin in vitro. *Biochimica et Biophysica Acta* **1233**, 134-44 (1995).

135. Ni, S., Stephenson, S.M. & Lee, R.J. Folate receptor targeted delivery of liposomal daunorubicin into tumor cells. *Anticancer Research* **22**, 2131-5 (2002).

136. Gabizon, A. et al. Targeting folate receptor with folate linked to extremities of poly(ethylene glycol)-grafted liposomes: in vitro studies. *Bioconjugate Chemistry* **10**, 289-98 (1999).

137. Pan, X.Q., Wang, H. & Lee, R.J. Antitumor activity of folate receptor-targeted liposomal doxorubicin in a KB oral carcinoma murine xenograft model. *Pharmaceutical Research* **20**, 417-22 (2003).

138. Deming, T.J. Facile synthesis of block copolypeptides of defined architecture. *Nature* **390**, 386-9 (1997).

139. Wang, S., Lee, R.J., Mathias, C.J., Green, M.A. & Low, P.S. Synthesis, purification, and tumor cell uptake of 67Ga-deferoxamine--folate, a potential radiopharmaceutical for tumor imaging. *Bioconjugate Chemistry* **7**, 56-62 (1996).

140. Ahsan, A., Jeske, W., Mardiguian, J. & Fareed, J. Feasibility study of heparin mass calibrator as a GPC calibrator for heparins and low molecular weight heparins. *Journal of Pharmaceutical Sciences* **83**, 197-201 (1994).

141. Ahsan, A. et al. Molecular profiling and weight determination of heparins and depolymerized heparins. *Journal of Pharmaceutical Sciences* **84**, 724-7 (1995).

142. Mathew, A.E., Mejillano, M.R., Nath, J.P., Himes, R.H. & Stella, V.J. Synthesis and evaluation of some water-soluble prodrugs and derivatives of taxol with antitumor activity. *Journal of Medicinal Chemistry* **35**, 145-51 (1992).

143. Deutsch, H.M. et al. Synthesis of congeners and prodrugs. 3. Water-soluble prodrugs of taxol with potent antitumor activity. *Journal of Medicinal Chemistry* **32**, 788-92 (1989).

144. Cavallaro, G., Licciardi, M., Caliceti, P., Salmaso, S. & Giammona, G. Synthesis, physico-chemical and biological characterization of a paclitaxel macromolecular prodrug. *European Journal of Pharmaceutics & Biopharmaceutics* **58**, 151-9 (2004).

145. Greenwald, R.B., Pendri, A. & Bolikal, D. Highly Water Soluble Taxol Derivatives: 7-Polyethylene Glycol Carbamates and Carbonates. *Journal of Organic Chemistry* **60**, 331-6 (1995).

146. Heller, J., Helwing, R.F., Baker, R.W. & Tuttle, M.E. Controlled release of water-soluble macromolecules from bioerodible hydrogels. *Biomaterials* **4**, 262-6 (1983).

147. Vilar, R.E. et al. Nitric oxide degradation of heparin and heparan sulphate. *Biochemical Journal* **324 (Pt 2)**, 473-9 (1997).

148. Dordunoo, S.K. & Burt, H.M. Solubility and stability of taxol: effects of buffers and cyclodextrins. *International Journal of Pharmaceutics* **133**, 191-201 (1996).

149. Lin, C.E. et al. Combination of paclitaxel and nitric oxide as a novel treatment for the reduction of restenosis. *Journal of Medicinal Chemistry* **47**, 2276-82 (2004).

150. Nakanishi, T. et al. Development of the polymer micelle carrier system for doxorubicin. *Journal of Controlled Release* **74**, 295-302 (2001).

151. Lee, Y., Nam, J.H., Shin, H.C. & Byun, Y. Conjugation of low-molecular-weight heparin and deoxycholic acid for the development of a new oral anticoagulant agent. *Circulation* **104**, 3116-20 (2001).

152. Lapierre, F. et al. Chemical modifications of heparin that diminish its anticoagulant but preserve its heparanase-inhibitory, angiostatic, anti-tumor and anti-metastatic properties. *Glycobiology* **6**, 355-66 (1996).

153. Brown, R.S. in The amide linkage: selected structural aspects in chemistry, biochemistry, and materials science (eds. Greenberg, A., Breneman, C.M. & Liebman, J.F.) 85-114 (Wiley-Interscience, New York, 2000).

154. Kerns, E.H., Volk, K.J., Hill, S.E. & Lee, M.S. Profiling taxanes in Taxus extracts using lc/ms and lc/ms/ms techniques. *Journal of Natural Products* **57**, 1391-403 (1994).

155. Auzenne, E. et al. Superior therapeutic profile of poly-L-glutamic acid-paclitaxel copolymer compared with taxol in xenogeneic compartmental models of human ovarian carcinoma. *Clinical Cancer Research* **8**, 573-81 (2002).

156. Parker, N. et al. Folate receptor expression in carcinomas and normal tissues determined by a quantitative radioligand binding assay. *Analytical Biochemistry* **338**, 284-93 (2005).

157. Ciardiello, F. et al. Antitumor activity of sequential treatment with topotecan and anti-epidermal growth factor receptor monoclonal antibody C225. *Clinical Cancer Research* **5**, 909-16 (1999).

158. Branda, R.F., Nigels, E., Lafayette, A.R. & Hacker, M. Nutritional folate status influences the efficacy and toxicity of chemotherapy in rats. *Blood* **92**, 2471-6 (1998).

159. Song, J., Medline, A., Mason, J.B., Gallinger, S. & Kim, Y.I. Effects of dietary folate on intestinal tumorigenesis in the apcMin mouse. *Cancer Research* **60**, 5434-40 (2000).

160. Song, J. et al. Chemopreventive effects of dietary folate on intestinal polyps in Apc+/-Msh2-/- mice. *Cancer Research* **60**, 3191-9 (2000).

161. Taxol Product Information. *Bristol-Myers Squibb*.

162. Abraxane Product Information. *Abraxis Oncology*.

163. Freireich, E.J., Gehan, E.A., Rall, D.P., Schmidt, L.H. & Skipper, H.E. Quantitative comparison of toxicity of anticancer agents in mouse, rat, hamster, dog, monkey, and man. *Cancer Chemotherapy Reports* **50**, 219-44 (1966).

164. Mabjeesh, N.J. et al. 2ME2 inhibits tumor growth and angiogenesis by disrupting microtubules and dysregulating HIF. *Cancer Cell* **3**, 363-75 (2003).

165. Folkman, J. The role of angiogenesis in tumor growth. *Seminars in Cancer Biology* **3**, 65-71 (1992).

166. Fidler, I.J. The pathogenesis of cancer metastasis: the 'seed and soil' hypothesis revisited. *Nature Reviews Cancer* **3**, 453-8 (2003).

167. Carmeliet, P. & Jain, R.K. Angiogenesis in cancer and other diseases. *Nature* **407**, 249-57 (2000).

168. Kerbel, R. & Folkman, J. Clinical translation of angiogenesis inhibitors. *Nature Reviews Cancer* **2**, 727-39 (2002).

169. Eberhard, A. et al. Heterogeneity of angiogenesis and blood vessel maturation in human tumors: implications for antiangiogenic tumor therapies. *Cancer Research* **60**, 1388-93 (2000).

170. Klauber, N., Parangi, S., Flynn, E., Hamel, E. & D'Amato, R.J. Inhibition of angiogenesis and breast cancer in mice by the microtubule inhibitors 2-methoxyestradiol and taxol. *Cancer Research* **57**, 81-6 (1997).

171. Lau, D.H., Xue, L., Young, L.J., Burke, P.A. & Cheung, A.T. Paclitaxel (Taxol): an inhibitor of angiogenesis in a highly vascularized transgenic breast cancer. *Cancer Biotherapy & Radiopharmaceuticals* **14**, 31-6 (1999).

172. Wang, J., Lou, P., Lesniewski, R. & Henkin, J. Paclitaxel at ultra low concentrations inhibits angiogenesis without affecting cellular microtubule assembly. *Anticancer Drugs* **14**, 13-9 (2003).

173. Lennernas, B., Albertsson, P., Damber, J.E. & Norrby, K. Antiangiogenic effect of metronomic paclitaxel treatment in prostate cancer and non-tumor tissue in the same animals: a quantitative study. *APMIS* **112**, 201-9 (2004).

174. Guo, W., Hinkle, G.H. & Lee, R.J. 99mTc-HYNIC-folate: a novel receptor-based targeted radiopharmaceutical for tumor imaging. *Journal of Nuclear Medicine* **40**, 1563-9 (1999).

175. Lu, Y., Sega, E., Leamon, C.P. & Low, P.S. Folate receptor-targeted immunotherapy of cancer: mechanism and therapeutic potential. *Advanced Drug Delivery Reviews* **56**, 1161-76 (2004).

176. Doucette, M.M. & Stevens, V.L. Folate receptor function is regulated in response to different cellular growth rates in cultured mammalian cells. *Journal of Nutrition* **131**, 2819-25 (2001).

177. Au, J.L., Jang, S.H. & Wientjes, M.G. Clinical aspects of drug delivery to tumors. *Journal of Controlled Release* **78**, 81-95 (2002).

178. Alakhov, V., Moskaleva, E., Batrakova, E.V. & Kabanov, A.V. Hypersensitization of multidrug resistant human ovarian carcinoma cells by pluronic P85 block copolymer. *Bioconjugate Chemistry* **7**, 209-16 (1996).

179. Diaz, J.F., Strobe, R., Engelborghs, Y., Souto, A.A. & Andreu, J.M. Molecular recognition of taxol by microtubules. Kinetics and thermodynamics of binding of fluorescent taxol derivatives to an exposed site. *Journal of Biological Chemistry* **275**, 26265-76 (2000).

180. Links, M. & Brown, R. Clinical relevance of the molecular mechanisms of resistance to anti-cancer drugs. *Expert Reviews in Molecular Medicine* **1999**, 1-21 (1999).

181. Krishna, R. & Mayer, L.D. Multidrug resistance (MDR) in cancer - Mechanisms, reversal using modulators of MDR and the role of MDR modulators in influencing the pharmacokinetics of anticancer drugs. *European Journal of Pharmaceutical Sciences* **11**, 265-283 (2000).

182. Rowinsky, E.K. & Donehower, R.C. Paclitaxel (taxol). *New England Journal of Medicine* **332**, 1004-14 (1995).

183. Schinkel, A.H. et al. Normal viability and altered pharmacokinetics in mice lacking mdr1-type (drug-transporting) P-glycoproteins. *Proceedings of the National Academy of Sciences of the United States of America* **94**, 4028-33 (1997).

184. Alvarez, M. et al. Generation of a drug resistance profile by quantitation of mdr-1/P-glycoprotein in the cell lines of the National Cancer Institute Anticancer Drug Screen. *Journal of Clinical Investigation* **95**, 2205-14 (1995).

185. Burns, B.S. et al. Selective drug resistant human osteosarcoma cell lines. *Clinical Orthopaedics and Related Research*, 259-67 (2001).

186. Tsuruo, T. Molecular cancer therapeutics: Recent progress and targets in drug resistance. *Internal Medicine* **42**, 237-243 (2003).

187. Gabizon, A., Shmeeda, H., Horowitz, A.T. & Zalipsky, S. Tumor cell targeting of liposome-entrapped drugs with phospholipid-anchored folic acid-PEG conjugates. *Advanced Drug Delivery Reviews* **56**, 1177-92 (2004).

188. Liscovitch, M. & Lavie, Y. Cancer multidrug resistance: a review of recent drug discovery research. *IDrugs* **5**, 349-55 (2002).

189. Chaplin, D.J. & Dougherty, G.J. Tumour vasculature as a target for cancer therapy. *British Journal of Cancer* **80 Suppl 1**, 57-64 (1999).

190. Evans, S.M. & Koch, C.J. Prognostic significance of tumor oxygenation in humans. *Cancer Letters* **195**, 1-16 (2003).

191. Tomasz, M. Mitomycin C: small, fast and deadly (but very selective). *Chemistry & Biology* **2**, 575-9 (1995).

192. Brown, J.M. SR 4233 (tirapazamine): a new anticancer drug exploiting hypoxia in solid tumours. *British Journal of Cancer* **67**, 1163-70 (1993).

193. Vrudhula, V.M., MacMaster, J.F., Li, Z., Kerr, D.E. & Senter, P.D. Reductively activated disulfide prodrugs of paclitaxel. *Bioorganic & Medicinal Chemistry Letters* **12**, 3591-4 (2002).

194. Hamdy, F.C. et al. Matrix metalloproteinase 9 expression in primary human prostatic adenocarcinoma and benign prostatic hyperplasia. *British Journal of Cancer* **69**, 177-82 (1994).

195. Naylor, M.S., Stamp, G.W., Davies, B.D. & Balkwill, F.R. Expression and activity of MMPS and their regulators in ovarian cancer. *International Journal of Cancer* **58**, 50-6 (1994).

196. Davies, B. et al. Levels of matrix metalloproteases in bladder cancer correlate with tumor grade and invasion. *Cancer Research* **53**, 5365-9 (1993).

197. Egeblad, M. & Werb, Z. New functions for the matrix metalloproteinases in cancer progression. *Nature Reviews Cancer* **2**, 161-74 (2002).

198. Turk, B.E., Huang, L.L., Piro, E.T. & Cantley, L.C. Determination of protease cleavage site motifs using mixture-based oriented peptide libraries. *Nature Biotechnology* **19**, 661-7 (2001).

199. Fryer, A. et al. Selective O-desulfation produces nonanticoagulant heparin that retains pharmacological activity in the lung. *Journal of Pharmacology and Experimental Therapeutics* **282**, 208-19 (1997).

VITA

Gloria J. Kim

Gloria was born in Waratah, New South Wales, Australia. She spent her childhood in Australia, Canada, Korea, and Germany. After graduating from Seoul Science High School, she attended Seoul National University where she received her BS in Chemistry in 1997. Under the guidance of Dr. Kam W. Leong, she earned her MSE in Biomedical Engineering from Johns Hopkins University in 2001. In 2002, she joined Dr. Shuming Nie's research group in the Department of Biomedical Engineering at Georgia Institute of Technology and Emory University. In addition to English, she is fluent in Korean and German. Her extracurricular activities include listening to NPR, inline skating, playing the piano, serving as an officer at Dogwood Toastmasters and rooting for the Baltimore Ravens.